Lappeenranta
University of Technology

Tuomas Rantalainen

SIMULATION OF STRUCTURAL STRESS HISTORY BASED ON DYNAMIC ANALYSIS

Thesis for the degree of Doctor of Science (Technology) to be presented with due permission for public examination and criticism in the Auditorium 1381 at Lappeenranta University of Technology, Lappeenranta, Finland on the 23rd of November, 2012, at noon.

Acta Universitatis
Lappeenrantaensis 494

Supervisor Professor Aki Mikkola
Department of Mechanical Engineering
Lappeenranta University of Technology
Finland

Reviewers Professor Shaoping Bai
Department of Mechanical and Manufacturing Engineering
Aalborg University
Denmark

Professor Ole Balling
Department of Mechanical Engineering
Aarhus University
Denmark

Opponents Professor Shaoping Bai
Department of Mechanical and Manufacturing Engineering
Aalborg University
Denmark

Professor Ole Balling
Department of Mechanical Engineering
Aarhus University
Denmark

ISBN 978-952-265-325-3
ISBN 978-952-265-326-0 (PDF)
ISSN 1456-4491

Lappeenranta University of Technology
Yliopistopaino 2012

Preface

The research work for this thesis was carried out between 2007 and 2012 in the Laboratory of Machine Design at the Lappeenranta University of Technology. Most of the funding for the work was provided by the Finnish National Graduate Program of Engineering Mechanics. I also received support for which I am very grateful from the KAUTE Foundation.

During the years I spent working on my thesis and educating myself, I had the opportunity to meet and work with many intelligent and gifted individuals. I enjoyed philosophical, technical, and political discussions with them that cleared my head as deadlines approached. I can say without exaggeration that the team spirit in our laboratory is outstanding. I enjoyed going to work and always having someone there willing to discuss a challenging problem. There have been and are many excellent persons forming our research group. I cannot mention everyone by name, but you all should know that you were and are responsible for the spirit of the group. As a researcher working in the Laboratory of Machine Design, I have been privileged with an additional family, a professional one.

Many people helped me directly with my dissertation work, and I would like to mention them by name.

First, I would like to thank Professor Aki Mikkola for providing me this opportunity to prepare my thesis and for giving me professional and encouraging supervision. I would also like to thank Doctor Rami Al Nazer, who gave me the initial inspiration towards my doctoral dissertation, and with whom I began my doctoral studies. Doctor Oleg Dmitrochenko has helped me from the very beginning of my work, and with him I enjoyed long discussions and philosophical sauna evenings. Doctor Marko Matikainen always encouraged me to continue and pushed me through my difficulties. Doctor Adam Kłodowski began his doctoral research shortly after I did, and with him, I shared virtually all the practical problems I encountered in my work. Antti Valkeapää also deserves my appreciation, since I shared and sometimes solved numerous practical problems with him. Finally, I am grateful to Scott Semken, who helped me with the English language and contributed to the readability of this thesis.

In addition to the previously mentioned colleagues, Emil Kurvinen and John Bruzzo contributed to this work by proofreading the manuscript and pointing out numerous errors in writing.

I am a big fan of an open source ideology, and therefore I would like to thank all the contributors to open source tools such as LaTeX, Inkscape, and Linux.

I received help from my parents Elisa and Juha in many ways. They provided me with a reasoning mind and supported me with practical help, such as taking care of my children. Thank you, mother and father, for all your support.

At last, I want to express my deepest gratitude to my lovely wife Hanna; my daughters Iidasofia, Aino-Ilona, and Elsa-Inkeri; and my son Urho-Viljami. You motivated me in the mornings and saw me swiftly off to my research. You are the purpose of my life.

Lappeenranta, November 2012

Tuomas Rantalainen

Abstract

Tuomas Rantalainen
Simulation of structural stress history based on dynamic analysis
Lappeenranta, 2012
122 pages

Acta Universitatis Lappeenrantaensis 494
Dissertation. Lappeenranta University of Technology

ISBN 978-952-265-325-3
ISBN 978-952-265-326-0 (PDF)
ISSN 1456-4491

Modern machine structures are often fabricated by welding. From a fatigue point of view, the structural details and especially, the welded details are the most prone to fatigue damage and failure. Design against fatigue requires information on the fatigue resistance of a structure's critical details and the stress loads that act on each detail. Even though, dynamic simulation of flexible bodies is already current method for analyzing structures, obtaining the stress history of a structural detail during dynamic simulation is a challenging task; especially when the detail has a complex geometry. In particular, analyzing the stress history of every structural detail within a single finite element model can be overwhelming since the amount of nodal degrees of freedom needed in the model may require an impractical amount of computational effort.

The purpose of computer simulation is to reduce amount of prototypes and speed up the product development process. Also, to take operator influence into account, real time models, *i.e.* simplified and computationally efficient models are required. This in turn, requires stress computation to be efficient if it will be performed during dynamic simulation.

The research looks back at the theoretical background of multibody dynamic simulation and finite element method to find suitable parts to form a new approach for efficient stress calculation. This study proposes that, the problem of stress calculation during dynamic simulation can be greatly simplified by using a combination of floating frame of reference formulation with modal superposition

and a sub-modeling approach. In practice, the proposed approach can be used to efficiently generate the relevant fatigue assessment stress history for a structural detail during or after dynamic simulation.

In this work numerical examples are presented to demonstrate the proposed approach in practice. The results show that approach is applicable and can be used as proposed.

Keywords: floating frame of reference, fatigue design, sub-modeling, flexible multibody dynamics

UDC 519.62 / 64 : 531.3 : 004.942

Tiivistelmä

Tuomas Rantalainen
Dynamiseen analyysiin perustuva rakenteellisen jännityshistorian simulointi
Lappeenranta, 2012
122 sivua

Acta Universitatis Lappeenrantaensis 494
Väitöskirja. Lappeenrannan teknillinen yliopisto

ISBN 978-952-265-325-3
ISBN 978-952-265-326-0 (PDF)
ISSN 1456-4491

Modernien koneiden rakenteet valmistetaan usein hitsaamalla. Väsymiskestävyyden näkökulmasta rakenteen yksityiskohdat ja etenkin hitsatut yksityiskohdat ovat erityisen herkkiä väsymään ja sitä kautta vaurioitumaan. Väsymiselle alttiiden rakenteiden suunnittelu tarvitsee onnistuakseen tietoa kriittisten yksityiskohtien väsymiskestosta ja jokaisen rakenneyksityiskohdan kuormituksesta. Vaikka joustavien kappaleiden dynamiikan simulointi on yleisesti käytössä oleva menetelmä rakenteiden analyysiin, rakenneyksityiskohdan jännityshistorian simuloiminen dynaamisen analyysin aikana on haastava tehtävä. Haasteellisuus korostuu etenkin silloin kun yksityiskohdan geometria on monimutkainen. Rakenteen jokaisen yksityiskohdan jännityshistorian analysoiminen yhdellä tarkalla elementtimallilla voi olla ylitsepääsemätön tehtävä, sillä mallin sisältämän suuren solmuvapausasteiden määrän käsittely ylittää käytännössä käytössä olevan laskentatehon.

Tietokonesimuloinnin käytön tarkoitus on vähentää tarvittavien prototyyppien määrää ja nopeuttaa tuotekehitysprosessia. Mikäli suunniteltavan koneen käyttäjän vaikutus halutaan ottaa huomioon koneen toimintaa simuloitaessa, on reaaliaikamallin käyttö tarpeellista. Reaaliaikamallilla tarkoitetaan tässä mallia, joka on yksinkertaistettu ja laskennallisesti niin tehokas, että sitä voidaan ajaa pöytäkoneella. Jos jännityshistoria lasketaan reaaliaikaisen dynaamisen simuloinnin aikana, asettaa se tiukat vaatimukset myös jännitysten simuloinnin laskentatehokkuudelle.

Tutkimuksessa poimitaan monikappaledynamiikan ja elementtimenetelmän teoreettisesta taustasta sopivia palasia uudenlaisen ja tehokkaan menetelmän koostamiseksi jännitysten laskentaa varten. Tässä työssä esitetään, että ongelmaa jännitysten laskennasta dynaamisen simuloinnin aikana voidaan huomattavasti yksinkertaistaa yhdistämällä kelluvan koordinaatiston menetelmää, muotojen superponointia ja alimallinusta. Kehitettyä menetelmää voidaan käyttää väsymisen kannalta oleellisten rakenneyksityiskohtien jännityshistorioiden tehokkaaseen tuottamiseen dynaamisen simuloinnin aikana tai sen jälkeen.

Työssä kuvattua uutta menetelmää ja sen käyttöä on esitelty numeerisin esimerkein. Tulokset osoittavat, että lähestymistapa on toimiva ja menetelmä on käyttökelpoinen.

Hakusanat: kelluvan koordinaatiston menetelmä, väsymismitoitus, alimallinnus, joustava monikappaledynamiikka

UDC 519.62 / 64 : 531.3 : 004.942

SYMBOLS

$\boldsymbol{0}$	zero vector
$\mathbf{0}$	zero matrix
A	loaded end of the large-scale element model
$\mathbf{A}^i$	rotation matrix of body i
$\mathbf{A}_f^{iP}$	rotation matrix that describes orientation due to deformation
$\mathbf{B}^i$	kinematic matrix of body i
$\mathbf{B}^{ik}$	kinematic matrix of body i belonging to element k
$\boldsymbol{c}$	position vector of a material point
C	constrained end of the large-scale element model
C_0	power law constant (material parameter)
$\boldsymbol{C}$	constraint vector for the system
$\dot{\boldsymbol{C}}$	first time derivate of constraints for the system
$\ddot{\boldsymbol{C}}$	second time derivative of constraints for the system
$\mathbf{C}_{\boldsymbol{q}}$	constraint Jacobian matrix for the system
$\mathbf{C}^i_{\boldsymbol{q}^i}$	constraint Jacobian matrix of body i
d	differential operator
$\frac{\mathrm{d}a}{\mathrm{d}N}$	crack growth rate
D	crack length
D_0	initial crack length
D_f	final crack size
e	nominal strain
E	elastic modulus
$\mathbf{E}^{ik}$	matrix of elastic coefficients of body i of an element k
$F(D)$	crack function that takes into account the shape of the crack
F_h	harmonic force
$\boldsymbol{F}^i$	external force vector of body i
$\boldsymbol{F}^i_k$	k^{th} force acting on body i
$\boldsymbol{F}^i_r$	vector of constraint forces of body i
$\boldsymbol{F}^{iI}$	vector of forces acting on internal nodes of body i
$\boldsymbol{F}^{iP}$	externally applied force per unit volume
$\boldsymbol{g}^i$, $\boldsymbol{g}^j$	nodal coordinates of body i and j, respectively
$\boldsymbol{g}^{ij}$	nodal coordinates of body i or j
$\boldsymbol{g}^s$	displacements vector of the interface element
$\mathbf{G}^{ij}$	surface integral of bodies i or j

$\bar{\mathbf{G}}^i$	local velocity transformation matrix of body i
$\dot{\bar{\mathbf{G}}}^i$	first time derivative of local velocity transformation matrix of body i
$\mathbf{H}^i$	matrix of elastic coefficients of body i
i	flexible body i
$\mathbf{I}$	identity matrix
$\bar{\mathbf{I}}^i_{\theta\theta}$	inertia tensor of body i
$\bar{\mathbf{I}}^i_{\theta p}$	interconnection matrix of rotational coordinates and modal coordinates
$\mathbf{I}^{i1}$	mass of body i
$\mathbf{I}^{i2}$	first static moment of body i
$\mathbf{I}^{i3}$	correction of location of center of mass of body i
$\mathbf{I}^{i4}$	first order correction of coupling between deformation and rotation
$\mathbf{I}^{i5}$	second order correction of coupling between deformation and rotation
$\mathbf{I}^{i6}$	modal mass of flexible body i
$\mathbf{I}^{i7}$	inertia of body i
$\mathbf{I}^{i8}$	first order inertia correction
$\mathbf{I}^{i9}$	second order inertia correction
$\mathbf{I}^{i5}_j$	(3 x 3) matrix of $\mathbf{I}^{i5}$ that is related to j^{th} mode
$\mathbf{I}^{i8}_j$	(3 x 3) matrix of $\mathbf{I}^{i8}$ that is related to j^{th} mode
$\mathbf{I}^{i9}_{jh}$	(3 x 3) matrix of $\mathbf{I}^{i9}$ that is related to multiplication of h^{th} mode and j^{th} mode
j	flexible body j
k_f	fatigue strength reduction factor (or fatigue notch factor)
k_t	elastic stress concentration factor
k_ε	strain concentration factor
k_σ	stress concentration factor
$\mathbf{K}$	stiffness matrix of the system
$\mathbf{K}^i$	stiffness matrix of body i in modal coordinates
$\hat{\mathbf{K}}^i$	stiffness matrix of body i in nonorthogonal modal coordinates
$\mathbf{K}^i_i$	stiffness matrix of original finite element of body i
$\mathbf{K}^i_o$	orthogonalized stiffness matrix
m	exponent of the power law (material parameter)
m_n	mass of node n
m^{iP}	nodal mass of particle P^i
M_k	function that takes local notch effect into account

$\mathbf{M}$	mass matrix of the system
$\mathbf{M}^i$	mass matrix of body i
$\hat{\mathbf{M}}^i$	mass matrix of body i in nonorthogonal modal coordinates
$\mathbf{M}^i_o$	orthogonalized mass matrix
$\mathbf{M}^i_{RR}$,$\mathbf{M}^i_{\theta\theta}$,$\mathbf{M}^i_{pp}$	diagonal parts of mass matrix $\mathbf{M}^i$
$\mathbf{M}^i{}_{R\theta} = \mathbf{M}^{i\,\mathrm{T}}_{\theta R}$	part of mass matrix $\mathbf{M}^i$
$\mathbf{M}^i_{Rp} = \mathbf{M}^{i\,\mathrm{T}}_{pR}$	part of mass matrix $\mathbf{M}^i$
$\mathbf{M}^i_{\theta p} = \mathbf{M}^{i\,\mathrm{T}}_{p\theta}$	part of mass matrix $\mathbf{M}^i$
$\mathbf{M}^{ij}$	surface integral
n	node
n_{cb}	number of Craig-Bampton modes
n_F	number of externally applied forces
n_n	number of nodes
n_p	number of modal coordinates or modal shapes
$n_{\Delta\sigma}$	number of counted stress amplitudes with certain stress level σ_1
n^i_j	j^{th} Craig-Bamton eigenvector of body i
N	number of cycles
N_1, N_2	number of cycles subjected to stress level σ_{a1} and σ_{a2}
N_{f1},N_{f2}	number of cycles to failure with certain stress level σ_{a1} and σ_{a2}
N_{fi}	number of cycles to failure with i^{th} stress level $\sigma_a i$
N_i	number of cycles with i^{th} stress level $\sigma_a i$
$\mathbf{N}^i$	orthogonal modal matrix of body i
$\mathbf{N}^{ij}$	element shape function matrix on a surface s of body i or j
$\mathbf{N}^j$	matrix of element shape functions of body j
p^i_j	j$^{\text{th}}$ modal coordinate of body i
$\boldsymbol{p}^i$	vector of modal coordinates of body i
$\dot{\boldsymbol{p}}^i$	first time derivative of modal coordinates of body i
$\ddot{\boldsymbol{p}}^i$	second time derivative of modal coordinates of body i
$\hat{\boldsymbol{p}}^i$	vector of modal coordinates of body i for nonorthogonal modes
P^i	particle in body i
P^i_0	particle in body i at the initial configuration
q	notch sensitivity index
$\boldsymbol{q}$	vector of generalized coordinates
$\boldsymbol{q}^i$	vector of generalized coordinates of body i
$\boldsymbol{q}^s$	displacement field of interface element surface s
$\dot{\boldsymbol{q}}^i$	generalized velocity coordinates of body i
$\ddot{\boldsymbol{q}}$	vector of accelereration of generalized coordinates
$\ddot{\boldsymbol{q}}^i$	generalized acceleration coordinates of body i

$\boldsymbol{Q}^c$	constraint force vector
$\boldsymbol{Q}^e$	vector of generalized forces of the system
$\boldsymbol{Q}^f$	vector of elastic forces of the system
$\boldsymbol{Q}^{ie}$	vector of generalized forces
$\boldsymbol{Q}_p^{ie}$	elastic components of the generalized force vector
$\boldsymbol{Q}_R^{ie}$	translational components of the generalized force vector
$\boldsymbol{Q}_\theta^{ie}$	rotational components of the generalized force vector
$\boldsymbol{Q}^{if}$	vector of elastic forces of body i
$\boldsymbol{Q}^{iv}$	quadratic velocity vector of body i
$\boldsymbol{Q}^v$	quadratic velocity vector of the system
$\boldsymbol{r}^{iP}$	location vector of particle P in body i
$\dot{\boldsymbol{r}}^{iP}$	velocity vector of particle P in body i
$\ddot{\boldsymbol{r}}^{iP}$	acceleration vector of particle P in body i
R	stress ratio
$\boldsymbol{R}^i$	translation of the local reference coordinate system of body i
$\dot{\boldsymbol{R}}^i$	vector of velocity of the local reference frame of body i
$\ddot{\boldsymbol{R}}^i$	vector of acceleration of the local frame of body i
$\mathbf{R}^{ij}$	matrix of interpolation functions of body i or j
$\boldsymbol{s}$	interface surface between domains $\boldsymbol{\Omega}^i$ and $\boldsymbol{\Omega}^j$
S	nominal stress
S_1,S_2	certain nominal stress level 1 and 2, respectively
S_a	nominal stress amplitude (or stress range)
S_{ar}	completely reversed nominal stress
S_m	nominal mean stress
$\bar{\mathbf{S}}^i$	inertia shape integral
$\bar{\boldsymbol{S}}_I^i$	mass moment of inertia about local reference frame of body i
t	time
$\boldsymbol{t}^{ij}$	interface traction of body i or j
$\mathbf{T}$	transformation matrix between body frame and element frame
$\mathbf{T}^{ik}$	transformation matrix between element frame and body frame
$\mathbf{T}^s$	element shape function matrix of interface element surface s
$\boldsymbol{u}^i$,$\boldsymbol{u}^j$	vector of displacements of body i and j at a certain point, respectively
$\boldsymbol{u}^{ij}$	displacement vector on a surface s of body i or j
$\bar{\boldsymbol{u}}_{0n}^i$	undeformed displacement vector in local frame of node n
$\bar{\boldsymbol{u}}_f^i$	displacement vector in local frame for deformed configuration for all nodes
$\bar{\boldsymbol{u}}_n^i$	local position vector of a node n

$\bar{\boldsymbol{u}}^{ik}$	nodal coordinate vector of element k belonging to body i
$\bar{\boldsymbol{u}}^{iP}$	displacement vector in local frame of particle P^i
$\bar{\boldsymbol{u}}_0^{iP}$	displacement vector in local frame for the initial configuration
$\bar{\boldsymbol{u}}_f^{iP}$	displacement vector in local frame for deformed configuration
$\tilde{\bar{\boldsymbol{u}}}_{0n}^{i}$	skew symmetric form of undeformed displacement vector in local frame of node n
$\tilde{\bar{\boldsymbol{u}}}_{k}^{i}$	skew symmetric form of the location vector of the k^{th} force
$\tilde{\bar{\boldsymbol{u}}}_{f}^{iP}$	skew symmetric form of a displacement vector $\bar{\boldsymbol{u}}_f^{iP}$
$\boldsymbol{v}^s$	displacement vector of interface surface s
$\bar{\boldsymbol{v}}_0^{iP}$	undeformed direction vector for location of particle P^i
$\bar{\boldsymbol{v}}_f^{iP}$	deformed direction vector for location of particle P^i
V^i	volume of body i
x	distance from the edge of the discontinuity
x^i, y^i, z^i	Cartesian coordinates of body i in a local frame
x_{n1}^i,x_{n2}^i,x_{n3}^i	Cartesian coordinates of a node n in a local frame
X, Y, Z	Cartesian coordinates in the global frame
X^i, Y^i, Z^i	Cartesian coordinates of body i in the global frame

GREEK LETTERS

α	material constant
$\boldsymbol{\alpha}^{ij}$	vector of unknown coefficients
$\boldsymbol{\Gamma}^{ij}$	common surface between domains $\boldsymbol{\Omega}^i$ and $\boldsymbol{\Omega}^j$
δ	virtual change
$\delta\boldsymbol{q}^i$	virtual change of the generalized coordinates
$\delta\boldsymbol{r}^{iP}$	virtual displacement of the position vector
δW^i	virtual work done by inertial forces
δW^{ie}	virtual work done by externally applied forces
δW^{if}	virtual work done by elastic forces
$\boldsymbol{\delta}^B$	displacements of boundary nodes
$\boldsymbol{\delta}^I$	physical displacements of interior nodes
ΔK	range of stress intensity factor
ΔK_{eqv}	equivalent stress intensity factor
ΔK_{th}	threshold level of range of stress intensity factor
$\Delta\sigma$	stress range
$\Delta\sigma_0$	fatigue limit of notched specimen at nominal stress
$\Delta\sigma_1$	certain stress range
$\Delta\sigma_{hs}$	range of hot spot stress

$\Delta\sigma_{on}$	fatigue limit of unnotched specimen at nominal stress
ε	local strain
ε_{11},ε_{22},ε_{33}	tension components of the strain vector $\boldsymbol{\varepsilon}^i$
ε_{12},ε_{23},ε_{31}	shear components of the strain vector $\boldsymbol{\varepsilon}^i$
$\boldsymbol{\varepsilon}^i$	strain vector of body i
$\boldsymbol{\varepsilon}^{ik}$	strain vector of body i belonging to element k
$\boldsymbol{\varepsilon}_f^{iP}$	vector of rotation change for location on particle P
$\tilde{\boldsymbol{\varepsilon}}_f^{iP}$	skew symmetric form of $\boldsymbol{\varepsilon}_f^{iP}$
$\theta_0^{iE} \dots \theta_3^{iE}$	Euler parameters $0 \dots 3$
$\boldsymbol{\theta}^{iE}$	vector of Euler parameters
$\dot{\boldsymbol{\theta}}^{iE}$	first time derivative of vector of Euler parameters
$\ddot{\boldsymbol{\theta}}^{iE}$	second time derivative vector of Euler parameters
$\boldsymbol{\lambda}$	vector of Lagrange multipliers of the system
$\boldsymbol{\lambda}^i$	vector of Lagrange multipliers of body i
$\boldsymbol{\lambda}^{ij}$	Lagrange multipliers of body i or j
$\boldsymbol{\lambda}^j$	lagrange multipliers of body j
Π	potential energy
Π^{Ω^i}	potential energy of domain Ω^i
Π^{Ω^j}	potential energy of domain Ω^j
ρ	notch tip radius
ρ^i	density of body i
σ	local stress
σ_1, σ_2, σ_3	first, second, and third principal stresses
σ_a	stress amplitude
σ_{a1},σ_{a2},σ_{a3}	stress amplitude of certain stress level
σ_{ai}	i^{th} stress amplitude of certain stress level
σ_{ar}	completely reversed local stress
σ_b	bending stress over the width of the structure
σ_m	mean stress
σ_n	normal stress
σ_{max}	maximum stress
σ_{mbr}	membrane stress
σ_{min}	minimum stress
σ_{nlp}	nonlinear stress peak
σ_s	structural stress
$\sigma_X, \sigma_Y, \sigma_Z$	normal stress components
$\boldsymbol{\sigma}$	stress vector
$\boldsymbol{\sigma}^i$	stress vector of a body i

$\hat{\boldsymbol{\sigma}}^{ik}$	stresses of an element in coordinate frame of element k
τ	shear stress
$\tau_{23}, \tau_{13}, \tau_{12}$	principal shear stresses
$\tau_{YX}, \tau_{YZ}, \tau_{ZX}$	shear stress components
$\boldsymbol{\varphi}_{Rj}$	j^{th} eigenvector translational
$\boldsymbol{\varphi}_{\theta j}$	j^{th} eigenvector for rotational coordinates
$\boldsymbol{\varphi}^{iP}_{R1} \dots \boldsymbol{\varphi}^{iP}_{Rn_p}$	translation modal vectors from $1 \dots n_p$
$\boldsymbol{\varphi}^{iP}_{\theta 1} \dots \boldsymbol{\varphi}^{iP}_{\theta n_p}$	rotation modal vectors from $1 \dots n_p$
φ^{i}_{Rnh},φ^{i}_{Rnj}	h^{th} and j^{th} mode of a modal matrix, respectively
$\boldsymbol{\Phi}^{C}$	matrix of the static correction modes
$\boldsymbol{\Phi}^{i}$	modal matrix of body i
$\boldsymbol{\Phi}^{i}_{nlR}$	l^{th} row of shape matrix $\boldsymbol{\Phi}^{i}_{nR}$
$\boldsymbol{\Phi}^{i}_{nR}$	part of the shape matrix $\boldsymbol{\Phi}^{i}$ that is related to node n
$\boldsymbol{\Phi}^{iC}$	modal matrix that contains static correction modes of body i
$\boldsymbol{\Phi}^{ik}$	shape function matrix of element k
$\boldsymbol{\Phi}^{iP}$	modal matrix of particle P of body i
$\boldsymbol{\Phi}^{iP}_{R}$	translational modal matrix of particle P of body i
$\boldsymbol{\Phi}^{iP}_{\theta}$	rotational modal matrix of particle P of body i
$\hat{\boldsymbol{\Phi}}^{iP}$	nonorthogonal modal matrix of particle P of body i
ω	angular velocity of a harmonic load
ω^{i}_{j}	j^{th} eigenvalue of body i
$\bar{\boldsymbol{\omega}}^{i}$	angular velocity of body i
$\tilde{\bar{\boldsymbol{\omega}}}^{i}$	skew symmetric form of angular velocity vector of body i
$\boldsymbol{\Omega}^{i}$,$\boldsymbol{\Omega}^{j}$	domain in body i and j, respectively

SUBSCRIPTS

0	initial state
$0, 1, 2, 3$	1st, 2nd, 3rd and 4th variable, respectively
f	deformed state
i	index for summation
I	inertial
j and h	index of a mode or an eigenvalue
k	index of a force
l	row of a matrix
n	index of a node
p	modal coordinates
q	differentiated with respect to generalized coordinates

R	translational coordinates
θ	rotational coordinates

SUPERSCRIPTS

-1	matrix inversion
C	index for static correction mode
B	boundary degree of freedom
e	externally applied
E	index of Euler parameters
i	index of body i
I	interior degree of freedom
k	index of element k
N	index for normal mode
o	otrhogonalized matrix
P	index of particle P
T	transpose of vector or matrix
v	velocity

SYMBOLS ON TOP OF A SYMBOL

$\bar{}$	symbol is defined in local coordinate frame
$\dot{}$	first derivative with respect to time
$\ddot{}$	second derivative with respect to time
$\hat{}$	symbol is nonorthogonal
$\tilde{}$	vector is in skew symmetric form

ABBREVIATIONS

CPU	Central Processing Unit
DAE	Differential Algebraic Equation
DOF	Degrees Of Freedom
EPFM	Elasto-Plastic Fracture Mechanics
FEM	Finite Element Method
LEFM	Linear-Elastic Fracture Mechanics
MBS	Multibody System
NM	Notch Method
ODE	Ordinary Differential Equation

CHAPTER 1

Introduction

Multibody dynamic simulation represents a remarkable improvement in predicting machine performance compared to previous methods, which are often based on analytic equations or empirical testing. With the development of more computationally powerful computers over recent decades, multibody dynamic simulation has increasingly become a standard tool for comprehensive machine design. Furthermore, this continuously increasing computational power, combined with the availability of increasingly advanced codes, offers more and more possibilities for analyzing complex structures with the multibody dynamic simulation.

With a simulation model, it is both fast and advantageous to study the effects of design variables on the dynamic behavior of a machine. Without the help of computer-aided design tools, design feedback is not available until the first prototype is built. Computer simulation can replace some physical prototyping, and consequently, accelerate the product development cycle. Simulation makes it possible to study an event without risking injury to personnel or damage to the physical prototype. Vehicle stability and crash testing is an example of potentially hazardous testing. Simulation can also be used, for example, in accident investigations to reconstruct specific scenarios. Finally, simulation is necessary in cases where experimentation is impractical or impossible, such as in the performance testing of outer space structures.

To assess the performance of a machine using computerized methods, the system dynamics must be solved. A number of studies on how to solve the dynamics of a machine can be found in the literature. Generally, these studies can be categorized into two different fields of research. In the first, tailored approaches that are designed to solve the dynamics of particular machine components are employed.

Due to the tailored nature of this approach, it is difficult to use for modeling complete machines. However, tailored approaches are powerful when components such as bearings, gearings, belt rollers, and shafts are under consideration. In the second field of research, general methods for machine dynamics are developed. Among these methods are the multibody dynamic simulation approach [64] and the finite element approach [5].

Using multibody dynamic simulation to determine stresses for flexible bodies also provides an opportunity to predict the fatigue life of a structure in practical applications. Currently in engineering applications, the prediction of fatigue life for a structure is thought to be a separate stage of design due its complexity and computational burden. If fatigue life prediction is implemented efficiently in multibody codes, it could be used throughout all stages of design without dedicating discrete designing stages to it. These two scenarios about how the fatigue analysis can be related to the workflow of a design process are depicted in Figure 1.1.

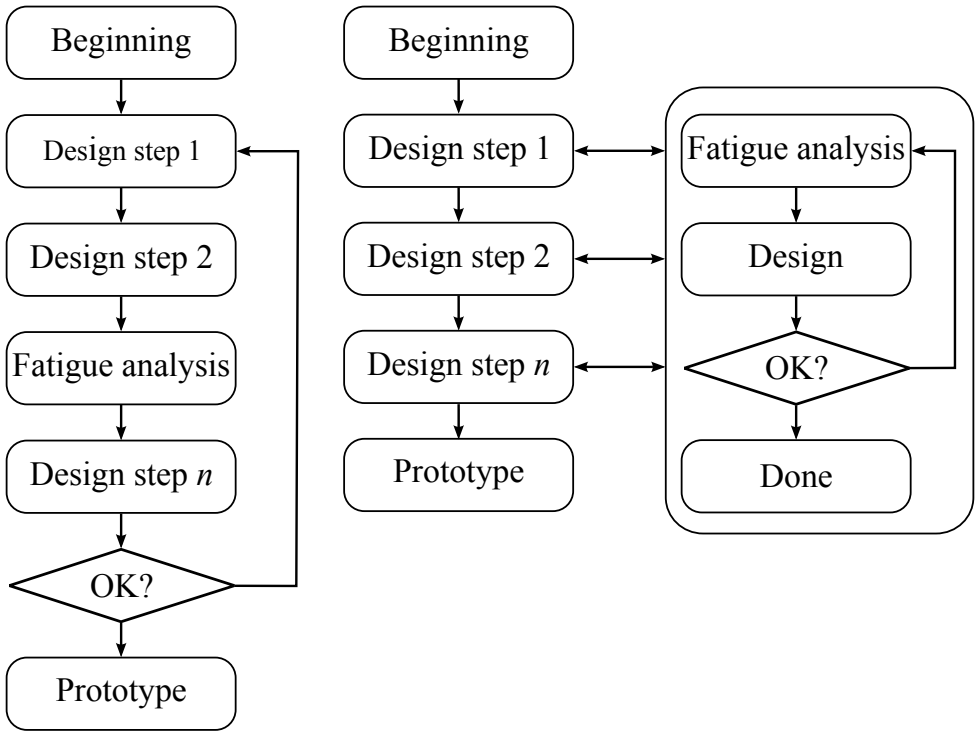

Figure 1.1. Workflow of a design process with integrated fatigue analysis

Instead of being an explicit design step, fatigue analysis can be included into the

design process (Figure 1.1 right). This makes fatigue analysis an integrated part of the design process, and from a design point of view, fatigue analysis is taken into account automatically. To perform mutual integration, efficient methods for performing fatigue analysis are required.

Dynamically loaded structures such as booms are typically manufactured by welding. By definition, fluctuating loads result in fatigue damage to a structure. Without post-weld treatment, welds are prone to fatigue [38, 27]. In dynamic analysis, structural details that do not affect the dynamic behavior of a structure are often neglected. Typically, this means that stress raisers are not analyzed in dynamic simulation even though they might be a possible location for fatigue. If treated separately, more work is required in fatigue analysis (Figure 1.1 left). In Figure 1.2, an excavator crane is depicted to illustrate the possible locations that might be vulnerable to fatigue and should be taken into consideration when predicting the fatigue life of a crane.

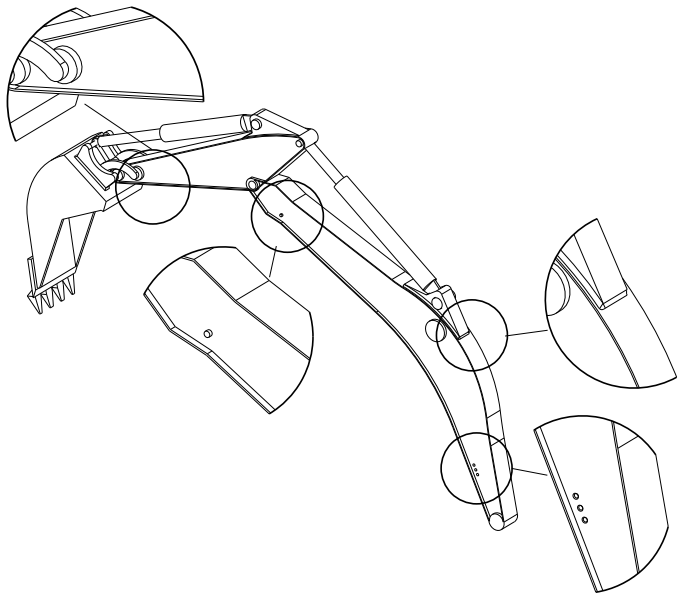

Figure 1.2. A crane with numerous discontinuities, which can be prone to fatigue

For stress history prediction, a welded structure requires particular attention. In addition, as computational power increases, there is increasing interest in predicting fatigue life for dynamically loaded structures. Even though computational capabilities have been greatly increased, the need remains for using coordinate reduction methods, especially in the case of large and complicated structures.

Multibody dynamic simulation can be used to analyze the dynamics of complex mechanical systems. It can also be used to determine dynamic loads or even stresses for further fatigue analysis. Obtaining stress data for fatigue analysis from multibody system simulation is a main component of this work.

A new strategy developed in this work combines three commonly used engineering approaches: the finite element method, the floating frame of reference formulation, and the sub-modeling approach. This strategy can be used when carrying out dynamic simulation to obtain, efficiently, the stress history of an arbitrary notch. In literature it is shown that computer simulations can be used for fault diagnosis [34]. Moreover, this stress history can further be used as initial data for the fatigue analysis; also discussed in this work. In addition to efficient stress history calculation, the proposed combined methods strategy offers other beneficial features, such as the possibility of attaching structural details to a simulation model without modifying the original simulation model. Furthermore, since structural detail does not affect the overall behavior of a simulation, the number of details can be changed arbitrary and separately.

To approximate, efficiently, the fatigue life of a structure or structural detail, some simplifying assumptions must be made. These assumptions decrease the quality of fatigue life estimation, especially in high frequency loading. For this work, a linear strain-stress relationship is assumed. In addition, presumptions have been made related to cumulative damage counting. For example, since fatigue damage can be linearly accumulated, structural failure is predicted when the entire available fatigue life is consumed. The focus here is on linear deformation, so in this work the concept of fatigue is also treated from that point of view. The strategy considers plastic deformation only local to the tip of a crack. Material nonlinearities fall outside the scope of this work. However, fatigue life estimation gives useful information when comparing alternative structures.

1.1 Flexible multibody system

For stress history prediction, a welded structure requires particular attention. In addition, as computational power increases, there is increasing interest in predicting fatigue life for dynamically loaded structures. Even though computational capabilities have been greatly increased, the need remains for using coordinate reduction methods, especially in the case of large and complicated structures. Multibody dynamic simulation is a computer-based approach to solving dynamic problems for a mechanical system. With a multibody approach, the feedback cycle from design to designer is faster than with empirical testing, and therefore,

the study of the effects of design variables is more efficient. In this work, the focus is on flexible multibody dynamics. Various formalisms for analyzing multibody systems that differ in computational burden and in purpose can be found in the literature [63, 61].

A description of body deformation is required to predict stresses and stress distributions inside a flexible body. Structural flexibility can be described by various methods, such as the linear theory of elastodynamics [77, 63] in which rigid body dynamics is first obtained, and then linear displacement is superimposed. In the lumped mass method [64] the system of interest is described using mass points that are connected to each other with massless stiffness elements. In the floating frame of reference formulation [64], structural flexibility can be described with respect to a frame of reference. The frame of reference is used to describe large displacements and rotations. The deformations of a flexible body with respect to a frame of reference can be described with a number of methods. A truly straightforward and computationally efficient way of describing deformations is the use of linear deformation modes of the body. Deformation modes can be formulated using a finite element model of the body. The floating frame of reference formulation can be applied to bodies that experience large rigid body displacements and rotations as well as elastic deformations.

Some approximations for simplicity are made in this work regarding the description of structural flexibility. Large rigid body displacements and rotations are taken into account while, however, large deformations are neglected. This means that deformations are assumed small and linear. Material properties are assumed linear. Timoshenko beam elements were used in this work, and for simplicity, beams were assumed to have uniform cross section. By using Timoshenko beam elements, shear deformation was taken into account.

1.2 Fatigue of welded structures

Fatigue is a failure that occurs after cyclic loading, and it is a common cause of structural fracture. Fatigue damage is one of the most common faults in dynamically loaded structures. In principle, the entire development of fatigue damage can be described as follows: one or more cracks form in the structure, and the cracks grow until fatigue failure takes place.

Avoiding fatigue failure is a fundamental object in the design of many dynamically loaded structures that are exposed to cyclic loading or vibrations. Many structures that are exposing fatigue loading are manufactured using welding. Cranes, vehicle

frames, and machines are just some examples of welded structures that are dynamically loaded. As a structural detail, a weld is initially prone to fatigue due to the notch effect, high tensile residual stresses, and welding flaws. High-strength steels, which are seeing increasing use, are even more sensitive to this phenomenon. In general, high strength steels are chosen to achieve larger payloads with more slender structural elements. As a trade off, the slender structures are subject to increased nominal stresses and welds became more prone to fatigue due to the higher stresses. Typically, structural welds are at or near areas of structural discontinuity. The weld itself is a structural discontinuity. Furthermore, welding processes typically introduce flaws in the weld or weld toe such as undercuts, the inclusion of impurities, and cold laps. These flaws are sources of incipient cracking.

Without post-weld treatments, the existence of incipient cracks can be assumed [38]. Therefore, the fatigue life of a weld is determined mainly by crack propagation. The fatigue life of a welded structure can be improved by designing for lower stress levels, moving the welds from structurally critical locations, or using post-weld treatments. Reducing nominal stress levels or moving welds into less critical areas are elements of the design process. Modifying local geometry lowers the stress raiser effect and may remove or diminish open cracks, so that fatigue life becomes dominated by crack initiation. Post-weld treatments should be considered if the other solutions cannot be fulfilled by design. Post-weld treatments can be divided into two main categories: methods that alter residual stress distribution and methods that modify weld geometry. Many treatment methods affect both categories. Residual stresses can be eliminated or even made compressive to gain more fatigue resistance [27]. Post-melting procedures aim at closing or diminishing already initiated cracks.

The fatigue life of a structure under dynamic load can be estimated by assuming it to have some initial amount of fatigue endurance and then assuming that one load cycle will result in fatigue damage of some amount. This idea is commonly known as Palmgren-Miner's rule, and it was first published in 1924 by Palmgren [48] for ball bearings. In 1945, Miner made it more general [43]. It was suggested that fatigue damage could be accumulated linearly for a certain amplitude value. Finally, when all fatigue endurance has been depleted, failure is expected. A large amount of fatigue test data can be found in the literature, and stress histories can be obtained experiments or by simulation.

In this work, Palmgren-Miner's rule is assumed valid and changes in geometry due to crack propagation are neglected since crack size is assumed small compared to the overall structural size.

1.3 Sub-modeling

Sub-modeling is an approach that is used together with the finite element method to combine two different finite element meshes. There are several reasons the sub-modeling approach is powerful. It can be used to connect or attach finite element models into a larger assembly. The approach does not require meshes to be similar and even element types can differ. Currently available methods do not require any coincident nodes. These beneficial features can be utilized to combine separately constructed models or refine the element mesh in a certain area without taking care of refining the mesh smoothly. In addition, a sub-model can be changed easily without modifying other parts of the model. Problems arise if the level of refinement differs significantly between two different models. A coarse mesh tends to be too stiff and displacements are underestimated, and if those underestimated displacements are used as boundary conditions for the refined model, calculated stress levels will be non-conservative.

Sub-modeling is traditionally used to attach dissimilar meshes together. For instance, local refinement without sub- modeling requires matching meshes. In addition, a sub-model can be attached on top of another model or it can replace some parts of it. A sub-model can make the overall structure stiffer, or it can only carry boundary conditions without affecting the stiffness of a large-scale structure. Traditionally, sub-modeling was clearly distinguished from substructuring, but nowadays the distinction is not that clear, since methods for connecting dissimilar meshes have been improved. From a philosophical point of view, the difference between substructuring and sub-modeling is that in sub-modeling, one model is hosting another, and the hosted model does not affect the overall behavior of the hosting model. In substructuring, the original model is divided into separate components to reduce the demand for limited computational resources.

Sub-models describe structural details, and only those that are interesting from a design point of view can be attached to a flexible multibody model. Connections between a multibody model and its sub-models are one-directional, guaranteeing that the multibody simulation is not affected by the sub-model. For instance, if a flexible multibody model is a part of a real-time simulation, it will be a real-time simulation even if sub-models are active. In this work, one way of attaching sub-models to the larger multibody model is introduced, but the concept is general.

1.4 Stress in multibody system

Rigid body multibody dynamics is dedicated to motion analysis. In rigid multibody dynamics, the stresses caused by dynamic loading cannot be obtained efficiently, because in rigid body dynamics body deformation does not occur and stresses have to be determined using constraint forces. Flexible multibody dynamics simulation results can be used as initial condition data for fatigue analysis.

Stress recovery methods for a flexible multibody system can be divided into two main categories. One is the stress-mode-based method, which determines the body's stress state using a linear combination of stress modes and elastic coordinates. The other is the finite element post-processing method, in which stresses are calculated by a finite-element code, and multibody simulation data is used as to define the initial condition. Both approaches have benefits, but in general, the method based on finite-element post-processing is more accurate, althought computationally heavier.

The literature provides a number of alternative approaches to determining stress histories from multibody simulation. The first to combine the multibody dynamic approach and stress calculation was Melzer [41]. Yim *et al.* [80] obtained dynamic stress histories by using constraint forces solved in a multibody system. Dietz *et al.* [18] described an approach for using multibody simulation to obtain all forces and torques for finite element analysis. They also selected the most severe time steps for which stresses of the complete structure were later analyzed in finite element code. Later, Dietz *et al.* [19] combined multibody dynamic simulation and fatigue life prediction. They obtained the load history from multibody simulation and calculated stress histories for selected locations using a stress load matrix. Stress histories were analyzed in a post-processing stage to predict fatigue life. Dietz [17] presented a systematic way of combining multibody dynamic simulation and fatigue analysis using stress component modes. Claus [11] generalizes the deformation-based stress recovery approach to multipurpose finite element codes. More recently, Jun *et al.* [31] used the modal stress recovery approach to obtain stress for fatigue analysis. They also discussed the reliability of fatigue life calculation. Lee *et al.* [36] studied the fatigue life for various parts of a guideway vehicle by coupling multibody dynamics and fatigue analysis. They determined stresses using the modal stress method or quasi-static force method depending on the loading conditions of the part. Braccesi and Cianetti [7] used a modal approach to recover stresses. Arczewski and Frączek [4] compared and discussed differences between force-based and deformation-based

stress recovery methods in multibody system (MBS). More recently, Tobias and Eberhard [71] obtained stresses using a reduced MBS model and stress modes. They concluded the stress state in any particular point of a flexible body could be expressed as a linear combination of global shape functions for stresses and nodal coordinates. In experiments, fatigue life prediction is mainly related to uniaxial cyclic loading. This leads to discussion about damage hypothesis, and the question arises about which damage hypothesis should be used. This work focuses on welded structures, which can be studied under the assumption of cumulative damage counting. Welded structures without any post-weld treatments have large tensile residual stresses, even nominally as large as the yield strength of the material. In this case, initial compressive loading closes an incipient crack and residual stresses open it again. This leads to a situation in which even a fully compressive loading cycle will result in full fatigue damage. This means the von Mises damage hypothesis cannot be selected as the only criteria. In this work, linear hot spot extrapolation [54] is selected, for both simplicity and robustness in use, even though, it may underestimate the effect of shear stress, which might be significant in, *e.g.*, the case of booms under torsion load.

1.5 Objectives and outline of the dissertation

The simulated user input in an off-line simulation is usually modeled as a simple function. It is also recognized in industry that machine lifetime depends heavily on the habits of the user. One method for overcoming the problem of defining proper user input is to use a real operator as the source of input. To accomplish this, real-time simulation is needed. Although the cost of computational power today is low (and becoming lower), it is still too expensive to run non-optimized or reduced models. So reducing model size is still one of the key issues in the simulation world. There are many techniques mentioned in the literature [55] to reduce model size without significantly losing accuracy. The floating frame of reference formulation is discussed and used in this work.

With multibody dynamic simulation, a large amount of raw data can be derived for fatigue analysis. In addition, measurements can produce a large amount of data, which needs to be processed before it can be used further. The processing of measured or derived data begins by employing classifications familiar from the fatigue analyses of mechanical parts [45]. With the help of classifications, characteristic features such as stress cycles can be identified. Hence, typical stress cycles can be extracted from the measured data. Rainflow counting approaches [22] are examined in this study. In addition, reliability and the

required confidence limits of cycle counting procedures are studied. A key in this study is the reliability of each step, so particular attention is given to this issue.

Because dynamic simulation demands so much computational power, real-time models can accurately describe only the general state of a complex machine. In real-time simulation, small details are not modeled. However, fatigue damage often occurs in the small details, for instance in a notch or groove [22]. In this study, method for taking into account small details and their contribution to fatigue damage during multibody dynamic simulation is presented.

Computational approaches also are developed in this work, as is the knowledge of the modeling of simulated stress histories. Specifically, the study strives to define a general procedure that can be used to obtain a simulated stress history for the simulation model of any machine. This important development makes it possible to use simulation extensively in the machine design process. Consequently, the traditional trial-and-error of physical prototype testing and evaluation can be reduced. Accordingly, product development time and the associated costs can be dramatically reduced. Multibody dynamics and fatigue life prediction are coupled here with sub-modeling and the stress recovery method. The approach is a combination of widely used formulations, and this thesis examines their theoretical background. Crane structures are the focus. In this work, all numerical examples are applied to the analysis of cranes.

As its main objective, this work explores a general method for determining the stress histories of flexible bodies using multibody dynamic simulation. This goal is achieved by coupling the finite element method, multibody dynamics, the floating frame of reference formulation [64], the Craig-Bampton method [15, 14], and the sub-modeling approach. In the literature several approaches for recovering stresses in multibody dynamic analysis can be found, they are briefly discussed. In this work, the focus was to recover stresses in large and complex structures that are dynamically loaded. Structures can contain hundreds of details prone to fatigue. The main idea was to produce reduced and simplified model for flexible multibody simulation and then attach sub-models. A sub-model takes nodal displacements as inputs and treats them as displacement boundary conditions. After the boundary conditions are analyzed, the sequence and stress history for a detail is obtained, and it is ready for cumulative fatigue damage counting. A method is introduced along with numerical examples.

This study is divided into five sections, the first being the introduction chapter. The second section presents methods used in this study. That section is divided into four chapters in a way that one method is discussed on it's own chapter. In third section, numerical examples are introduced and results are briefly discussed.

Finally, the fourth section covers the analysis work based on the introduced approach and summarizes the work done.

1.6 Contribution of the dissertation

On this thesis, the objective was to combine dynamic simulation and fatigue life prediction. This thesis proposes a novel approach to multibody dynamic simulation for producing stress histories for selected details. A particular focus is to develop a practical and computationally effective implementation to obtain stress histories. Consequently, assumptions are made from a practical engineering point of view. A commercial finite element code (ANSYS[1] 11.0 for Linux) and the computational environment (MATLAB[2] 7.9 for Linux) were the tools selected for the for the multibody simulation implementation.

The main scientific contribution of the thesis is to introduce a general approach for combining dynamic simulation and fatigue life prediction. The introduced approach assumes simulation to be independent from life prediction. Fatigue analysis and simulation are combined using sub-modeling approach. Stresses are determined by analyzing sub-models using the finite element models with simulated displacement history data as input. Cranes were the subject of the numerical examples presented in the thesis. To complete the stress histories, linear hot spot surface extrapolation was included as a measured stress [57].

[1]Website of Ansys software: http://www.ansys.com/Products/
[2]Website of Matlab software: http://www.mathworks.com/products/matlab/

CHAPTER 2

Description of structural flexibility in multibody dynamics

Multibody dynamic simulation, which is based on system kinematics, is capable of solving for static and dynamic equilibrium. This approach is general and can be applied to a wide variety of engineering problems. The term flexible multibody dynamic simulation refers to the analysis of the dynamics of a system that contains more than one body and at least one of the bodies is not rigid, *i.e.*, deformable. A multibody system is as a collection of bodies that interact with each other through joints that kinematically limit relative motion [28]. The system can also contain force components other than constraint forces, such as external forces and volume forces, *e.g.*, the force of gravity. The bodies and forces together form a system that has behavior, topology, and function. Often, the bodies are assumed rigid, and this assumption can be accurate enough for many engineering applications. In some cases, however, body flexibility should be taken into account to improve the accuracy of the system's predicted behavior. There are various methods to model flexibility [74].

Simple and computationally efficient approaches can be used if deformations are small and elastic material models are used, *i.e.*, the stress-strain relation is linear. With increased computational burden as the trade off, there are also formulations that can describe nonlinear displacement-strain relations with nonlinear material models [23]. Assuming linear flexibility is typically appropriate for the simulation of fatigue failures. To produce a stress distribution useful for fatigue analysis, at a minimum, a linear description of structural flexibility is needed; and available description methods include the linear theory of elastodynamics [77, 64], the lumped mass method [64], and the floating frame of reference formulation.

2.1 The floating frame of reference formulation

The floating frame of reference formulation is typically applicable to systems with large displacements and rotations and small deformations, even though the method can be used for large deformation problems [73]. The method is based on describing the deformations of a flexible body with respect to a frame of reference. With the frame of reference, large displacements and rotations can be described. The deformations of a flexible body in relation to its frame of reference can be described with a number of methods, but in the present study, deformation can be depicted with orthonormalized Craig-Bampton modes [15]. In it, eigenmodes are used together with static modes to describe structural deformation. The modes can be obtained using a finite element method.

The formulation separates the deformation of the body from the reference motion. The dynamics of the body can be generated using reference motion that is superposed by the deformation of the body. The interaction between the reference motion and deformation is accounted for with a mass matrix and quadratic velocity vector. This permits even mass distribution and inertia modeling [64].

Figure 2.1 illustrates the position of particle P^i within a flexible body i. In the deformed state, the position of the particle in the local reference frame of the body can be determined by vector $\bar{\boldsymbol{u}}_0^{iP}$.

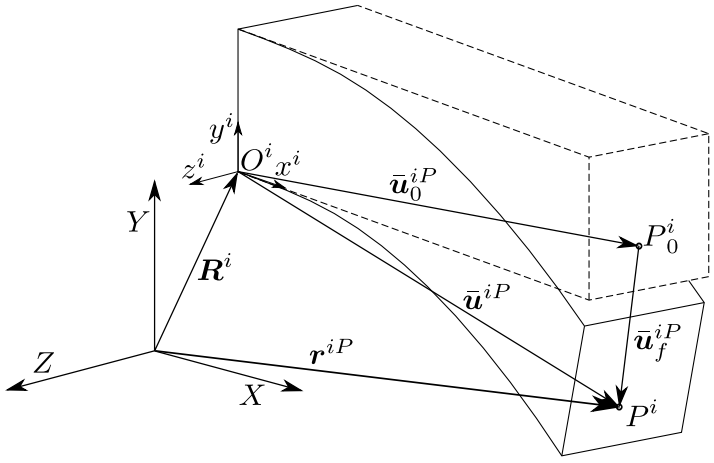

Figure 2.1. Position of particle P^i in a flexible body

As body i is deformed (Figure 2.1), the position of particle P^i changes according to the vector $\bar{\boldsymbol{u}}_f^{iP}$. The global reference frame is represented (Figure 2.1) using

Cartesian coordinates X, Y, and Z. Respectively, the local reference frame of body i consists of coordinates x^i, y^i, and z^i. Therefore, the location of the particle in a global reference frame can be defined with the vector $\boldsymbol{r}^{iP}$ as follows.

$$\boldsymbol{r}^{iP} = \boldsymbol{R}^i + \mathbf{A}^i \left(\bar{\boldsymbol{u}}_0^{iP} + \bar{\boldsymbol{u}}_f^{iP} \right), \tag{2.1}$$

where $\boldsymbol{R}^i$ is translation of the local reference coordinate system of body i in the global coordinate system, and matrix $\mathbf{A}^i$ is the rotation matrix, which is expressed here in terms of four Euler parameters.

In Equation 2.1, $\bar{\boldsymbol{u}}_0^{iP}$ is the position vector of particle P^i in the local reference coordinate system for the undeformed configuration, and $\bar{\boldsymbol{u}}_f^{iP}$ is the displacement vector in the local reference coordinate system for the deformed configuration. The behavior of the vector $\bar{\boldsymbol{u}}_f^{iP}$ can be described with a series of parallel differential equations. By separating the variables, if possible, the equation results in an infinite series that describes the deformations. For computational reasons, the infinite series cannot be applied to the analysis of flexible bodies. In practical application, the vector $\bar{\boldsymbol{u}}_f^{iP}$ is described using the finite element method.

The rotation matrix $\mathbf{A}^i$ using Euler parameters can be formulated as follows.

$$\mathbf{A}^i = 2 \begin{bmatrix} \frac{1}{2} - \left(\theta_2^{iE}\right)^2 - \left(\theta_3^{iE}\right)^2 & \theta_1^{iE}\theta_2^{iE} - \theta_0^{iE}\theta_3^{iE} & \theta_1^{iE}\theta_3^{iE} + \theta_0^{iE}\theta_2^{iE} \\ \theta_1^{iE}\theta_2^{iE} + \theta_0^{iE}\theta_3^{iE} & \frac{1}{2} - \left(\theta_1^{iE}\right)^2 - \left(\theta_3^{iE}\right)^2 & \theta_2^{iE}\theta_3^{iE} - \theta_0^{iE}\theta_1^{iE} \\ \theta_1^{iE}\theta_3^{iE} - \theta_0^{iE}\theta_2^{iE} & \theta_2^{iE}\theta_3^{iE} + \theta_0^{iE}\theta_1^{iE} & \frac{1}{2} - \left(\theta_1^{iE}\right)^2 - \left(\theta_2^{iE}\right)^2 \end{bmatrix}, \tag{2.2}$$

where θ_0^{iE}, θ_1^{iE}, θ_2^{iE}, and θ_3^{iE} are Euler parameters, which can be defined in vector form as.

$$\boldsymbol{\theta}^{iE} = \begin{bmatrix} \theta_0^{iE} & \theta_1^{iE} & \theta_2^{iE} & \theta_3^{iE} \end{bmatrix}^{\mathrm{T}} \tag{2.3}$$

Euler parameters are used, in this study, to avoid singular conditions, which can occur when Euler or Bryant angles are used [47]. The following mathematical constraint must be taken into consideration when Euler parameters are applied.

$$\left(\theta_0^{iE}\right)^2 + \left(\theta_1^{iE}\right)^2 + \left(\theta_2^{iE}\right)^2 + \left(\theta_3^{iE}\right)^2 = 1 \tag{2.4}$$

The first time derivative of the Euler parameters $\dot{\boldsymbol{\theta}}^{iE}$ and the angular velocity vector $\bar{\boldsymbol{\omega}}^i$ has the following linear connection.

$$\bar{\boldsymbol{\omega}}^i = \bar{\mathbf{G}}^{i^{\mathrm{T}}} \dot{\boldsymbol{\theta}}^{iE} \tag{2.5}$$

Local velocity transformation matrix $\bar{\mathbf{G}}^i$ depends on the selected generalized coordinates. Using Euler parameters, the matrix $\bar{\mathbf{G}}^i$ can be expressed as

$$\bar{\mathbf{G}}^i = \begin{bmatrix} -\theta_1^{iE} & \theta_0^{iE} & \theta_3^{iE} & -\theta_2^{iE} \\ -\theta_2^{iE} & -\theta_3^{iE} & \theta_0^{iE} & \theta_1^{iE} \\ -\theta_3^{iE} & \theta_2^{iE} & -\theta_1^{iE} & \theta_0^{iE} \end{bmatrix} \tag{2.6}$$

2.2 Modal reduction in the floating frame of reference formulation

The finite element model often consists of a large number of nodal degrees of freedom, and the use of large finite element models to describe flexibility may be computationally inefficient. For this reason, the floating frame of reference formulation is often used together with a modal reduction method in which the deformation is described with structural modes. Modes may be the presumed forms of deformation, but most often, they are eigenmodes of structural vibrations. The eigenmodes can be obtained from a finite element model of the structure. By employing a component mode synthesis, the displacement vector $\bar{\boldsymbol{u}}_f^{iP}$ can be expressed in modal coordinates with a modal matrix.

$$\bar{\boldsymbol{u}}_f^{iP} = \boldsymbol{\Phi}_R^{iP}\, \boldsymbol{p}^i, \tag{2.7}$$

where $\boldsymbol{\Phi}_R^{iP}$ is the modal matrix whose columns describe the translation of particle P^i within the assumed deformation modes of the flexible body i [64], and $\boldsymbol{p}^i$ is a vector of modal coordinates.

Modal reduction can be performed by selecting only limited number of component modes. Equation 2.7 can be approximated with an n_p number of modal coordinates, thus the displacement vector $\bar{\boldsymbol{u}}_f^{iP}$ for a particle P^i can be written as follows.

$$\bar{\boldsymbol{u}}_f^{iP} \approx \sum_{j=1}^{n_p} \boldsymbol{\varphi}_{Rj}^i p_j^i = \boldsymbol{\Phi}_R^{iP} \boldsymbol{p}^i, \tag{2.8}$$

where p_j^i is one modal coordinate in the modal coordinate vector that corresponds to the j^{th} modal shape. In general, the complete modal matrix $\boldsymbol{\Phi}^{iP}$ for body i

obtained from the finite element method contains the location translation and orientation of particle P^i. In multibody dynamics, the modal matrix should separate translation and orientation descriptions into their own components. Accordingly, the modal matrix can be divided into two components as follows.

$$\boldsymbol{\Phi}^{iP} = \begin{bmatrix} \boldsymbol{\Phi}_R^{iP} \\ \boldsymbol{\Phi}_\theta^{iP} \end{bmatrix}, \tag{2.9}$$

where $\boldsymbol{\Phi}_R^{iP} = (\boldsymbol{\varphi}_{R1}^{iP} \dots \boldsymbol{\varphi}_{Rn_p}^{iP})$ is the modal matrix that describes the translation of particle P^i, and $\boldsymbol{\Phi}_\theta^{iP} = (\boldsymbol{\varphi}_{\theta 1}^{iP} \dots \boldsymbol{\varphi}_{\theta n_p}^{iP})$ is the modal matrix that describes the location orientation of particle P^i. In the three-dimensional case, the dimensions of both matrices $\boldsymbol{\Phi}_R^{iP}$ and $\boldsymbol{\Phi}_\theta^{iP}$ are $3 \times n_p$, where n_p is the number of modal shapes. In practice, the orthogonal modal matrix can be formulated using the Craig-Bampton method [15]. The local displacement vector $\bar{\boldsymbol{u}}_f^{iP}$ in Equation 2.7 can be approximated using a reduced amount of modes.

Using the model reduction method, the position of an arbitrary particle P^i in the global coordinate system can be expressed as.

$$\boldsymbol{r}^{iP} = \boldsymbol{R}^i + \mathbf{A}^i \left(\bar{\boldsymbol{u}}_0^{iP} + \boldsymbol{\Phi}_R^{iP} \boldsymbol{p}^i \right) \tag{2.10}$$

Equation 2.10 is determined using a collection of modes, not a continuous system. The vector $\bar{\boldsymbol{u}}_0^{iP}$ and the modal matrix $\boldsymbol{\Phi}_R^{iP}$ are constant with time. Consequently, they only need to be calculated once, at the beginning of the simulation. The vector of generalized coordinates of the flexible body i can be written as follows.

$$\boldsymbol{q}^i = \begin{bmatrix} \boldsymbol{R}^{i\mathrm{T}} & \boldsymbol{\theta}^{iE\mathrm{T}} & \boldsymbol{p}^{i\mathrm{T}} \end{bmatrix} \tag{2.11}$$

The vector of generalized velocity coordinates of the flexible body i can be written as follows.

$$\dot{\boldsymbol{q}}^i = \begin{bmatrix} \dot{\boldsymbol{R}}^{i\mathrm{T}} & \dot{\boldsymbol{\theta}}^{iE\mathrm{T}} & \dot{\boldsymbol{p}}^{i\mathrm{T}} \end{bmatrix} \tag{2.12}$$

The velocity of particle P^i can be determined by differentiating Equation 2.1 with respect to time as follows.

$$\dot{\boldsymbol{r}}^{iP} = \begin{bmatrix} \mathbf{I} & -\mathbf{A}^i \tilde{\bar{\boldsymbol{u}}}_f^{iP} \bar{\mathbf{G}}^i & \mathbf{A}^i \boldsymbol{\Phi}_R^{iP} \end{bmatrix} \begin{bmatrix} \dot{\boldsymbol{R}}^i \\ \dot{\boldsymbol{\theta}}^{iE} \\ \dot{\boldsymbol{p}}^i \end{bmatrix}, \tag{2.13}$$

where $\mathbf{I}$ is (3x3) identity matrix. The ~ symbol above a variable indicates the skew-symmetric form. Note the vector, in the right hand of Equation 2.13, describes the velocity of the generalized coordinates of a flexible body i. Differentiating the velocity of a particle Equation 2.13 with respect to time, the acceleration of a particle can be written in this manner.

$$\begin{aligned}\ddot{\boldsymbol{r}}^{iP} = &\begin{bmatrix}\mathbf{I} & -\mathbf{A}^i\tilde{\bar{\boldsymbol{u}}}^{iP}\bar{\mathbf{G}}^i & \mathbf{A}^i\boldsymbol{\Phi}_R^{iP}\boldsymbol{R}^{iP}\end{bmatrix}\begin{bmatrix}\ddot{\boldsymbol{R}}^i\\ \ddot{\boldsymbol{\theta}}^{iE}\\ \ddot{\boldsymbol{p}}^i\end{bmatrix}\\ &+\begin{bmatrix}\mathbf{0} & -\mathbf{A}^i\tilde{\bar{\boldsymbol{\omega}}}^i\tilde{\bar{\boldsymbol{u}}}^{iP}\bar{\mathbf{G}}^i & 2\mathbf{A}^i\tilde{\bar{\boldsymbol{\omega}}}^i\boldsymbol{\Phi}_R^{iP}\end{bmatrix}\begin{bmatrix}\dot{\boldsymbol{R}}^i\\ \dot{\boldsymbol{\theta}}^{iE}\\ \dot{\boldsymbol{p}}^i\end{bmatrix},\end{aligned} \tag{2.14}$$

where $\ddot{\boldsymbol{R}}^i$, $\ddot{\boldsymbol{\theta}}^{iE}$, and $\ddot{\boldsymbol{p}}^i$ are accelerations of translational coordinates, Euler parameters, and modal coordinates of body i.

The orthogonal shape matrix can be formulated from the eigenmodes of the body. Typically, the shape superposition technique yields acceptably accurate results even though only a few differential equations are applied.

Rotations due to body deformation do not have any direct use in the floating frame of reference formulation, and therefore they are usually ignored. However, rotation modes can be used in the description of constraint equations applied to rotational degrees of freedom [33]. Rotational modes are used here to connect sub-models to large-scale models. With the rotational modal matrix $\boldsymbol{\Phi}_\theta^{iP}$, the rotation change $\boldsymbol{\varepsilon}_f^{iP}$ resulting from deformation can be approximated as follows.

$$\boldsymbol{\varepsilon}_f^{iP} \approx \sum_{j=1}^{n_p}\boldsymbol{\varphi}_{\theta j}^i p_j^i = \boldsymbol{\Phi}_\theta^{iP}\boldsymbol{p}^i, \tag{2.15}$$

where p_j^i is j^{th} modal coordinate of body i. A rotation matrix $\mathbf{A}_f^{iP}$ that describes orientation due to deformation at the location of particle P^i with respect to the reference frame can be composed like this.

$$\mathbf{A}_f^{iP} = \mathbf{I} + \tilde{\boldsymbol{\varepsilon}}_f^{iP}, \tag{2.16}$$

whre $\mathbf{I}$ is (3x3) identity matrix. The orientation at the location of particle P^i within the frame of reference can be expressed as follows.

$$\bar{\boldsymbol{v}}_f^{iP} = \mathbf{A}_f^{iP} \bar{\boldsymbol{v}}_0^{iP}, \tag{2.17}$$

where $\bar{\boldsymbol{v}}_0^{iP}$ is the orientation of the location of particle P^i in the undeformed state.

2.3 Craig-Bampton method

Even though the shape matrix $\boldsymbol{\Phi}^i$ can be obtained using element shape functions [64], in most engineering cases, structures can be large and complex and can contain a large number of nodal variables. Furthermore, dynamic analysis based completely on a finite element model will be computationally inefficient, due to the large number of degrees of freedom. Component mode synthesis is one of the most efficient methods developed to reduce the number of coordinates. In component mode synthesis, eigenmodes are usually obtained from an eigenmode analysis performed on the finite element model. The eigenmodes and related frequencies can be obtained by solving the eigenvalue problem in this manner.

$$\left[\mathbf{K}^i - \left(\omega_j^i\right)^2 \mathbf{M}^i\right] \boldsymbol{\varphi}_j^i = 0, \tag{2.18}$$

where $\mathbf{K}^i$ and $\mathbf{M}^i$ are the stiffness and mass matrices of the body i, and ω_j^i is the j^{th} eigenvalue of the body i and $\boldsymbol{\varphi}_j^i$ j^{th} eigenvector.

Following eigenmode analysis, the shape matrix contains as many degrees of freedom as the original finite element model. Model reduction can be accomplished by neglecting some modes. Because neglecting modes leads to a trade off between accuracy and computational efficiency, a general rule regarding which modes should be selected cannot be made. Some guidelines can be found in the literature [1, 78]. In practice, an efficient way to select the modes is to perform a test simulation and select those modes that describe the largest proportion of deformation energy. In general, approximately 95 percent of the deformation energy can be described by accounting for 5 percent of the modes. For engineering applications, the energy-based method results in an appropriate selection of modes.

Eigenmode analysis can be applied to constrained or unconstrained structures. The unconstrained case is more general, but its description of local deformations caused by constraint forces can be inaccurate and a significantly large number of modes are needed. To overcome this problem, static correction modes can be used. The concept of static correction modes was introduced in the Craig-Bampton method [15], in which the structure is divided into its interior and its boundary

degrees of freedom. In the divided form, the stiffness and mass matrices of the structure can be expressed as follows.

$$\mathbf{K}^i = \begin{bmatrix} \mathbf{K}^{iBB} & \mathbf{K}^{iBI} \\ \mathbf{K}^{iIB} & \mathbf{K}^{iII} \end{bmatrix} \tag{2.19}$$

$$\mathbf{M}^i = \begin{bmatrix} \mathbf{M}^{iBB} & \mathbf{0} \\ \mathbf{0} & \mathbf{M}^{iII} \end{bmatrix} \tag{2.20}$$

The superscripts B and I signify boundary and interior, respectively. In the first stage, the boundary degrees of freedom are treated as fixed, and therefore the eigenmode analysis is carried out by solving the following.

$$\left[\mathbf{K}^{iII} - \left(\omega_j^{iN}\right)^2 \mathbf{M}^{iII} \boldsymbol{\varphi}_j^{iN}\right] = 0 \tag{2.21}$$

Superscript N signifies the normal mode. Sometimes eigenmodes coming from eigenmode analysis are called normal modes to distinguish them from static correction modes. A shape matrix $\boldsymbol{\Phi}^{iN}$ that contains only normal modes can be constructed like this.

$$\boldsymbol{\Phi}^{iN} = \left[\boldsymbol{\varphi}_1^{iN}, \boldsymbol{\varphi}_2^{iN}, \ldots, \boldsymbol{\varphi}_j^{iN}\right] = 0 \tag{2.22}$$

Static correction modes, which are sometimes referred as constraint modes, are the modal shapes of the interior degrees of freedom when one boundary degree of freedom has a unit displacement and all other boundary nodes are fixed. The constrained modes can be obtained from the static force equilibrium in Equation 2.23 by setting all forces $\boldsymbol{F}^{iI}$ acting at the interior degrees of freedom to zero resulting in the following matrix equation.

$$\begin{bmatrix} \boldsymbol{F}^{iB} \\ \boldsymbol{F}^{iI} \end{bmatrix} = \begin{bmatrix} \mathbf{K}^{iBB} & \mathbf{K}^{iBI} \\ \mathbf{K}^{iIB} & \mathbf{K}^{iII} \end{bmatrix} \begin{bmatrix} \boldsymbol{\delta}^{iB} \\ \boldsymbol{\delta}^{iI} \end{bmatrix} \tag{2.23}$$

$\boldsymbol{\delta}^{iI}$ and $\boldsymbol{\delta}^{iB}$ are the physical displacements of the interior and boundary nodes, respectively.

$$\boldsymbol{\delta}^{iI} = -\left(\mathbf{K}^{iII}\right)^{-1} \mathbf{K}^{iIB} \boldsymbol{\delta}^{iB} = \boldsymbol{\Phi}^{iC} \boldsymbol{\delta}^{iB}, \tag{2.24}$$

where $\boldsymbol{\Phi}^{iC}$ is the matrix of the static correction modes.

The coordinate transformation from nodal coordinates to the nonorthogonal Craig-Bampton coordinates can be expressed as follows.

$$\bar{\boldsymbol{u}}_f^i = \begin{bmatrix} \boldsymbol{\delta}^{iB} \\ \boldsymbol{\delta}^{iI} \end{bmatrix} \simeq \begin{bmatrix} \mathbf{I} & \mathbf{0} \\ \boldsymbol{\Phi}^{iC} & \boldsymbol{\Phi}^{iN} \end{bmatrix} \begin{bmatrix} \hat{\boldsymbol{p}}^{iC} \\ \hat{\boldsymbol{p}}^{iN} \end{bmatrix} = \hat{\boldsymbol{\Phi}}^i \hat{\boldsymbol{p}}^i, \tag{2.25}$$

where the superindex C indicates static correction and N indicates normal mode. $\hat{\boldsymbol{\Phi}}^i$ is a generalized, but not orthogonal, shape matrix. The generalized stiffness and mass matrices of the structure can be obtained with these equations.

$$\hat{\mathbf{K}}^i = \hat{\boldsymbol{\Phi}}^{i\mathrm{T}} \mathbf{K}^i \hat{\boldsymbol{\Phi}}^i \tag{2.26}$$

$$\hat{\mathbf{M}}^i = \hat{\boldsymbol{\Phi}}^{i\mathrm{T}} \mathbf{M}^i \hat{\boldsymbol{\Phi}}^i \tag{2.27}$$

These generalized matrices are Craig-Bampton representations of the original system. Static correction modes are not orthogonal, and coupling between modal coordinates cannot be removed. If the modal matrix contains nonorthogonal modes, the generalized stiffness and mass matrices will contain non-zero off-diagonal terms. Nonorthogonal modes can be orthogonalized by solving the eigenvalues from the nonorthogonal Craig-Bampton representation of a structure as follows.

$$\left[\hat{\mathbf{K}}^i - \left(\omega_j^i\right)^2 \hat{\mathbf{M}}^i\right] \boldsymbol{n}_j^i = 0 \tag{2.28}$$

The orthogonal modal matrix can be defined as follows.

$$\mathbf{N}^i = \left[\boldsymbol{n}_1^i, \boldsymbol{n}_2^i, \ldots, \boldsymbol{n}_{n_{cb}}^i\right] \tag{2.29}$$

The sub index n_{cb} is the number of Craig-Bampton modes. The final modal shapes and physical degrees of freedom can be represented as follows.

$$\boldsymbol{\Phi}^i = \hat{\boldsymbol{\Phi}}^i \mathbf{N}^i \tag{2.30}$$

$$\bar{\boldsymbol{u}}_f^i \simeq \boldsymbol{\Phi}^i \boldsymbol{p}^i \tag{2.31}$$

As a result of the orthogonalization procedure, the stiffness and mass matrices become diagonal with these equations.

$$\mathbf{K}_o^i = {\mathbf{\Phi}^i}^{\mathrm{T}} \hat{\mathbf{K}}^i \mathbf{\Phi}^i = \mathrm{diag}\left(\hat{\boldsymbol{\omega}}_1^i, \hat{\boldsymbol{\omega}}_2^i, \ldots, \hat{\boldsymbol{\omega}}_{n_{cb}}^i\right) \tag{2.32}$$

$$\mathbf{M}_o^i = {\mathbf{\Phi}^i}^{\mathrm{T}} \hat{\mathbf{M}}^i \hat{\mathbf{\Phi}}^i = \mathbf{I} \tag{2.33}$$

After orthogonalization, all modes have an associated frequency in order of their frequency contribution to the dynamics system. The physical meaning of the static correction normal modes is lost. Regardless, local deformations near constraints can be described using a relative low number of modes.

2.4 Forces of a flexible body

Forces applied to a flexible body are usually not constant, but change as a function of time. In flexible multibody dynamics, forces applied to the body are rarely sequential, which means that the response of the flexible body must be analyzed with respect to time.

According to the D'Alembert principle, inertial forces can be treated as external forces, thus forces of the body i can be written as follows.

$$\boldsymbol{F}^i = \int_{V^i} \rho^i \ddot{\boldsymbol{r}}^{iP} \mathrm{d}V^i, \tag{2.34}$$

where ρ^i is density and V^i is the volume of a body i, respectively. By applying the D'Alembert principle, the virtual work done by the inertial forces can be represented as.

$$\delta W^i = \int_{V^i} \rho^i \delta {\boldsymbol{r}^{iP}}^{\mathrm{T}} \ddot{\boldsymbol{r}}^{iP} \mathrm{d}V^i \tag{2.35}$$

The virtual displacement of the position vector $\delta \boldsymbol{r}^{iP}$ can be expressed as.

$$\delta \boldsymbol{r}^{iP} = \frac{\delta \boldsymbol{r}^{iP}}{\delta \boldsymbol{q}^i} \delta \boldsymbol{q}^i = \begin{bmatrix} \mathbf{I} & -\mathbf{A}^i \tilde{\bar{\boldsymbol{u}}}^{iP} \bar{\mathbf{G}}^i & \mathbf{A}^i \mathbf{\Phi}_R^{iP} \end{bmatrix} \delta \boldsymbol{q}^i, \tag{2.36}$$

where $\bar{\boldsymbol{u}}^{iP}$ is the displacement vector in local frame of particle P^i. By substituting the virtual displacement Equation 2.36 into the equation for virtual work 2.35 and separating terms related to acceleration and quadratic velocity vector, the following equation can be obtained.

$$\delta W^i = \delta \boldsymbol{q}^i \left[\mathbf{M}^i \ddot{\boldsymbol{q}}^i + \boldsymbol{Q}^{iv} \right], \tag{2.37}$$

where $\delta \boldsymbol{q}^i$ is virtual change of the generalized coordinates, $\boldsymbol{Q}^{iv}$ is quadratic velocity vector of body i, and $\mathbf{M}^i$ is the mass matrix that can be written as follows.

$$\mathbf{M}^i = \int_{V^i} \rho^i \begin{bmatrix} \mathbf{I} & -\mathbf{A}^i \tilde{\bar{\boldsymbol{u}}}^{iP} \bar{\mathbf{G}}^i & \mathbf{A}^i \boldsymbol{\Phi}_R^{iP} \\ & -\bar{\mathbf{G}}^{i\mathrm{T}} \tilde{\bar{\boldsymbol{u}}}^{iP} \tilde{\bar{\boldsymbol{u}}}^{iP} \bar{\mathbf{G}}^i & \bar{\mathbf{G}}^{i\mathrm{T}} \tilde{\bar{\boldsymbol{u}}}^{iP} \boldsymbol{\Phi}_R^{iP} \\ \mathrm{sym} & & \boldsymbol{\Phi}_R^{iP\mathrm{T}} \boldsymbol{\Phi}_R^{iP} \end{bmatrix} \mathrm{d}V^i \tag{2.38}$$

Note that the use of Euler parameters leads to $\dot{\bar{\mathbf{G}}}^i \dot{\boldsymbol{\theta}}^{iE} = 0$. Thus, the quadratic velocity vector $\boldsymbol{Q}^{iv}$ can be presented with following matrix equation.

$$\boldsymbol{Q}^{iv} = \int_{V^i} \rho^i \begin{bmatrix} \mathbf{A}^i \tilde{\bar{\boldsymbol{\omega}}}^i \tilde{\bar{\boldsymbol{\omega}}}^i \bar{\boldsymbol{u}}^{iP} + 2\mathbf{A}^i \tilde{\bar{\boldsymbol{\omega}}}^i \boldsymbol{\Phi}_R^{iP} \dot{\boldsymbol{p}}^i \\ -\tilde{\bar{\boldsymbol{u}}}^{iP\mathrm{T}} \tilde{\bar{\boldsymbol{\omega}}}^i \tilde{\bar{\boldsymbol{\omega}}}^i \bar{\boldsymbol{u}}^{iP} \bar{\mathbf{G}}^i - 2\tilde{\bar{\boldsymbol{u}}}^{iP\mathrm{T}} \tilde{\bar{\boldsymbol{\omega}}}^i \boldsymbol{\Phi}_R^{iP} \dot{\boldsymbol{p}} \bar{\mathbf{G}}^i \\ \boldsymbol{\Phi}_R^{iP\mathrm{T}} \tilde{\bar{\boldsymbol{\omega}}}^i \tilde{\bar{\boldsymbol{\omega}}}^i \bar{\boldsymbol{u}}^{iP} + 2\boldsymbol{\Phi}_R^{iP\mathrm{T}} \tilde{\bar{\boldsymbol{\omega}}}^i \boldsymbol{\Phi}_R^{iP} \dot{\boldsymbol{p}} \end{bmatrix} \mathrm{d}V^i \tag{2.39}$$

Vector $\bar{\boldsymbol{S}}_I^i$ represents the components of the moment of mass of the body i about the axes of the local coordinate system, $\bar{\mathbf{S}}^i$ is inertia shape integral, $\bar{\boldsymbol{I}}_{\theta\theta}^i$ is the inertia tensor of the body i, and $\bar{\mathbf{I}}_{\theta p}^i$ is a matrix that connects rotations and modal coordinates. These components are defined as follows.

$$\bar{\boldsymbol{S}}_I^i = \sum_{n=1}^{n_n} m_n \bar{\boldsymbol{u}}_n^i \tag{2.40}$$

$$\bar{\mathbf{S}}^i = \sum_{n=1}^{n_n} m_n \boldsymbol{\Phi}_{nR}^i \tag{2.41}$$

$$\bar{\boldsymbol{I}}_{\theta\theta}^i = \sum_{n=1}^{n_n} m_n x_{nk}^i x_{nl}^i \quad k,l = 1,2,3 \tag{2.42}$$

$$\bar{\mathbf{I}}_{\theta p}^i = \sum_{n=1}^{n_n} m_n x_{nk}^i \boldsymbol{\Phi}_{nlR}^i \quad k,l = 1,2,3, \tag{2.43}$$

where $\bar{\boldsymbol{u}}_n^i = \begin{bmatrix} x_{n1}^i & x_{n2}^i & x_{n3}^i \end{bmatrix}$ is the position vector of the node n, m_n is the mass of the node, $\boldsymbol{\Phi}_{nlR}^i$ is the l^{th} row of shape matrix $\boldsymbol{\Phi}_{nR}^i$, and n_n is number of nodes in body i.

The virtual work of externally applied forces can be defined as.

$$\delta W^{ie} = \int_{V^i} \delta \boldsymbol{r}^{iP\mathrm{T}} \boldsymbol{F}^{iP} \mathrm{d}V^i = \delta \boldsymbol{q}^{i\mathrm{T}} \boldsymbol{Q}^{ie}, \tag{2.44}$$

where $\boldsymbol{F}^{iP}$ is externally applied force per unit volume, and $\boldsymbol{Q}^{ie}$ is the vector of generalized forces, which can be expressed as follows.

$$\boldsymbol{Q}^{ie} = \begin{bmatrix} \boldsymbol{Q}_R^{ie} \\ \boldsymbol{Q}_\theta^{ie} \\ \boldsymbol{Q}_p^{ie} \end{bmatrix}, \tag{2.45}$$

where $\boldsymbol{Q}_R^{ie}$ is translational components, $\boldsymbol{Q}_\theta^{ie}$ is rotational components, and $\boldsymbol{Q}_p^{ie}$ is elastic components of the generalized force vector, respectively. Defining generalized forces allows moving external forces and torques affecting a certain point of the body to the generalized coordinates of the body. The vector of generalized forces consists of the following components.

$$\boldsymbol{Q}_R^{ie} = \sum_{k=1}^{n_F} \boldsymbol{F}_k^i \tag{2.46}$$

$$\boldsymbol{Q}_\theta^{ie} = \sum_{k=1}^{n_F} \tilde{\tilde{\boldsymbol{u}}}_k^i \mathbf{A}^{i\mathrm{T}} \boldsymbol{F}_k^i \tag{2.47}$$

$$\boldsymbol{Q}_p^{ie} = \sum_{k=1}^{n_F} \boldsymbol{\Phi}_k^{i\mathrm{T}} \mathbf{A}^{i\mathrm{T}} \boldsymbol{F}_k^i, \tag{2.48}$$

where $\boldsymbol{F}_k^i$ is the k^{th} force acting on body i, $\tilde{\tilde{\boldsymbol{u}}}_k^i$ is the skew symmetric form of the location vector of the k^{th} force, and $\boldsymbol{\Phi}_k^i$ is the terms of the modal matrix associated with the acting node of the k^{th} force. In previous equations, n_F is the number of externally applied forces.

The elastic forces can be described using modal coordinates and the stiffness matrix in modal coordinates $\mathbf{K}^i$. The stiffness matrix in modal coordinates can be obtained using component mode synthesis. The virtual work of the elastic forces can be expressed as.

$$\delta W^{if} = \delta \boldsymbol{p}^{\mathrm{T}} \mathbf{K}^i \boldsymbol{p}^i \tag{2.49}$$

The vector of elastic forces can be represented as follows.

$$\boldsymbol{Q}^{if} = \begin{bmatrix} \mathbf{0} \\ \mathbf{0} \\ \mathbf{K}^i \boldsymbol{p}^i \end{bmatrix} \tag{2.50}$$

In Equation 2.50 stiffness matrix related to modal coordinates $\boldsymbol{p^i}$ can be computed as follows.

$$\mathbf{K}^i = {\mathbf{\Phi}^i}^{\mathrm{T}} \mathbf{K}_i^i \mathbf{\Phi}^i, \tag{2.51}$$

where $\mathbf{K}_i^i$ is the stiffness matrix of original finite element model.

2.5 Formulation of equations of motion

In multibody dynamics, different types of joints between bodies are accounted for with kinematic constraints applied on generalized coordinates. Algebraic equations are used for the description of constraints between bodies. By examining only holonomic constraints, constraint equations can be expressed as follows.

$$\boldsymbol{C}(\boldsymbol{q}) = \boldsymbol{0} \tag{2.52}$$

where, $\boldsymbol{C}$ is the constraint vector for the system. Equations of motion may be formulated using the widely known Lagrange method, in which kinematic constraints are accounted for as supplementary algebraic equations with the help of Lagrange multipliers. The method is called global formulation since it does not differentiate between open and closed kinematic chains, as topological methods do. After employing the concept of virtual work to externally applied forces and then introducing constraints with help of Lagrange multipliers, the equation of motion can be written in the form of a differential algebraic equation (DAE).

$$\mathbf{M}\ddot{\boldsymbol{q}} + \mathbf{K}\boldsymbol{q} + \mathbf{C}_{\boldsymbol{q}}^{\mathrm{T}} \boldsymbol{\lambda} = \boldsymbol{Q}^e + \boldsymbol{Q}^v - \boldsymbol{Q}^f, \tag{2.53}$$

where $\mathbf{M}$ is the mass matrix, $\mathbf{K}$ is the stiffness matrix, $\mathbf{C}_{\boldsymbol{q}}^{\mathrm{T}}$ is transpose of the constraint Jacobian matrix, $\boldsymbol{\lambda}$ is the vector of Lagrange multipliers, and $\boldsymbol{Q}^e$ is the vector of generalized forces, $\boldsymbol{Q}^v$ is the quadratic velocity vector (which includes the Coriolis and centrifugal forces that depend on the square velocity), and $\boldsymbol{Q}^f$ is the vector of elastic forces. If the origin of the frame of reference is placed at the

centre of mass of the rigid body, the translational terms of vector $\boldsymbol{Q}^v$ are zero. In the case of flexible bodies, however, a corresponding choice of reference frame does not lead to the same result because irrespective of the frame of reference, the description of mass inertias is not constant and terms in $\boldsymbol{Q}^v$ do not equal zero.

Equations 2.52 and 2.53 form a set of differential algebraic equations, which can be converted to ordinary differential equations (ODE) to solve for the dynamic response of the multibody system in the time domain. To be able to apply traditional ODE solvers to the system of equations, the constraint equations must be differentiated twice with respect to time.

$$\ddot{\boldsymbol{C}}\left(\boldsymbol{q}, \dot{\boldsymbol{q}}, \ddot{\boldsymbol{q}}\right) = \mathbf{C}_{\boldsymbol{q}}\ddot{\boldsymbol{q}} + \left(\mathbf{C}_{\boldsymbol{q}}\dot{\boldsymbol{q}}\right)_{\boldsymbol{q}}\dot{\boldsymbol{q}} = \boldsymbol{0}, \tag{2.54}$$

where $\boldsymbol{Q}^c = -\left(\mathbf{C}_{\boldsymbol{q}}\dot{\boldsymbol{q}}\right)_{\boldsymbol{q}}\dot{\boldsymbol{q}}$ is the constraint force vector for the system. As a result, the final matrix form of equations of motion describing the system dynamics looks as following.

$$\begin{bmatrix} \mathbf{M} & \mathbf{C}_{\boldsymbol{q}}^{\mathrm{T}} \\ \mathbf{C}_{\boldsymbol{q}} & \mathbf{0} \end{bmatrix} \begin{bmatrix} \ddot{\boldsymbol{q}} \\ \boldsymbol{\lambda} \end{bmatrix} = \begin{bmatrix} \boldsymbol{Q}^e + \boldsymbol{Q}^v - \boldsymbol{Q}^f \\ \boldsymbol{Q}^c \end{bmatrix}, \tag{2.55}$$

Because the constraint equations are differentiated, equation 2.55 satisfies the constraint equations only at the acceleration level. This leads to error accumulation in the kinematic constraints for long simulations. This problem can be solved by applying a constraint stabilization method, which decreases the error caused by the violation of constraint equations. Alternatively, Equations 2.52 and 2.53 may be integrated directly using integration methods that are suitable for DAE systems.

2.6 Mass invariants

Mass matrix M^i in Equation 2.38 is determined using consistent mass. In a case of discrete bodies, body mass is distributed among all nodes. This approach is called the lumped mass technique, which focuses on the nodes. Mass matrix M^i is a function of the rotational coordinates and the deformations of flexible body i.

In the lumped mass approach, the mass matrix M^i, shown in Equation 2.38, can be expressed with nine submatrices like this.

$$\mathbf{M}^i = \begin{bmatrix} \mathbf{M}^i_{RR} & \mathbf{M}^i_{R\theta} & \mathbf{M}^i_{Rp} \\ \mathbf{M}^i_{\theta R} & \mathbf{M}^i_{\theta\theta} & \mathbf{M}^i_{\theta p} \\ \mathbf{M}^i_{pR} & \mathbf{M}^i_{p\theta} & \mathbf{M}^i_{pp} \end{bmatrix} \tag{2.56}$$

Subscripts R, θ, and p refer to translational, rotational, and modal coordinates, respectively. Due to mass normalizing, $\mathbf{M}_o^i = \mathbf{M}_{pp}^i = \mathbf{I}$. Using Euler parameters, the submatrices and their dimensions (Equation 2.56) can be expressed as follows.

$$\mathbf{M}_{RR}^i = \int_{V^i} \rho^i \mathbf{I} \mathrm{d}V^i = \mathbf{I}^{i1}\mathbf{I} \tag{2.57}$$

$$\mathbf{M}_{R\theta}^i = -\int_{V^i} \rho^i \mathbf{A}^i \left(\tilde{\tilde{\boldsymbol{u}}}_0^{iP} + \tilde{\tilde{\boldsymbol{\Phi}}}_R^i \boldsymbol{p}^i\right) \bar{\mathbf{G}}^i \mathrm{d}V^i = -\mathbf{A}^i \mathbf{I}^{i2} + \sum_{j=1}^{n_p} \mathbf{I}_j^{i3} p_j^i \bar{\mathbf{G}}^i \tag{2.58}$$

$$\mathbf{M}_{Rp}^i = \int_{V^i} \rho^i \mathbf{A}^i \boldsymbol{\Phi}_R^i \mathrm{d}V^i = \mathbf{A}^i \mathbf{I}^{i3} \tag{2.59}$$

$$\begin{aligned} \mathbf{M}_{\theta\theta}^i &= \int_{V^i} \rho^i \bar{\mathbf{G}}^{i^{\mathrm{T}}} \left(\tilde{\tilde{\boldsymbol{u}}}_0^{iP} + \tilde{\tilde{\boldsymbol{\Phi}}}_R^i \boldsymbol{p}^i\right)^{\mathrm{T}} \left(\tilde{\tilde{\boldsymbol{u}}}_0^{iP} + \tilde{\tilde{\boldsymbol{\Phi}}}_R^i \boldsymbol{p}^i\right) \bar{\mathbf{G}}^i \mathrm{d}V^i \\ &= \bar{\mathbf{G}}^{i^{\mathrm{T}}} \left[\mathbf{I}^{i7} - \left[\mathbf{I}_j^{i8} + \mathbf{I}^{i8^{\mathrm{T}}}\right] p_j - \mathbf{I}_j^{i9} p_j p_k\right] \bar{\mathbf{G}}^i \end{aligned} \tag{2.60}$$

$$\mathbf{M}_{\theta p}^i = -\int_{V^i} \rho^i \bar{\mathbf{G}}^{i^{\mathrm{T}}} \left(\tilde{\tilde{\boldsymbol{u}}}_0^{iP} + \tilde{\tilde{\boldsymbol{\Phi}}}_R^i \boldsymbol{p}^i\right)^{\mathrm{T}} \boldsymbol{\Phi}_R^i \mathrm{d}V^i = \bar{\boldsymbol{G}}^{i^{\mathrm{T}}} \left[\mathbf{I}^{i4} + \mathbf{I}_j^{i5} p_j\right] \tag{2.61}$$

$$\mathbf{M}_{pp}^i = -\int_{V^i} \rho^i \boldsymbol{\Phi}_R^{i^{\mathrm{T}}} \boldsymbol{\Phi}_R^i \mathrm{d}V^i = \mathbf{I}^{i6} \tag{2.62}$$

$$\mathbf{M}_{pR}^i = \mathbf{M}_{Rp}^{i^{\mathrm{T}}} \tag{2.63}$$

$$\mathbf{M}_{\theta R}^i = \mathbf{M}_{R\theta}^{i^{\mathrm{T}}} \tag{2.64}$$

$$\mathbf{M}_{p\theta}^i = \mathbf{M}_{\theta p}^{i^{\mathrm{T}}}, \tag{2.65}$$

where n_p is the number of modal shapes.

The mass matrix has to be updated every time step, and because it contains some time independent components, they can be partitioned. These time independent components of mass matrix are called mass invariants. They can be calculated before integrating the equations of motion with respect to time. The mass invariants can be calculated as volume integrals, or for the lumped mass approach, as summations. In the lumped mass approach, rotational degrees of freedom are neglected. Mass invariants can be expressed as follows.

Total mass of a flexible body i is defined as follows.

$$\mathbf{I}^{i1} = \int_{V^i} \rho^i \mathrm{d}V^i \simeq \sum_{n=1}^{n_n} m_n, \tag{2.66}$$

where n_n is number of nodes and m_n is the mass of node n.

The first static moment is expressed in this manner.

$$\mathbf{I}^{i2} = \int_{V^i} \rho^i \bar{\boldsymbol{u}}_0^i \mathrm{d}V^i \simeq \sum_{n=1}^{n_n} m_n \bar{\boldsymbol{u}}_{0n}^i \tag{2.67}$$

The correction for the location of the centre of mass is as follows.

$$\mathbf{I}_j^{i3} = \int_{V^i} \rho^i \boldsymbol{\varphi}_{Rj}^i \mathrm{d}V^i \simeq \sum_{n=1}^{n_n} \sum_{j=1}^{n_p} m_n \varphi_{Rnj}^i, \tag{2.68}$$

where n_p is the number of modes.

The first order correction for cross coupling between the deformations and the rotations is given in this manner.

$$\mathbf{I}^{i4} = \int_{V^i} \rho^i \tilde{\bar{\boldsymbol{u}}}_0^i \boldsymbol{\Phi}_R^i \mathrm{d}V^i \simeq \sum_{n=1}^{n_n} m_n \tilde{\bar{\boldsymbol{u}}}_{0n}^i \boldsymbol{\Phi}_{Rn}^i \tag{2.69}$$

The second order correction for cross coupling between the deformations and the rotations consists of n_p number of (3 x 3) matrices that can be calculated as follows.

$$\mathbf{I}_j^{i5} = \int_{V^i} \tilde{\boldsymbol{\varphi}}_{Rj}^i \boldsymbol{\Phi}_R^i \rho^i \mathrm{d}V^i \simeq \sum_{n=1}^{n_n} \sum_{j=1}^{n_p} m_n \varphi_{Rnj}^i \boldsymbol{\Phi}_{Rn}^i \tag{2.70}$$

Modal mass for a flexible body looks like this.

$$\mathbf{I}^{i6} = \int_{V^i} \rho^i \boldsymbol{\Phi}^{i\,\mathrm{T}} \boldsymbol{\Phi}^i \mathrm{d}V^i \simeq \sum_{n=1}^{n_n} m_n \boldsymbol{\varphi}_{Rn}^{i\,\mathrm{T}} \boldsymbol{\varphi}_{Rn}^i \tag{2.71}$$

The following equation defines the inertia of a flexible body.

$$\mathbf{I}^{i7} = \int_V^i \rho^i \tilde{\bar{\boldsymbol{u}}}_0^{i\,\mathrm{T}} \tilde{\bar{\boldsymbol{u}}}_0^i \mathrm{d}V^i \simeq \sum_{n=1}^{n_n} m_n \tilde{\bar{\boldsymbol{u}}}_{0n}^{i\,\mathrm{T}} \tilde{\bar{\boldsymbol{u}}}_{0n}^i \tag{2.72}$$

The first order inertia correction consists of n_p number of (3 x 3) matrices that are as follows.

$$\mathbf{I}_j^{i8} = \int_{V^i} \rho^i \tilde{\bar{\boldsymbol{u}}}_0^{i\,\mathrm{T}} \tilde{\boldsymbol{\varphi}}_{Rj}^i \mathrm{d}V^i \simeq \sum_{n=1}^{n_n} \sum_{j=1}^{n_p} m_n \tilde{\bar{\boldsymbol{u}}}_0^i \varphi_{Rnj}^i \tag{2.73}$$

Finally, the second order inertia correction consists of ${n_p}^2$ number of (3 x 3) matrices that come from this equation.

$$\mathbf{I}^{i9}_{jh} = \int_{V^i} \rho^i \tilde{\boldsymbol{\varphi}}^i_j \tilde{\boldsymbol{\varphi}}^i_k \mathrm{d}V^i \simeq \sum_{n=1}^{n_n} \sum_{j=1}^{n_p} \sum_{h=1}^{n_p} m_n \varphi^i_{Rnj} \varphi^i_{Rnh} \tag{2.74}$$

A model can be simplified to reduce computational time by neglecting selected invariants. The trade off is reduced accuracy. Computationally, the most demanding invariants are $\mathbf{I}^{i5}$ and $\mathbf{I}^{i9}$, the second order corrections for cross coupling and inertia, and they should be neglected first.

CHAPTER 3

Fatigue phenomena

Empirical testing with actual parts or complete systems for fatigue analysis is time consuming and laborious. Traditionally, the approach to avoiding fatigue failures in a new system is to fatigue test specific structural details before integrating them into the system design. In fact, fatigue life predictions for many kinds of typical welded details can be found commonly in the literature including fillet welds, corner joints, and butt joints. This approach has several weaknesses. For example, all pertinent structural details to be used should be tested under various loading conditions if the fatigue evaluation is to be comprehensive. Also, the approach ignores other parameters that may relate to a particular joint, such as the number of weld beads or other geometrical and technical details. Obviously, for a complex system with an arbitrary number of structural details subjected to various multi-axial loading scenarios, it is practically impossible to use this traditional approach.

More recently, numerical methods have been developed to estimate fatigue life allowing the designer to more effectively consider the effects of fatigue [27]. Today, the finite element method has become a standard approach for estimating the fatigue life of a structure. Nonetheless, even though computational capacity is increasing all the time, applying the finite element approach to a complex structure subject to dynamic multi-axial loading presents an overwhelming computational burden.

A common cause of structural fracture, fatigue failure occurs because of cyclic loading. In essence, fatigue damage progresses in two stages; the crack initiation stage, in which one or more small cracks begin to form in the material, and the crack growth stage. In the crack growth stage, the initial crack propagates

until it results in the failure of the structural material. Avoiding fatigue failure is a fundamental principle in the design of structures that are exposed to cyclic loading and vibration. Fatigue can be classified as one of two types depending on the number of load cycles prior to failure. High-cycle fatigue failure results after millions of load cycles. Failures resulting from a lower number of load cycles, thousands or less, are low-cycle fatigue failures. In low-cycle fatigue, the deformations due to load are mainly plastic, whereas high-cycle fatigue deformations are elastic. The focus of this work is high-cycle fatigue.

Fatigue design approaches can be differentiated according to how cracks initiate. In some applications, such as rotating axles, fatigue life is practically equivalent to the duration of the crack initialization stage. Because of the notch effect, the crack in these applications quickly results in failure. For larger structures, such as machine frames or many welded structures, cracks are present from the beginning, so fatigue life is the determined by the length of time it takes the initial cracks to propagate.

Three finite element analysis methods are available for predicting fatigue life: nominal stress, local yielding, and total-life fracture mechanics. The nominal stress method is straightforward. In this method, experimental fatigue data is typically presented in a form of S-N curves, which present the number of constant amplitude load cycles leading to failure. Using the local yielding method to predict fatigue life requires an approach to determining local plasticity, such as Neuber's law. Finally, the total-life fracture mechanics method relates mainly to the observation of crack propagation, which is cumbersome to implement into a multibody system simulation. Propagating cracks may affect the geometry and inertial properties of a flexible body.

3.1 Fatigue stresses

The entire area of fatigue damage analysis relies on the results of empirical testing. Traditionally, the focus has been on one-dimensional loading. To extrapolate one-dimensional test results to a more complex configuration, damage hypotheses are needed to estimate equivalent loading. In the literature, studies about test setups more complex than one-dimensional loading can be found [67]. The main interest of this work is to produce stress data. From that point of view, the relative fatigue life of individual structural detail is more critical than the absolute fatigue life of a particular structural system. Even though measuring the fatigue life of a structural detail subject to a complex load history is problematic, some kind of estimate can be made and more importantly can be used to make comparisons.

3.1.1 Stress components

The stress state of a particle in a structural material is a function of all loads applied. At any point, the direction of stresses and strains can be estimated. A stress state can be fully described with a stress vector comprised of three normal and three shear stress components. This assumption can be made, since adjacent shear stresses in a matrix form are equal [81]. Thus, stress vector $\boldsymbol{\sigma}$ can be expressed as follows.

$$\boldsymbol{\sigma} = \begin{bmatrix} \sigma_X & \sigma_Y & \sigma_Z & \tau_{YX} & \tau_{YZ} & \tau_{ZX} \end{bmatrix}^{\mathrm{T}} \tag{3.1}$$

In Figure 3.1, stress components are depicted on three orthogonal planes in Cartesian coordinates.

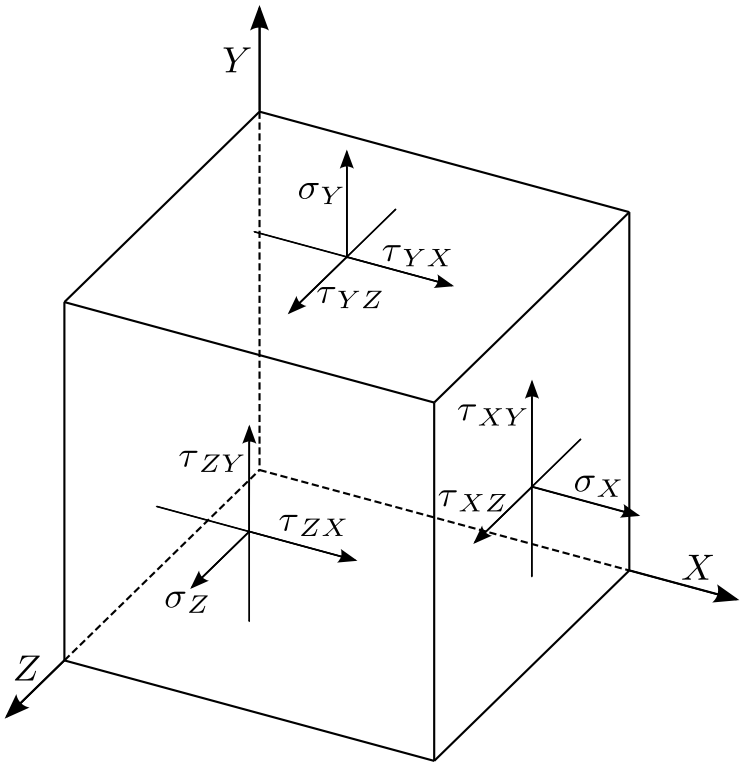

Figure 3.1. Components of the stress vector

Normal stresses σ_X, σ_Y, and σ_Z are along indicated coordinate axes X, Y, and Z; respectively. Shear stresses τ_{XY}, τ_{YZ}, and τ_{ZX} are indicated with two subindices.

The first is for the acting plane, and the second for the direction. The shear stress plane is perpendicular to the nominated coordinate axis. The positive and negative signs on the stress points along the coordinate axis are reversed. Shear stresses are paired such as, $\tau_{XY} = \tau_{YX}$, $\tau_{YZ} = \tau_{ZY}$, and $\tau_{ZX} = \tau_{XZ}$; therefore, only three shear components and three normal components are needed to describe the complete stress state of a given point. At any point, the coordinate frame can be oriented so the shear stresses disappear. The coordinate axes of this rotated coordinate frame are called principal axes. The orientation of the principal axes is independent of the orientation of the original coordinate frame of observation. Principal stress values can be found by solving for the roots of the following equation.

$$\begin{aligned}\sigma^3 - &\sigma^2 \left(\sigma_X + \sigma_Y + \sigma_Z\right) \\ &+\sigma \left(\sigma_X\sigma_Y + \sigma_Y\sigma_Z + \sigma_X\sigma_Z - \tau_{XY}^2 - \tau_{YZ}^2 - \tau_{ZX}^2\right) \\ &- \left(\sigma_X\sigma_Y\sigma_Z + 2\tau_{XY}\tau_{YZ}\tau_{ZX} - \sigma_X\tau_{XY}^2 - \sigma_Y\tau_{YZ}^2 - \sigma_Z\tau_{ZX}^2\right) = 0\end{aligned} \tag{3.2}$$

The largest root is nominated σ_1, and σ_3 is the smallest. Principal shear planes can be found by rotating principal normal stress planes 45°. The principal shear stresses can be obtained as follows.

$$\begin{aligned}\tau_{23} &= \frac{|\sigma_2 - \sigma_3|}{2} \\ \tau_{13} &= \frac{|\sigma_1 - \sigma_3|}{2} \\ \tau_{12} &= \frac{|\sigma_1 - \sigma_2|}{2}\end{aligned} \tag{3.3}$$

The principal stresses can be visualized using Mohr's circle representation of a stress state as depicted in Figure 3.2.

In Figure 3.2, τ is the shear stress and σ_n is the normal stress. Mohr's circle illustrates that principal stresses occur where the shear stresses are zero. Conversely, normal stresses are non-zero on the principal shear planes.

Typically, fatigue testing is uniaxial, and therefore complex multiaxial stress is reduced into equivalent uniaxial stress. Methods for calculating equivalent uniaxial stress are called yield criteria. There is no single all-purpose yield criterion, and selection of the one most appropriate to a particular analysis

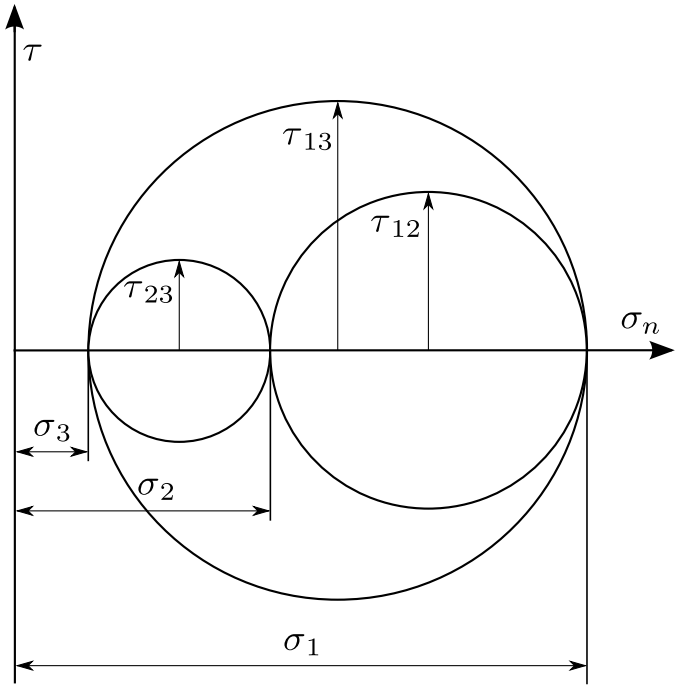

Figure 3.2. Mohr's circle representation

depends on material parameters and the way loads are applied. Three of the most commonly used yield criteria are described here briefly.

The most used equivalent stress criterion is the von Mises yield criterion. It is based on energy and is, therefore, independent of coordinate system orientation. The complex multiaxial stress state is reduced as.

$$\sigma = \frac{1}{\sqrt{2}}\sqrt{(\sigma_X - \sigma_Y)^2 + (\sigma_Y - \sigma_Z)^2 + (\sigma_X - \sigma_Z)^2 + 6\left(\tau_{XY}^2 + \tau_{YZ}^2 + \tau_{ZX}^2\right)} \tag{3.4}$$

A second important equivalent stress criterion is the Tresca yield criterion, wherein yield is assumed to occur when the maximum principal shear stress equals the yield strength. Tresca's yield criterion suits for ductile material. The second principal normal stress is always orthogonal to the plane where the maximum principal shear occurs, and therefore has no influence on maximum shear. Equivalent stress can be computed as follows.

$$\sigma = \sigma_1 - \sigma_3 \tag{3.5}$$

The original yield hypothesis criterion is the maximum principal stress hypothesis, which is suitable for brittle materials. The maximum principal stress hypothesis is formulated as follows.

$$\sigma = \max\left(|\sigma_1|, |\sigma_2|, |\sigma_3|\right) \tag{3.6}$$

Generally, in dynamic cases, the principal normal stress coordinates for any material point varies in direction and magnitude. This complicates making comparisons between stress results and fatigue test results. Yield hypotheses require the computation of the principal normal stress directions. Loading is considered proportional if the principal stress directions remain constant with respect to the applied loads. Otherwise, the loading is referred to as non-proportional.

3.1.2 Types of stresses

Stress σ acting on a structural detail can be divided into three components.

$$\sigma = \sigma_{mbr} + \sigma_b + \sigma_{nlp}, \tag{3.7}$$

where σ_{mbr} is membrane stress, sometimes referred as nominal stress or primary stress, σ_b is bending stress over the width of a bent structure, and σ_{nlp} is the nonlinear stress peak. The superposition of membrane stress and bending stress is called σ_s or the structural stress.

In fatigue analysis, hot-spot stress is also used [30]. Hot-spot stress is the value of structural stress slightly below the surface, where fatigue cracking is assumed to initiate. The nonlinear stress peak is not included in the hot-spot stress.

Primary stress is an artificial entity contrived to facilitate stress calculation. It is defined as the minimum stress state where external loads and internal loads are in balance. When calculating primary stress, the loaded material is assumed fully elastic. Additive to primary stress, secondary stress includes residual stresses and stresses produced by notches, discontinuities, and temperature differences. Secondary stresses tend to relax over time due to material plasticity. Also, secondary stress takes into account stresses caused by the material model. Typically, the finite element method gives good approximations for the overall

stress state, but separating primary and secondary stresses is difficult [21]. This is mainly because the ratio between stress components depends on mesh size.

Nonlinear stress peaks can also be considered secondary stresses, but because they are localized phenomena, they can be treated separately as a unique category. Even though the nonlinear stress peak value at a given structural location may approach the material's tensile strength, there may be no visible deformation.

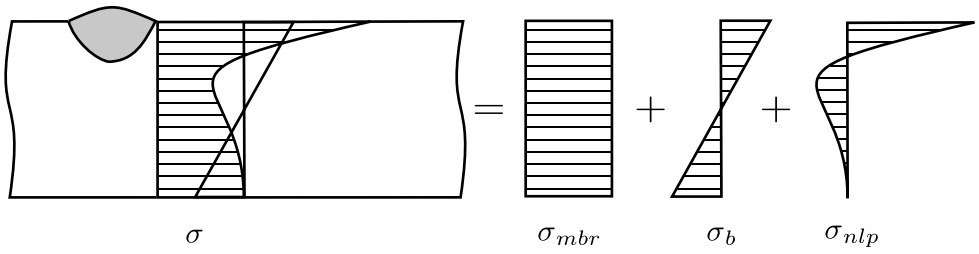

Figure 3.3. Three components of the stress

In Figure 3.3, the primary stress, secondary stress, and nonlinear stress peak distributions are illustrated. Primary stress is a product of the applied nominal tension force. Bending caused by local structural discontinuity results in the secondary stress distribution. Finally, the notch effect leads adds the nonlinear stress peak distribution. The secondary (or structural) stress and the nonlinear stress peak are self-balancing, which means their sum over any region of observation equals zero.

3.1.3 S-N-curves

The cyclic variation of mean stress produced by cyclic loading conditions affects the life of a structure. To evaluate their fatigue life, material samples are typically exercised to failure by cyclically loading them to produce a constantly varying mean stress. The amplitude of this mean stress is then recorded along with the number of cycles to failure. From numerous tests covering a range of mean stress amplitudes, a stress-life diagram relating stress amplitude (S_a) to number of cycles to failure (N) can be produced for any given material. This S-N diagram is an important and standard way of presenting fatigue data. Another equivalent type of S-N diagram can be produced by plotting stress ratio with respect to the number of cycles to failure.

For metallic materials, increased mean stress results in lower fatigue life [37]. One of the first attempts to find a relationship between mean stress and fatigue strength

and provide a border between safe and unsafe conditions was the Gerber parabola. Some decades later, the relationship was approximated with the Goodman line. Both curves are depicted in Figure 3.4. Most experimental test data falls between the Goodman line and the Gerber parabola.

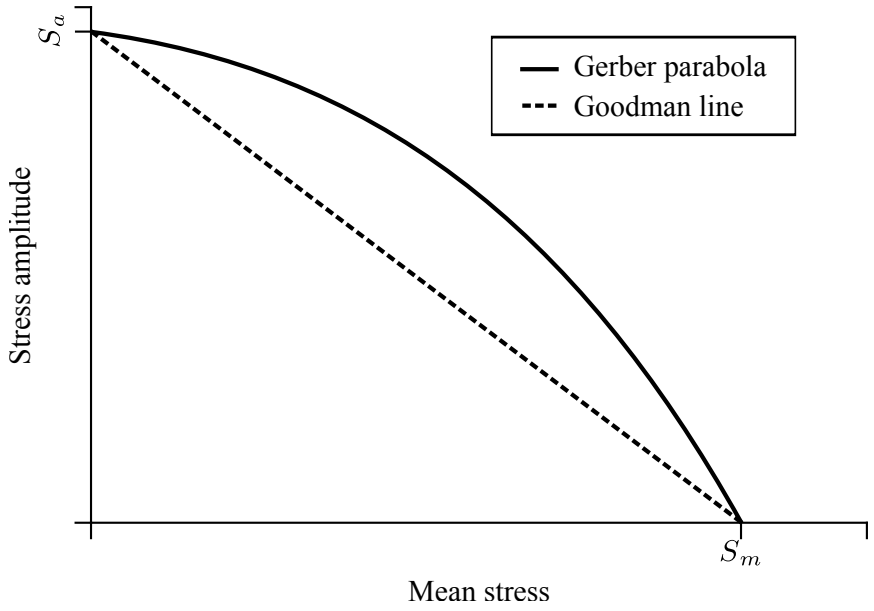

Figure 3.4. The Goodman line and Gerber parabola on the same graph

One basic idea behind fatigue testing is constant amplitude loading, that is, fatigue loading in which the applied cyclic load is sinusoidally shaped and of constant amplitude and frequency. The load cycle is the smallest repeating period of the resulting mean stress history. Following the commonly used convention for stress notation, over one full load cycle, $\S_a$ is nominal stress amplitude or alternating stress, $\S_m$ is nominal mean stress. For local stresses, σ_a is stress amplitude and σ_m is mean stress. σ_{max} is maximum stress, and σ_{min} is minimum stress. The load cycle is noted mathematically as $\sigma_m \pm \sigma_a$. Tensile stresses have positive values, and negative values are compressive stresses. According to this notation and considering the sign convention, the following equations for maximum, mean, and minimum stress can be expressed.

$$\sigma_{max} = \sigma_m + \sigma_a \tag{3.8}$$

$$\sigma_{min} = \sigma_m - \sigma_a \tag{3.9}$$

$$\sigma_m = \frac{\sigma_{max} + \sigma_{min}}{2} \tag{3.10}$$

The stress range is denoted as $\Delta\sigma = 2\sigma_a = \sigma_{max} - \sigma_{min}$, and the stress ratio is $R = \sigma_{min}/\sigma_{max}$.

3.1.4 Cumulative damage counting

Fatigue test results are usually presented as an S-N-graph with logarithmic cycles to failure on the x-axis and (usually) linear stress amplitude on the y-axis. There has been a great deal of constant amplitude testing done for unnotched specimens, and a large number of resulting S-N-curves can be found in the literature, see [60]. A large number of tests have been carried out using specimens with circular cross section and rotating bend loading with a stress ratio $R = -1$. Constant specimen rotation produces sinusoidal loading cycles. The results of this kind of testing is typically presented as an S-N-curve in which stress amplitude, with some certain levels, and the number of cycles to failure is plotted, and an appropriate curve is then fitted through individual data points. S-N-graphs are sometimes called Wöhler diagrams after the German engineer who first used them as a way of presenting his fatigue data. In Figure 3.5, S-N-curve is shown schematically in linear scale. Stress amplitude, at level S_1, leads to the failure after N_{f1} cycles.

In Figure 3.6, m is the exponent of the power law and it is a material parameter. The left uppermost horizontal line in the graph on the right represents the static limit, which means it is not reasonable to estimate fatigue life for a structure that fails during the first cycle. The second horizontal line (with the "S-N-curve" label) represents the level of threshold stress change, which can be found experimentally. All stress change levels below the threshold lead to approximately infinite fatigue life. To be on the safe side, a hypothetical S-N-curve is added that eliminates the prediction of infinite fatigue life for low stress levels. Structural failure that occurs at stress levels even slightly below the fatigue limit can require load cycles in the region of 10 raised to the power of 9. Fatigue failure occurring in this region is referred to as gigacycle fatigue, which combined with the large scatter on results for low-level stresses led to the use of the hypothetical addition. The hypothetical addition to the S-N curve increases the safety margin.

In design, deciding how to predict fatigue life for a structure that is loaded by wide variety of amplitudes is a difficult problem. In reality, the problem is highly complicated, but some approaches have come from empirical tests. For example, one way of estimating the fatigue life of a structure is to give it some initial amount

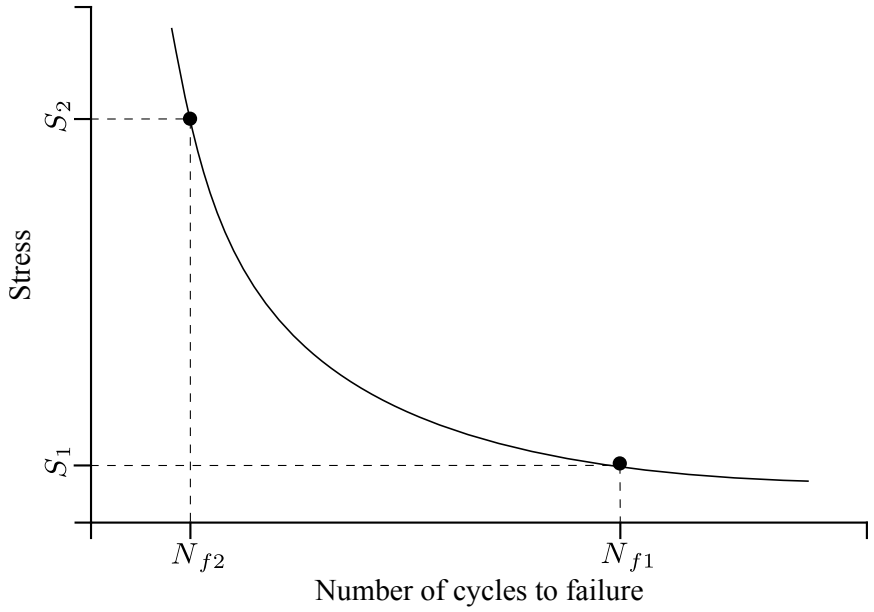

Figure 3.5. Schematic representation of S-N-curve in a linear scale

of fatigue endurance, and then assume that one load cycle will shorten its fatigue life by some amount. This idea was first published in 1924 by Palmgren [48] for ball bearings. Later, Miner made it more general [43]. Palmgren and Miner suggested that fatigue damage could be accumulated linearly and that failure occurs once the fatigue endurance limit has been reached. The Palmgren-Miner rule states that if a specimen is stressed with a stress level σ_{1a} and has a fatigue life of N_{f1} cycles, the damage after N_1 cycles will be $\frac{N_1}{N_{f1}}$ and the damage caused by one cycle will be $\frac{1}{N_{f1}}$. The idea can be expanded for varying stress conditions and is referred to as the Palmgren-Miner equation, which can be expressed as follows.

$$\frac{N_1}{N_{f1}} + \frac{N_2}{N_{f2}} + ... + \frac{N_n}{N_{fn}} = \sum_{i=1}^{n} \frac{N_i}{N_{fi}} = 1, \tag{3.11}$$

where N_1 denotes the amount of load cycles with stress amplitude of σ_{a1}, and N_{f1} is the number of cycles with stress amplitude σ_{a1} that leads to failure. When the sum of all the fractions reaches 1, the fatigue life of the material is exhausted. The Palmgren-Miner approach is straightforward, but makes several assumptions that

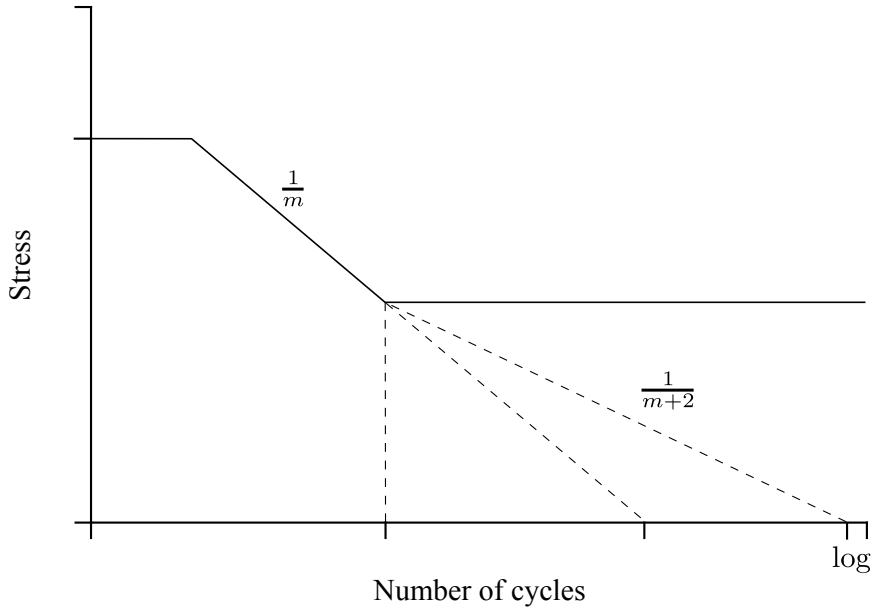

Figure 3.6. Schematic S-N-curve in a logarithmic scale

could largely impact the accuracy of the fatigue life prediction. If the material has a pre-existing crack, and if the bulk of the fatigue life takes place in the propagation phase, the Palmgren-Miner approach does not take into account the geometrical change of the structure due to crack growth. Another problem with the Palmgren-Miner hypothesis is the wide variation in experimental data that defines values used in Equation 3.11 [53].

Fatigue is a random process, and fatigue testing produces scattered data. This scatter increases as the number of load cycles required for failure increases. Problems associated with data scatter can be and are already mitigated by applying statistical methods to analyze the data. Nonetheless, scatter in the data exists and has to be taken into account in design. Fatigue test data scatter can be described with the log-normal distribution, although other distributions also can be used [44]. S-N-curves can be drawn with different probabilities of failure. Then, the curves are referred to as P-S-N-curves. Figure 3.7 is a schematic representation of a P-S-N-curve.

The curves, in Figure 3.7, represent failure probabilities of 1, 50 and 99 percent. The figure also illustrates that scatter increases with measured fatigue life. For

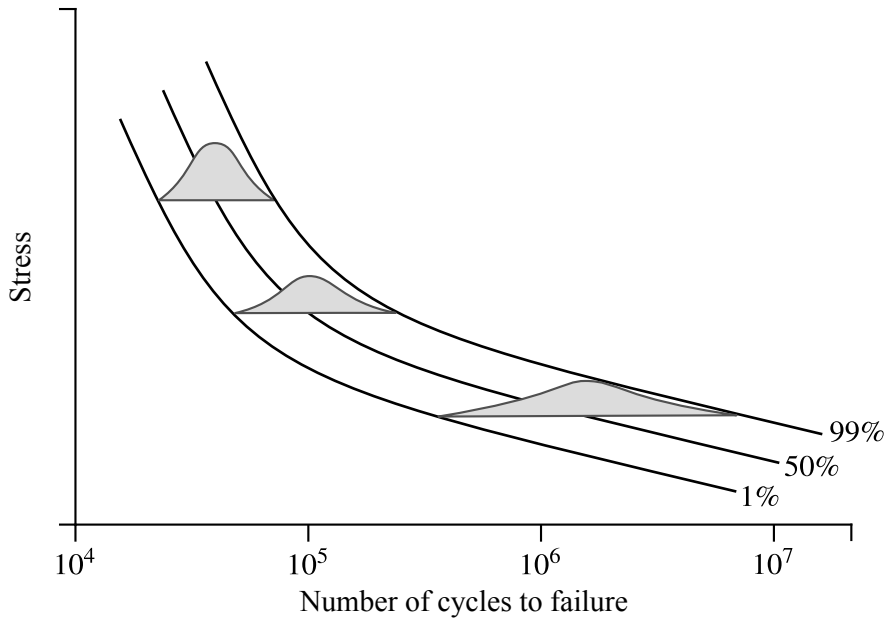

Figure 3.7. Schematic representation of P-S-N diagram

low failure probability, significantly lower stress levels than suggested by the nominal S/N assumption should be used.

3.1.5 Stress history

Before computer workstations were readily available, obtaining a reasonable stress history was a problem. Now, stresses can be measured directly using strain gauges affixed to the material of interest. Also, the finite element method has become a standard tool for fatigue life estimation, even though computational requirements still prevent using the method to produce complete stress histories for a dynamically loaded structure. Today, multibody simulation tools promise to provide the needed stress information and stress histories for structural details, extracting them directly from the simulation.

Palmgren-Miner rule requires cyclic loading as an input. During fatigue analysis, it is rarely practical to work with entire load histories. A cycle counting method is needed to classify continuous load history into discrete cycles before Palmgren-Miner's rule can be applied. Several cycle counting methods can be found in the literature [75, 24, 68]. One of the most common method for identifying

individual cycles is the rainflow counting method [44] or variations of it [3]. This method can be used to determine both the stress range $\Delta\sigma$ and the mean stress σ_m for a cycle [39]. The basic idea in the counting methods is to count individual hysteresis loops in a stress history. In Figure 3.8, schematic example of a stress history is shown as a graph. In the counting, the number of cycles in a stress history will be equivalent to the number of peaks. The development of cycle counting methods is based on empirical tests, and candidates for new methods are verified by comparing analytical with experimental results. Results obtained by different counting methods vary widely in their detail.

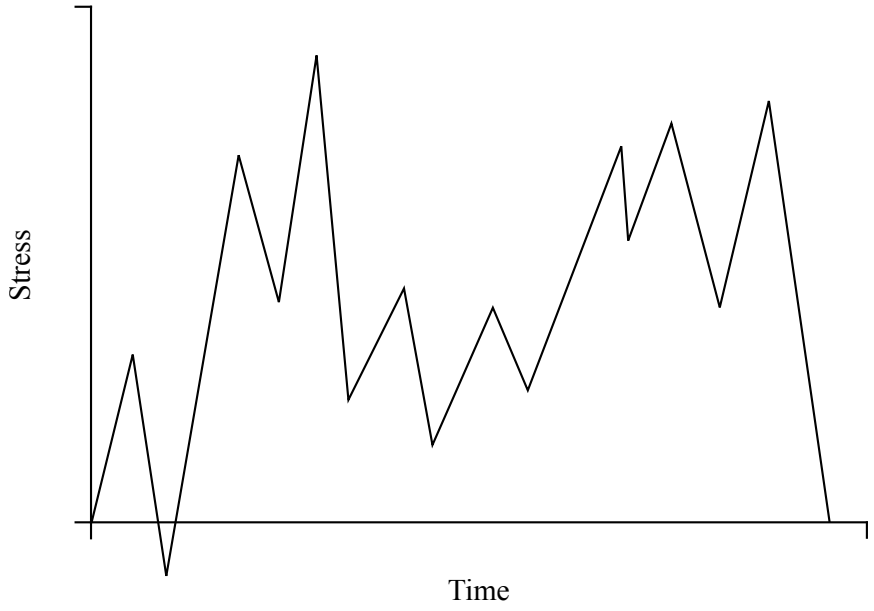

Figure 3.8. Example of the stress history for fatigue cycle counting

3.2 Discontinuities

Discontinuities act as stress raisers and when determining the fatigue life of a structure, they are the key issue. For a notched feature, fatigue strength in cases of long fatigue life is reduced by the factor k_f. However, the notch geometry is not the only factor that reduces fatigue life. Tensile loading is more severe from a fatigue point of view than bending, mainly because the tensile stress acts upon a larger material volume. The surface condition of the material plays a significant

role. Typically, presented results are obtained from polished specimens, and the fatigue strength values for cast specimens without surface finishing can be half the nominal values.

The effect of size is also mentioned in the literature [22]. Usually, fatigue tests are carried out using relative small specimens, *i.e.*, 8 mm in diameter. A larger material volume means a larger stress volume, and the probability of fatigue failure is greater for a larger stress volume.

3.2.1 Effect of notches

Discontinuities can rarely be avoided in the design of machine parts or structural members, although they can be positioned to minimize their affect on fatigue life. Welds, holes, grooves, or bracket features all result in notch geometries that act locally as stress raisers. The presence of a stress raiser shortens the fatigue life of a machine part or structural member, because it induces locally higher stresses that cause cracks to initiate. The fatigue life of a notched specimen depends on material and the geometry of the notch. The elastic stress concentration factor is the ratio of local stress σ to nominal stress S, that is, $k_t = \sigma/S$. It can be used to quantify the seriousness of a notch. Thus, notches are usually characterized by the elastic stress concentration factor. Even though the concept of k_t is appropriate for analyzing notches in fatigue, additional phenomena should be taken into account to study the fatigue behavior of a crack subject to multiaxial loading. In a ductile material, the tip of a crack will deform plastically, and stress peaks are redistributed into a larger volume. Plastic deformation of the crack tip may then result in a local change in mean stress.

In a simplified case, it might seem that unnotched and notched specimens will have the same fatigue life if $\sigma = S$ in the unnotched specimen and $\sigma = k_t S$ in the notched specimen. Experimental observation shows that a notch has less effect than k_t predicts. The actual reduction factor k_f, especially for long fatigue life, is called the fatigue notch factor. Defined as follows, the fatigue notch factor or fatigue strength reduction factor is the ratio of the equivalent completely reversed (*i.e.*, zero mean stress) amplitudes for the unnotched σ_{ar} and notched S_{ar} cases.

$$k_f = \frac{\sigma_{ar}}{S_{ar}} \tag{3.12}$$

For relatively large notches, or more precisely, for a large crack radius, $k_f = k_t$. As crack radius becomes smaller, k_f becomes smaller than k_t.

Stress decreases rapidly with increasing distance from a notch. The slope $d\sigma/dx$ of the stress distribution is called the stress gradient, and for sharp cracks, the stress gradient is high. The inequality between k_t and k_f is related to stress gradient. In a smooth specimen, stress is applied to a large volume that probably contains flaws, micro cracks, or weak spots to promote crack initialization. In a notched specimen, the higher stress is applied to a much smaller volume that according to probability will have no flaws. Another explanation is that in the notched specimen case, fatigue life is mostly dominated by crack growth. That is, cracks grow rapidly in a notched specimen until the nominal stress becomes relatively low, whereas in an unnotched specimen, an incipient crack will always be located in a highly stressed volume.

For different geometries, values for k_t can be found in the literature [52]. Experiments have shown that some materials are more prone to notch fatigue. A notch sensitivity index q defined by Equation 3.13 quantifies this effect [51].

$$q = \frac{k_f - 1}{k_t - 1} \tag{3.13}$$

If $q = 1$, a material is said to be fully notch sensitive, and if $q = 0$ a material is said to be fully notch insensitive. The notch sensitivity index q is not a material constant even though it is related to the material. Typically, q increases with increasing material tensile strength and increasing notch sharpness, or in the case of a round notch, with decreasing radius. Values for q and k_f can be estimated using empirical material constants that do not depend on notch geometry. According the Peterson, the notch sensitivity factor q also can be written as follows [51].

$$q = \frac{1}{1 + \frac{\alpha}{\rho}} \tag{3.14}$$

In the denominator, ρ is the notch tip radius, and α is a material constant defined in millimeters. Material constants can be found in the literature [51].

3.2.2 Crack initiation

Typically, crack initiation covers 80 % of the total fatigue life for a structure, and crack growth covers the remaining 20 %. Failure analysis often shows that a crack starts where several kinds of discontinuities exist simultaneously. Geometric discontinuities are usually referred as notches, without considering the actual

shape of the geometry. Cracks initiate near notches because the stresses there are higher than the nominal mean stresses. In cases where crack initiation dominates fatigue durability, geometric changes due to crack growth can be neglected, because structural failure occurs as soon as the crack begins. For crack initiation dominated cases, surface finish plays a crucial role, especially for long design fatigue life. This is understandable, because a rough surface can act as a notch and promote crack formation. Surface finish relates to manufacturing. In the literature, many experimental studies relate surface roughness to different manufacturing techniques.

There is no way to describe surface roughness generally using a single parameter that describes everything about the surface, but at least the literature provides qualitative advice on the influence of the effects. One way to treat surface problems is to introduce the concept of intrinsic fatigue strength [25], *i.e.* fatigue strength for carefully polished specimens without any residual stress or hardness variation. This intrinsic fatigue strength then can be treated as a nominal case given a surface factor of 1. For real design cases, the surface quality factor can be expected to be less than 1. In general, higher tensile strength materials are more sensitive to surface defects.

Residual stresses in a material are additive. In other words, they simply superimpose onto the stress fields resulting from applied loads. Residual stresses that are compressive lower the mean stress, and tensile residual stress increases mean stress. In practice, it is sometimes difficult to determine residual stresses, but once determined, superposing them onto the mean stress field is straightforward.

3.2.3 Crack propagation

Often, tiny cracks are present from the beginning in many structural members or machine parts. In particular, metal casting and welding are two manufacturing processes that introduce cracks. For existing cracks, fatigue life can be predicted by determining the number of load cycles needed to grow from the initial crack size D_0 to the final crack size D_f, where the material fails due to static load. There are several methods for determining fatigue life in materials with pre-existing cracks. Fatigue cracking can be divided into three phases: crack initiation, microcrack propagation, and macrocrack growth. Figure 3.9 illustrates crack grow phases in a schematic way.

Microcrack initiation and microcrack growth are together refered as stage I crack growth. It is driven mainly by plasticity and the direction of a crack growth is not changing. The direction of a crack growth on a stage I is along highest shear stress.

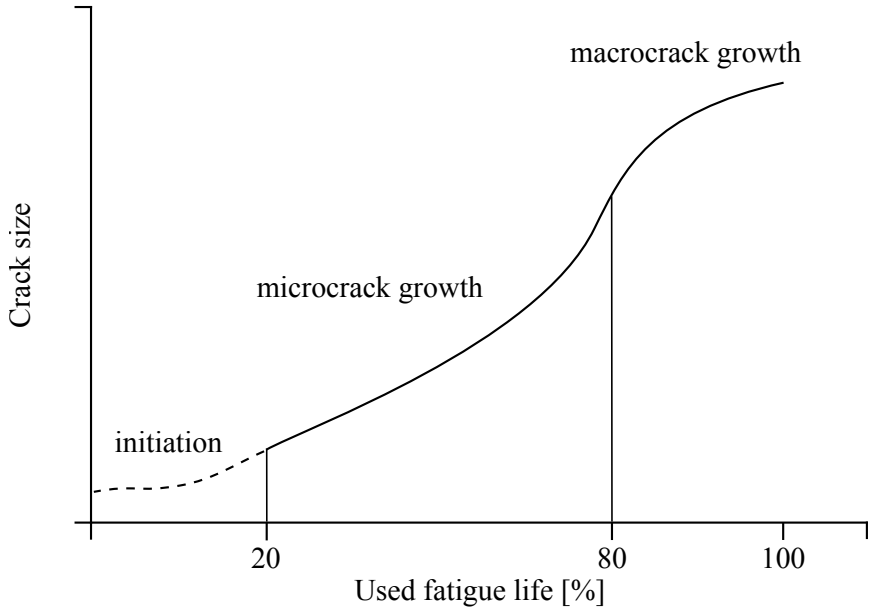

Figure 3.9. Phases of the crack growth

Once the Stage I crack achieves a critical length, it will become a Stage II crack. In Stage II, crack growth changes direction and begins propagating normal to the maximum principal stress. One reason crack propagation must be considered during dynamic analysis is the effect it has on material geometry that may, in turn, affect dynamic response. The fundamental basis behind the analysis of stage II crack growth is that criteria must be met for propagation [13]. According to the thermodynamic criterion, there should be enough energy to drive propagation. According to the stress criterion, the stress at the tip of the crack should be high enough to force propagation. Below the fatigue threshold, these criteria are not met. Crack propagation releases energy that is absorbed by plastic deformation. For a brittle material, the released energy exceeds the absorption capacity of the material, crack propagation continues unstably, and the material fractures in a brittle way.

3.3 Fatigue in welded structures

Welded joints always contain welding flaws that cause plastic deformation locally even though nominal stresses are relatively small compared to yield strength.

Welded joints also contain internal stresses that are equal to the material yield strength. These internal stresses remain if they are not subsequently removed by tempering or controlled overloading.

Residual stresses caused by rapid solidification from a molten state are tensile and of the same order of magnitude as the yield strength of the material. In practice, this means that even a compressive load cycle will result in full fatigue damage. The residual stresses keep the crack open, and then compressive loading closes the crack. Removing the load completes a fully effective load cycle.

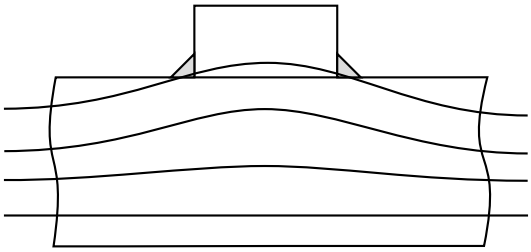

Figure 3.10. Locally increased stress due to weld

Fatigue failure is common in a welded structure due to the small defects and discontinuities created during the welding process. These small defects act as pre-existing cracks. Furthermore, the weld bead is in itself a structural discontinuity, and welds are often located near large changes in structural shape where high secondary stresses exist. In Figure 3.10, the change in tension stress flow due to welded joint is shown schematically. Finally, there are residual stresses caused by the weld that raises the local mean stress. All these are cumulative, and they lead a well-known conclusion: welded structures are prone to fatigue failure if loaded dynamically.

3.3.1 Avoiding fatigue failure

There are two fundamental ways to prolong fatigue life: improve the design or improve the mechanical properties of a material, *i.e.*, use a more fatigue resistant material, employ better manufacturing methods, or add thermal and mechanical treatments. From an economics point of view, it is usually more beneficial to improve structural design than to upgrade material, because material costs are recurring, while making the design improvements requires only a single initial investment. With respect to improving the design, fatigue analysis results can identify any existing problem areas and suggest likely strategies for improvement.

Improving mechanical properties
Two important approaches for improvement are modifying local geometries to reduce stress levels (*e.g.*, removing notches or increasing the radius of structural discontinuities) and moving problematic features into areas of lower mean principal stress. Often approaches are combined.

Several mechanical treatments are available that can increase fatigue life. Grinding and polishing material surfaces removes micro notches, heat treatment removes residual stresses, and remelting weld beads decreases weld defects. Introducing compressive residual stresses into material surfaces with pneumatic hammering or shot peening also increases fatigue life by inhibiting crack initiation. A commonly used method is to overload material volumes suspected of containing pre-existing cracks, plastically deforming them to produce compressive residual stresses that bind the crack tips. After overloading is relaxed, residual compressive stresses remain on the crack tips. To cause fatigue damage, these residual stresses must be overcome before cracks will begin to open and propagate. This kind of overloading is usually referred as proof loading.

Improving the design
There are a number of fundamental concepts that define good design with respect to fatigue. One is to eliminate or reduce the effect of stress raisers by minimizing their severity. This leads to minimizing the elastic stress concentration factor k_t, which will decrease the fatigue notch factor k_f and raise the fatigue limit and raise the overall S-N curve. Also beneficial is removing eccentricity that results in unwanted bending.

By design it is beneficial to move stress raisers from high stress regions to locations where nominal stress is relatively low. Fatigue damage occurs, almost without exception, around structural discontinuities. Designing against fatigue is paying careful attention to their placement. For grooves and different kind of holes, stress concentration factors are decreased by increasing the radii of the shapes.

For all of the concepts mentioned, stress distribution in the structural material is the key. Using a multibody simulation approach, the stress history for every material point can be determined, offering an excellent opportunity to improve structural fatigue life.

3.3.2 Fatigue design methods

Fatigue damage occurs after cyclic loading and is a common cause of structural fracture. Particularly in welded structures, residual stresses near the welds make

those areas prone to fatigue cracking. A major contributor to fatigue damage is insufficient knowledge of structural loading conditions. A fatigue failure occurs when a crack grows large enough to undermine the structural strength of the material. Designing structures to resist fatigue damage requires accurate information about the loading conditions affecting the structural material and its detailed behavior.

Stress amplitude, *i.e.*, the difference between maximum and minimum stress, plays a critical role in fatigue. This applies especially to the heat affected zones of structural welds, where there can be high residual stress levels caused by uncontrolled weld cooling. A commonly applied method to calculate the fatigue life of a structure is based on the use of the rainflow counting algorithm [44]. The method classifies the stress range $\Delta\sigma$ for a certain measurement period, and calculates their number $n_{\Delta\sigma}$. Measurement data can be obtained either from the actual machine with a strain gauge or through a computer simulation. With the rainflow counting method, stress amplitudes can be classified simply based on their magnitude, with or without the mean stress level. The method is based on the empirically verified concept that stress amplitude of a certain magnitude and a certain mean stress causes fatigue damage of a certain size. The concept can be extended by a real-time classification and calculation to assess the remaining fatigue life of the structure and the extent of its current fatigue damage.

Without making actual measurements or performing simulations, designers generally have limited possibilities to assess structural loads. Using off-line computer simulations to determine loading conditions has been problematic, because the simulations have not properly accounted for machine operator behavior. The way a machine system is operated greatly influences its fatigue life. With real-time simulation, the activities of the operator can be included. Thus, the machines stresses in the simulation are often closer to reality than in off-line simulations.

The fatigue life for a structural detail can be estimated in several ways, but these can be categorized into two basic methods.

1) Methods based on S-N-curves (nominal stress, hot-spot)
2) Methods based on fracture mechanics (fracture mechanics)

3.3.3 Methods based on S-N-curves

Approaches based on experimentally obtained S-N-curves include nominal stress, hot-spot stress, and local notch stress. The nominal stress approach is not highly accurate, but still widely used. In the nominal stress approach, a large number of specimens featuring a particular joint are tested. Afterwards, the specimens are

classified according to their fatigue durability, which is quantified for a predefined level of nominal stress. The main problem with this method is that it does not pay any specific attention to material discontinuity or notch geometries. The only information the method offers is that one specific joint belongs to one specific nominal stress class.

The hot spot stress method requires definition of the structural stresses at the point where fatigue cracks are assumed to grow. In this method, all welded geometries are assumed equivalent in terms of fatigue, so notch stress is included in the fatigue strength data. The fatigue strength data can be expressed in a single S-N curve, which simplifies fatigue testing. Finite element analysis can be used to determine hot-spot stress. For large local stresses and plastic deformations, fatigue life prediction is conservative. The hot spot stress method can be considered as efficient and straightforward.

The local notch stress approach requires estimation of the nonlinear stress peak at the point of crack growth. Estimating the nonlinear stress peak may be cumbersome if the local geometry of the stress is unknown. The local notch stress method is best suited for estimating crack initiation and is used for improving weld quality.

Total fatigue life is the sum of crack initiation and propagation. Statistically, in test specimens the largest scatter comes from crack initiation even though it seems to be straightforward compared to arbitrarily propagating cracking.

Notch root strain is used as a characterizing parameter in local strain approaches, and it can be obtained using full elastic-plastic finite element analysis, which is computationally more demanding than linear-elastic finite element analysis. Local strains can be estimated from elastic analysis using approximation tools, such as Neuber's rule. In addition, detailed data for the material is needed, such as the cyclic stress-strain curve. With these methods, an elastoplastic material model is assumed. For Neuber's rule, it is necessary to define separate stress and strain concentration factors. They can be defined as.

$$k_\sigma = \frac{\sigma}{S} \tag{3.15}$$

$$k_\varepsilon = \frac{\varepsilon}{e}, \tag{3.16}$$

where σ is the stress on a notch, ε the corresponding strain, S is nominal stress, and e is nominal strain. Without full plastic yield, $e = S/E$, where E is the elastic modulus.

Neuber's rule states the geometric mean of the stress and strain concentration factors remains equal to k_t during plastic deformation. The rule can be formulated as follows.

$$\sqrt{k_\sigma k_\varepsilon} = k_t, \tag{3.17}$$

Combining previous equations, results in the following expression.

$$\sigma\varepsilon = \frac{(k_t S)^2}{E}. \tag{3.18}$$

Now, the product of stress and strain is a known constant. In cases where the product does not exceed yield strength, Neuber's rule gives results equivalent to elastic behavior.

Critical distance method allows the use of elastic analysis to predict fatigue life for notched components [69]. This prediction is made by introducing correction factors that are functions of the notch tip radius ρ. The fundamental idea is that the fatigue limit of an unnotched specimen must be exceeded, not only in tip of notch, but also within some area or volume ahead of the notch tip. This specific volume is referred to as the critical volume. In practice, stress is not measured at the hot spot, but at a critical distance away from the hot spot. The critical distance is determined empirically, measurement being the only way to find it. It is dependent on material, and typically is something between 0.1 ... 5 mm. The critical distance is small for high-strength materials, especially if they are sensitive to notches.

3.3.4 Methods based on fracture mechanics

The basic concept behind fracture mechanics approaches, which can be divided into linear-elastic fracture mechanics (LEFM) and elastic-plastic fracture mechanics (EPFM), is to approximate the rate of crack growth. Typically, only LEFM is used for analyzing welded structures. In LEFM, the stress field ahead of the crack is calculated using a range of stress intensity factor. Knowing the relationship between the stress intensity factor and the rate of crack growth makes it possible to predict the number of work cycles it takes to move from crack initiation to its maximum size. This method is versatile and can be used with initiated cracks or other similar discontinuities. However, the fracture mechanics approach cannot be used for to analyze the progression of crack propagation. Rule of thumb suggests that LEFM is most efficient when the length of the crack is more than 0.1 mm.

The fracture mechanics approach can be based on the empirically determined Paris equation, which defines the relationship between the rate of crack growth and the range of the stress intensity factor. The Paris equation can be expressed as follows.

$$\frac{\mathrm{d}a}{\mathrm{d}N} = C_0 \Delta K^m, \tag{3.19}$$

where $\frac{\mathrm{d}a}{\mathrm{d}N}$ is the crack growth rate, C_0 is power law constant, ΔK is the range of stress intensity factor, and factor m is the exponent of the power law. Constant C_0 and factor m are material parameters. In Equation 3.19, N is the number of cycles, and in fact as in practice, it is treated as a continuous variable, even though it is not. The range of stress intensity factor ΔK is a function of crack length D and must be updated for every stage of the growth. In reality, ΔK must exceed some threshold level ΔK_{th}, otherwise crack propagation cannot occur.

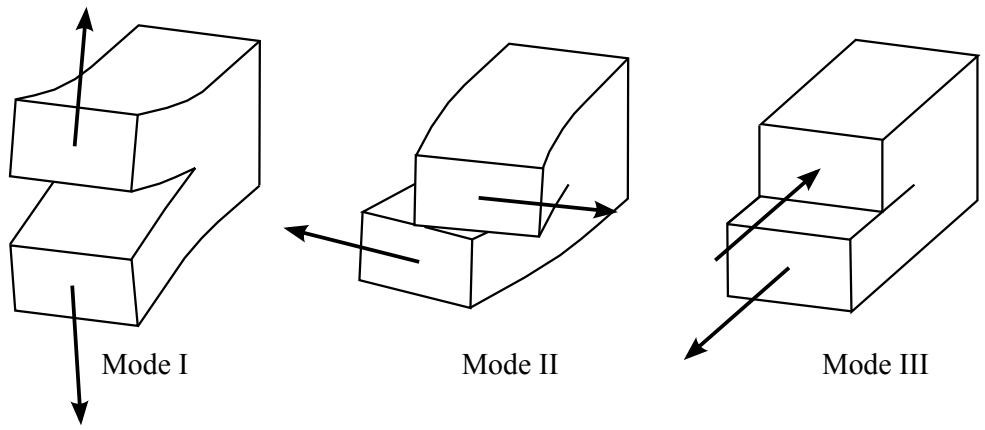

Figure 3.11. Crack opening modes

Crack opening can be classified into three modes: opening, Mode I; shearing or sliding, Mode II; and tearing or twisting, Mode III. In Figure 3.11 crack opening modes are visualized schematically. If only uniaxial tension is applied, the crack will open purely in Mode I. All modes can be superimposed onto each other and represented by an equivalent stress intensity factor ΔK_{eqv}. In practices, the opening mode (Mode I) is most dominant, and because it represents uniaxial cases there is plenty of test data available in the literature.

The Paris equation can be solved to give the number of cycles needed for a crack to propagate from its initial state to failure. Stress intensity factors can be estimated

using the finite element method. For some particular cases, the analytical solution for solving stress intensity factor is known. Generally, the equation for stress intensity factor can be written as follows.

$$\Delta K = F\Delta\sigma_{hs}\sqrt{\pi D} \tag{3.20}$$

The symbol F represents a function that takes the geometry, the shape, and the mode of the crack into account; D is the length of the crack; and $\Delta\sigma_{hs}$ is the range of hot spot stress.

In the Smith and Miller method, a crack is just a notch with a small radius ρ. The fatigue limit for the notch can be obtained by setting ρ to zero [66]. For a sharp notch, the fatigue limit can be expressed as follows.

$$\Delta\sigma_{on} = \frac{\Delta K_{th}}{\left[F\left(\pi D\right)^{1/2}\right]} \tag{3.21}$$

The fatigue limit $\Delta\sigma_{on}$ is for nominal stress of unnotched specimen, constant F is determined by the geometry of an equivalent crack, and D is the length of a crack.

For a blunt notch, the fatigue limit can be determined by assuming a hot-spot stress equal to the fatigue limit for an unnotched specimen as follows.

$$\Delta\sigma_{on} = \frac{\Delta\sigma_0}{K_t} \tag{3.22}$$

The Smith and Miller method can be applied to any notch, and given the two results, the analyst should used the largest fatigue limit value going forward. The biggest problem with this method is it requires values for F and D, which means that it can be only used for blunt notches or for notches of standard geometry.

3.4 Fatigue analysis and multibody simulation

Even though current fatigue analysis methods already provide various tools for estimating the fatigue life of a design, the concept of combining fatigue life prediction and multibody simulation is relatively new [61]. The need for the computational efficiency of multibody simulation and the requirement for a detailed deformation description are contradictory on a fundamental level. As a

result, compromise between requirements is necessary. From a fatigue analysis point of view, this means that fatigue life estimation must be made using inaccurate stress data or an insufficient amount of stress data. Because of this compromise, it is difficult to perform accurate absolute estimations of fatigue life, and more attention should be paid to relative life estimations.

Since the majority of multibody applications are intended to be computationally efficient, default multibody simulation can be assumed to provide only a rough estimation of stress distribution unless special techniques are used to improve accuracy locally. Some approaches noted in this chapter are summarized in the following Figure 3.12. In general, the multibody simulation obtains stress history for a structural detail, and the fatigue analysis uses this stress history as input and determines if the design is acceptable. In Figure 3.12, $F(D)$ is a function that takes into account the shape of the crack and $M_k(D)$ is a function that takes into account the local notch effect. $\Delta\sigma_h s$ is the range of hot spot stress and k_t is elastic stress concentration factor.

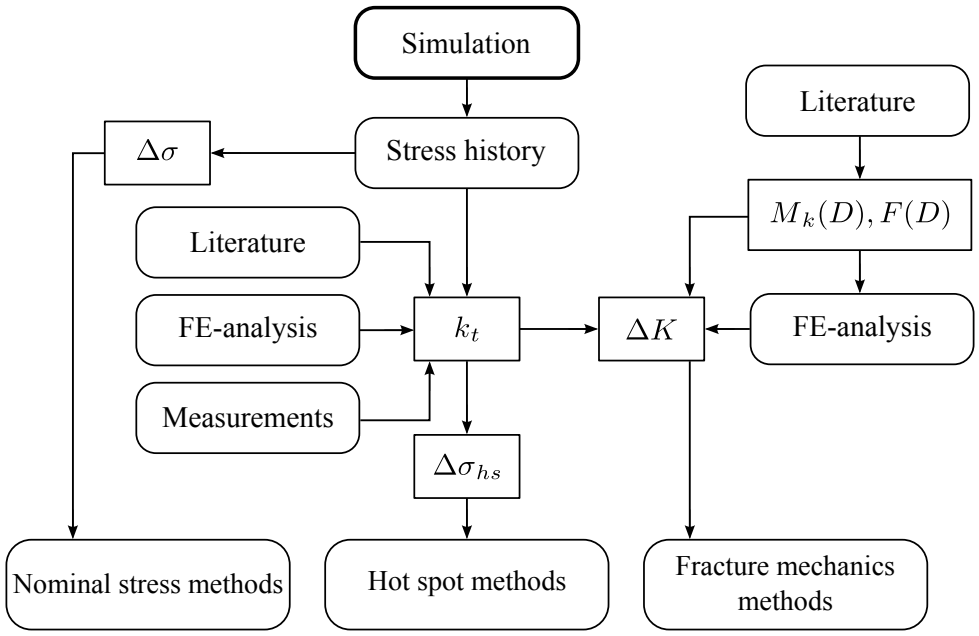

Figure 3.12. Combining simulated stress history and fatigue analysis approaches

CHAPTER 4

Stress calculation in multibody dynamic simulation

The multibody dynamic simulation approach has become a state-of-the-art method when complex machine systems need to be analyzed. This approach is based on the concept of replacing the actual system with an equivalent mathematical model made up from discrete members. Multibody simulation is powerful, especially when machine members undergo large translational and rotational motion. Consequently, multibody simulation can be used to analyze a wide variety of machines including robots, vehicles, manipulators, and mechanisms [42].

Mechanical industry products such as mobile machines and process machines comprise several different technology subsystems including mechanics, hydraulics, pneumatics, and control systems. These subsystems are in close interaction with each other. In mechatronic machines, mechanical components are driven by electronics under software control to define the behavior of the structural assembly. Therefore, the mechatronic machine must be analyzed as a coupled system to get accurate responses. Multibody simulation employs a generalized methodology that can describe coupled machine members using numerical methods to solve the nonlinear equations of motion with respect to time. Because of the generalized nature of the multibody simulation approach, equations that describe actuators and the control system can be coupled with the equations of motion [64]. In this way, several different engineering disciplines can be considered simultaneously and solved as a combined system.

Modern fabricated structures, especially load-bearing structures in mobile machinery, are susceptible to fatigue failure, because they contain multiple welded joints in which fatigue resistance is low. Fatigue life is normally assessed based

on simplified assumptions of machine usage. In some safety-critical structures, stress/strain histories are measured during service using strain gauges. More recently, stress histories are based on simulations combining multibody system models with finite element analysis. Stresses at critical locations in the structure are often the product of multi-degree-of-freedom loads. Consequently, three-dimensional multibody simulation models, including either a structural flexibility description or multi-degree-of-freedom strain gauge measurements, are required to determine the stress histories. Accurate stress information is essential to the design of safety-critical machine structures. In addition to being an important input in the design of structures, accurate stress information is crucial for the condition monitoring of the machine structures to estimate the remaining service life of the machine.

Stresses can somehow be obtained from rigid body dynamics by using simulated forces as force boundary conditions in finite element method. In general, to obtain structural stresses, structural flexibility should be taken into account. Concept of multibody dynamics gives attractive approach to simulate real operating conditions and thus obtain realistic loading conditions.

A stress history from a multibody dynamics simulation can be used as initial data for component dimensioning. Furthermore, it can provide loading data for the analyst that is otherwise difficult to obtain. Finally, the stress history can be used as input for the fatigue analysis of the component. In such cases, one should make sure that simulated operations describe the operating conditions of the machine with sufficient accuracy. With simulation, it is difficult to describe the impact of statistical issues, such as component wear and operator usage habits, on component loading. On the other hand, simulation helps to understand the causes and effects related to loading. This allows the use of optimization routines in component dimensioning. Simulation and measurement on a real-life machine can thus be considered to support each other, and using them together can help to reach an optimal solution.

4.1 Stress calculation methods

The displacement field in multibody dynamics for a flexible body i can be described using a vector of nodal displacement $\boldsymbol{u}^i$, which can be defined discretically with a modal matrix $\boldsymbol{\Phi}^i$ and a vector of generalized coordinates $\boldsymbol{q}^i$ as follows.

$$\boldsymbol{u}^i(\boldsymbol{c}, t) = \boldsymbol{\Phi}^i(\boldsymbol{c})\boldsymbol{q}^i(t), \tag{4.1}$$

where $\boldsymbol{u}^i$ is vector of displacements of body i at certain point and $\boldsymbol{c}$ is the position vector of a material point and $\boldsymbol{\Phi}^i(\boldsymbol{c})$ is a shape-function matrix that is only a function of spatial coordinates.

The displacement field can be used to describe the strain vector, which can be written as follows.

$$\boldsymbol{\varepsilon}^i = \begin{bmatrix} \varepsilon_{11} & \varepsilon_{22} & \varepsilon_{33} & 2\varepsilon_{12} & 2\varepsilon_{23} & 2\varepsilon_{31} \end{bmatrix}^{\mathrm{T}}, \tag{4.2}$$

where ε_{11}, ε_{22}, and ε_{33} are tension components and ε_{12}, ε_{23}, and ε_{31} are shear components of the strain vector $\boldsymbol{\varepsilon}^i$.

After completing the dynamic analysis, the time history for stresses $\boldsymbol{\sigma}^i(c,t)$ for all material point can be calculated from the strain vector. Stress history can be used, *e.g.*, for fatigue analysis and fatigue life prediction.

In multibody dynamics, stress calculation can be carried out using various methods that differ with respect to accuracy, computational efficiency, and usability. Ideally, the stress calculation method should contain all the necessary variables, should be simple to formulate, and should be numerically stable and efficient. The method should be useful for developing new designs or for analyzing existing designs. In addition, an ideal method should not contain independent procedures that are executed in series. Finally, method results should come in a simple and easily usable form. An ideal method does not yet exist. Therefore, the analyst must select the most appropriate method for a particular problem. Selecting the most suitable method can be straightforward, however, the selection should be given serious consideration.

There are three common approaches to obtaining stresses from multibody simulation: the force method, the displacement method, and the modal stress matrix method. In the force method, forces are obtained from simulation and later used as input for the finite element analysi to compute stress histories [59]. In practise, the approach also can be applied to compute nominal stresses for rigid bodies [19]. Arczewski and Fraczek described three categories of force-based methods [4], but in this work, all have been included in a single category. In the displacement method, displacements are obtained from simulation and are then used as boundary conditions for the finite element analysis [62, 11, 79]. In the modal stress matrix method, stresses are obtained using a modal stress matrix analogous to the modal matrix, but giving stress states instead of displacement fields [17, 7]. The following chapters briefly describe all three of the multibody simulation approaches to defining stresses.

Commercial multibody dynamics software programs often contain automatic routines that can develop loading cases for the finite element model from the loading data of the bodies. Usually, loading cases are determined for each simulated time step, which can result in a heavy computational burden for the finite element analysis. Alternatively, loading cases can be developed only for time steps in which stress values are relevant for design purposes. That is, loading cases are formulated only for time steps in which the largest and smallest stresses are seen. In practice, identifying such time steps is difficult and laborious.

4.2 The force method

Methods based on computed forces differ from each other in details and assumptions. Generally, in force-based methods, all the forces acting on a body over the desired time interval are taken from the dynamic simulation and applied to the body in the finite element analysis. According to D'Alembert's principle, all forces are dynamically in equilibrium for any point in time (during each time step). The finite element analysis is carried out in sequential linear steps, *i.e.*, it is a quasi-static analysis. To apply simulated forces during a finite element analysis, surface forces must be transformed at every time step into the local coordinate system of the body. Volumetric forces, such as gravity, can be accounted for separately [72]. As a result, a quasi-static stress distribution is obtained from the finite element analysis for the time interval of interest. Due to the quasi-static nature of the approach, high frequency loads are neglected. Since the highest excitation frequencies are typically much lower than the first eigenfrequency of a body, this simplification does not adversely affect the analysis results.

In the quasi-static analysis, the model is often simplified such that, for example, the behavior of tires and actuators is not taken into account. Flexibilities in a machine system, such as the flexibilities of mechanisms and actuators, interact. A flexible machine structure responds to a change in loading by immediately moving toward a new equilibrium state. The change in state is not instantaneous, and it is subject to inertial forces, which cause the structure to oscillate around the new equilibrium. Thus, the dynamic response of the system is composed of the combined effects of multiple different flexibilities. One must examine the activity of the entire mechanical system to establish its dynamic stresses accurately.

The equations of motion for a body i can be formulated using the Lagrange equation. In this approach, kinematic constraints can be taken into account as augmented algebraic equations by using Lagrange multipliers. The equations of motion for body i can be written as follows.

$$\mathrm{M}^i\ddot{\boldsymbol{q}}^i + \mathrm{K}^i\boldsymbol{q}^i + \mathrm{C}_{\boldsymbol{q}^i}^{i\,\mathrm{T}}\boldsymbol{\lambda}^i = \boldsymbol{Q}^{ik} + \boldsymbol{Q}^{iv} - \boldsymbol{Q}^{if}, \tag{4.3}$$

The equations of motion 4.3 can be solved for each time step giving the accelerations, velocities, positions, and Lagrange multipliers for the bodies in the system. With the help of constraint equations and Lagrange multipliers, constraint forces $\boldsymbol{F}_r^i$ applied to body i can be expressed as a vector:

$$\boldsymbol{F}_r^i = \mathrm{C}_{\boldsymbol{q}^i}^{i\,\mathrm{T}}\boldsymbol{\lambda}^i \tag{4.4}$$

In a dynamic analysis, the bodies of the multibody system are in equilibrium at each time step. For this reason, stresses in bodies can be calculated by estimating the velocities and accelerations, and the internal and external loading applied to the body. In simple cases, this can be done using analytical equations. For cases that are more complex, the finite element method is used. In the finite element method boundary conditions should approximately correspond to the constraints applied to the multibody model. The validity of the boundary conditions in the finite element model can be evaluated by examining the support reaction forces comparing them to reaction forces in multibody simulation. If the boundary conditions are realistic, the support reaction forces correspond approximately to the multibody dynamics results. Moreover, the load vectors obtained from multibody dynamic simulation are inputs for quasi-static finite element stress calculation. Instead of just computing stress distribution histories for the model, computation can be reduced to covering only selected critical points, *i.e.*, stress trajectories, if case-critical points are known in advance [19].

4.3 Displacement method

The displacement approach has its basis in the classical Ritz method, where deformation is described by a set of modal shape functions. In this approach, deformations obtained from multibody simulation are then transferred to the finite element analysis as boundary conditions.

The major drawback to the approach is that all nodes a certain body must be considered. This drawback can be overcome by dividing the bodies into sub-models. The displacement method can be extended by superposing the deformation modes that also include static correction modes.

The nodal displacement vector $\boldsymbol{u}^i$ can be obtained from multibody simulation. It works as an input for finite element analysis. Thus, the stress distribution in a selected domain can be computed as follows [11].

$$\boldsymbol{\sigma}^i(\boldsymbol{c},t) = \mathbf{H}^i(\boldsymbol{c})\mathbf{B}^i(\boldsymbol{c})\boldsymbol{u}^i(\boldsymbol{c},t), \tag{4.5}$$

where $\mathbf{H}^i$ is matrix of elastic coefficients, and $\mathbf{B}^i$ is the kinematic matrix that relates displacements to strains. Most conveniently, Equation 4.5 can be computed quasi-statically for every time step. Since the whole stress distribution can be computed, the highest stress concentrations can be found straightforwardly. The displacement approach can be applied to a sub-model to reduce coordinates for the overall stress calculation.

4.4 Modal stress matrix method

In modal methods, stresses for flexible bodies are reconstructed using the modal matrix. Strains are reconstructed after simulation, and stresses are then calculated based on strains. In these methods, the reconstructed dynamic responses of each component are focused into a body of the multibody simulation by transforming the physical coordinates of a body into modal coordinates using a modal matrix. The fundamental idea is to model the stress/strain field and then define the stresses using the finite element method [8].

Since the time history of all generalized coordinates contains the vector of modal coordinates $\boldsymbol{p}^i$, it is possible to use a modal stress matrix. The modal matrix $\boldsymbol{\Phi}^i$ which includes modal coordinates, gives the deformation distribution history for the elastic body for every time step. Multiplying the modal matrix and modal coordinates leads to the nodal displacement vector.

$$\bar{\boldsymbol{u}}_f^{iP} = \boldsymbol{\Phi}_R^{iP}\boldsymbol{p}^i \tag{4.6}$$

The displacement vector $\bar{\boldsymbol{u}}_f^{iP}$ can be evaluated for every time step, and therefore stresses can be calculated separately for every time step. This ensures that no relevant point in time is ignored.

The strains of the element can be calculated with the help of kinematic matrix $\mathbf{B}^{ik}$ as follows.

$$\boldsymbol{\varepsilon}^{ik} = \mathbf{B}^{ik}\bar{\boldsymbol{u}}^{ik}, \tag{4.7}$$

where $\bar{\boldsymbol{u}}^{ik}$ is the nodal coordinate vector of element k belonging to body i. The kinematic matrix of the element is obtained through partial differentiation of the shape function matrix with respect to nodal displacements. The element

stress state can be obtained from the strain vector $\boldsymbol{\varepsilon}^{ik}$ with the matrix of elastic coefficients $\mathbf{E}^{ik}$.

$$\boldsymbol{\sigma}^{ik} = \mathbf{E}^{ik}\boldsymbol{\varepsilon}^{ik} \tag{4.8}$$

By combining equations 4.7 and, 4.8, a connection between the modal coordinate vector of the body and the element stress state can be established as follows.

$$\boldsymbol{\sigma}^{ik} = \mathbf{E}^{ik}\mathbf{B}^{ik}\boldsymbol{\Phi}^{ik}\boldsymbol{p}^{i} \tag{4.9}$$

Matrix $\mathbf{E}^{ik}\mathbf{B}^{ik}\boldsymbol{\Phi}^{ik}$ allows the stress state of the element to be calculated when the modal coordinate values of the body are known. The accuracy of the stress state is affected by how well the shape functions used to describe flexibility can depict the deformation of a flexible body.

When the internal stresses of the element are examined, a transition must be made from body coordinates to element coordinates by multiplying the modal stress matrix with the inverse matrix of the transformation matrix $\mathbf{T}^{ik}$ as follows.

$$\hat{\boldsymbol{\sigma}}^{ik} = \mathbf{E}^{ik}\mathbf{B}^{ik}\mathbf{T}^{ik\,\mathrm{T}}\boldsymbol{\Phi}^{ik}\boldsymbol{p}^{i} \tag{4.10}$$

4.5 Stress calculation for the proposed method

As discussed, the literature provides several approaches to generate stress histories for a flexible body using multibody dynamic simulation results as input. In general, the quality of the stress results heavily depends on the accuracy of the description of flexibility. For the floating frame of reference formulation, proper mode selection plays an important role [11]. According to [4], force based methods suffer slightly from inaccuracies. Furthermore, the force boundary conditions are not trivial on sub-model boundaries. As a result, the force-based method will not be used in the method proposed here. In modal based approaches, the accuracy of stress results in places with structural discontinuities suffers because of the simplifications made in mode selection. In displacement-based methods, the accuracy of stress results near to structural discontinuities can be preserved by modeling stress raisers separately and adding them as sub-models. Therefore, the proposed method is based on the displacement-based stress recovery method.

In future development, it is important from the computational efficiency point of view to reduce sub-model coordinates using a modal reduction method. The

problem lies in the fact, that models that are described with modal coordinates cannot be constrained efficiently with nodal displacement boundary conditions, but mapping from modal to nodal and back must be done for every time step.

CHAPTER 5

Sub-modeling

A common cause of structural damage is local stress concentration due to structural geometry. Practically all structural damage occurs where one or more stress raisers are present. Problematic details are often combinations of several geometries that concentrate hazardous stresses. Stress raisers result from structural discontinuities in real structural features; such as welds, attachments grooves or holes. Typically, small discontinuities are neglected in dynamic simulation, since their effect on overall behavior is relatively small compared to their contribution to computational burden. Traditionally, the problem of stress raisers is solved by calculating nominal stress levels and then taking into account the effect of stress raisers by applying predefined stress concentration factors. The stress concentration factor concept cannot be a general approach, since it is obvious that all possible geometrical shapes and their combinations combined with complex loading cases cannot be predefined, especially if a specific but arbitrary level of accuracy is needed. Obviously, the general approach covering all kinds of geometrical combinations in the finite element method is to model them as they appear in the structure. Since stress values change drastically in the neighborhood of a structural discontinuity, a refined element mesh is required, which will lead to a large number of degrees of freedom. This approach is impractical due to the computational burden, especially in the case of dynamic simulation.

The sub-modeling approach is commonly used, and it can overcome the previously mentioned problems. With the approach some new problems arise, but they will be discussed later. In principal, a sub-model is a model inside of or on top of a large-scale model that describes a certain portion of the large-scale model. It can be used to attach a locally refined element mesh to the larger scale model, which

does not need to be changed. In sub-modeling, the simplified structural model is complemented by a more refined sub-model of structural details. The sub-models do not influence the operation of the system but get their boundary conditions and loading data from the larger simplified model. The sub-modeling approach is also referred to in the literature as the global/local approach [32].

In general, any model that is attached to the reduced model can be seen as a sub-model. The proposed method does not limit the methods that can be used to attach sub-models to the larger reduced model. sub-modeling was traditionally clearly distinguished from sub-structuring, but today the distinction is not that clear, since methods for connecting dissimilar meshes have been improved.

To clarify the difference between sub-structuring and sub-modeling, the sub-model, traditionally, does not affect the larger scale model, whereas a substructure does influence overall model behavior. A sub-model can be attached onto a model, whereas a sub-structure actually replaces parts of the larger model. A sub-model gets its boundary conditions from the large-scale model without affecting model stiffness. In contrast, a sub-structure is part of the larger scale structure, and in that sense affects its stiffness. In substructuring, the original model is divided into separate components to meet requirements caused by limited computational resources. In both approaches, sub-modeling and sub-structuring, similar methods for assembling models can be used. Since the beginning, the both methods have been approaching each other and it is not always clear, which of the methods is being used [12]. Even in a dynamic simulation, a sub-model is attached to the large-scale model quasi statically, which means that additional assumptions are not needed. In the case of the sub-structuring approach, additional approximations are imposed in dynamic simulation. A common name for dynamic sub-structuring is component mode synthesis. For component mode synthesis, many variants can be found in the literature [15, 40, 65]. Even though, Craig-Bampton method has some problems in high frequency range [35], it will be used in this work.

Sub-models can be used for local refining or to connect dissimilar meshes. Figure 5.1 illustrates the idea of sub-modeling. The two-dimensional plate structure has a groove as a structural discontinuity. The plate is first coarsely meshed. Then, the area around the groove is refined by attaching a sub-model. In Figure 5.1, the nodal divisions do not match, therefore nodal coupling cannot be applied straightforwardly. However, some boundary degrees of freedom interpolation method should be used. In general, attaching sub-models does not require overlapping nodes within the boundary region. Computation can be efficient if the general behavior of the structure is calculated with the simplified model and the details are examined separately.

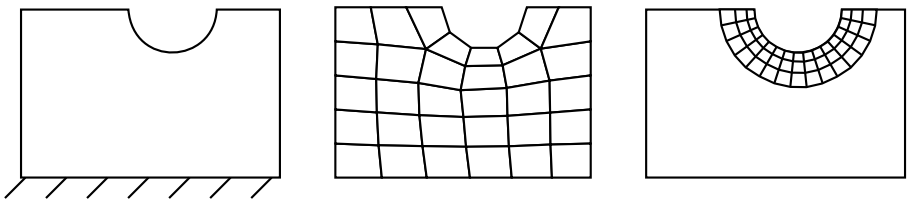

Figure 5.1. Schematic representation of the sub-modeling approach - For clarity, the coarse mesh is not shown together with the sub-model.

To study structural details in the framework of a finite element model, the element model should have a dense mesh. This, in turn, leads to finite element models with a large number of degrees of freedom, and therefore dynamic simulation becomes computationally burdensome. In this work, this problem is overcome by studying structural details separately and computing large-scale dynamics with a relatively coarser model. The coarse model does not account for the small details or the local stress concentrations. The rough model can be used to solve the general state of displacement of the structure. Details are modeled as sub-models that can be small but refined finite element models. Sub-models must be attached to the large-scale model. The following chapter discusses various methods of attaching sub-models to coarse dynamic models.

5.1 Assembling a finite element model by parts

Sub-modeling is an approach commonly used together with the finite element method. In the sub-modeling approach, two element models are combined. The most straightforward way of combining the sub-model domain into the large-scale domain is to use coupling equations with overlapping nodes. Coupling equations are easily applied, but the approach is not general. Typically, element model meshes can be dissimilar. In fact, connecting dissimilar meshes together has been, in the past, a key topic of sub-model discussion. There are also other aspects that make the approach of sub-modeling powerful. It can be used to combine the finite element models of sub-assemblies or assembly elements into a larger assembly. The approach does not require meshes to be similar and even element types can differ. Coincident nodes are not even required in some methods. The beneficial features of the sub-modeling approach can be used to assemble separate models or refine element meshing for a particular region without the need for a smooth refined mesh of the entire model. Furthermore, a sub-model can be changed out

with another sub-model without affecting the overall assembly. This improves the modularity of the design. For local refining, one of the biggest advantages is that meshes can be refined locally without modifying the overall assembly mesh.

As previously stated, the sub-modeling approach is often used to add needed detail to a particular local region. In the sub-modeling approach, there is no need for body meshes to match, which makes sub-modeling a means of increasing analytical efficiency. If the level of refinement differs significantly between two different models, *i.e.*, the gradient change of mesh size is too steep, some inaccuracies close to the boundary zones will result. In general, a coarse mesh tends to be too stiff, and displacements will be underestimated. If underestimated displacements are used as displacement boundary conditions, this will lead to non-conservative stress levels in the refined sub-model.

Moreover, the sub-modeling approach makes it possible to distribute large finite element models among multiple computers, which can be useful if computational power is a bottleneck in the design process.

5.2 Connecting dissimilar meshes

Similar meshes, in the matter of overlapping nodes and matching displacement interpolation functions between the nodes, can be connected by simply applying coupling equations. In general, meshes are dissimilar in a couple ways. Therefore, more general approaches should be considered.

In principle, dissimilar meshes are connected by projecting interface nodes onto the contacting surface. Or, they can already be defined to lay on the surface. This projection should be made to all contacting surfaces. After projection, the nodes are glued together with coupling equations. A common approach to connecting dissimilar meshes together in commercial software is to add a layer of interface elements between meshes.

In general, the connection between a sub-model and the larger model has many possible solutions. There are, in principle, two different approaches to attaching sub-models, which can be categorized as either meshless connection or connection using interface elements.

Several approaches in both categories for connecting dissimilar meshes can be found in the literature. Aminpour *et al.* [2] introduced the hybrid interface element formulation for connecting dissimilar meshes. Cho *et al.* [9] developed the concept of attaching dissimilar meshes using a penalty frame. Their method does not employ additional interface parameters that have to be solved, and it

preserves the symmetry of the global stiffness matrix. Another approach is to get boundary conditions from the coarse model and use them independently for the local model [56]. The latter approach leads to smaller dimensions and simpler modeling; therefore it is more practical in applications in which computational efficiency is crucial. Gmür and Schorderet [26] introduced three-dimensional interface elements to form a connection between solid elements and plate elements.

Furthermore, it is not uncommon that more than two meshes must be combined; and from a broader perspective, those multiple meshes may share the same boundary zone. Typically, this situation occurs when an entire model is made up of sub-models and is assembled out of those separate smaller parts. If element meshes have the same number of nodes, nodal coordinates, and element divisions; and if they used the same shape functions; the meshes can be combined by coupling their overlapping nodal degrees of freedom. Generally, this approach limits the element types that can be used and demands more effort in the mesh generation phase. [20]

Attaching dissimilar meshes leads to local disturbances at or near the contacting surfaces. Local disturbances are analogous to disturbances caused by boundary conditions, which are generated due to large force gradients. To overcome this problem, the point or area of interest should not be located too close to the connection zone. To test for the presence of disturbances, stresses can be computed on all surfaces near the connection zone. They should be approximately equal. For structural detail added to a larger model using sub-models, the boundary zone of the sub-model should be far away from the vicinity of interest, since the boundary conditions of the sub-model may introduce local disturbances. A common way to check if enough continuous material has been modeled around the detail of interest is to compare stress results for the boundary nodes of both models. The stress results should be approximately equal. In the sub-modeling approach, there is a risk of obtaining under predicted displacements from the coarse model that will result in underestimating stresses near a discontinuity. Typically coarse meshes are artificially stiffer than refined ones.

Connecting models together can be expressed mathematically, in general, as follows.

$$\boldsymbol{u}^i = \boldsymbol{u}^j \text{ on } \boldsymbol{s} = \boldsymbol{\Omega}^i \cap \boldsymbol{\Omega}^j, \tag{5.1}$$

where $\boldsymbol{u}^i$ and $\boldsymbol{u}^j$ are vectors of displacement for a particular point (not necessarily a node) in bodies i and j, respectively. In Equation 5.1, $\boldsymbol{s}$ is a common surface

between domains Ω^i and Ω^j. The boundary conditions are thus displacement boundary conditions or displacement control loading defined in advance for the sub-model.

5.3 Interface elements

In the literature, there are several classes and several methods for connecting sub-models using interface elements [56, 2, 20, 49, 10], in which a specific interface element layer is generated between the sub-model and master model. Interface elements are sometimes referred to as contact elements. In interface element methods, one layer of contact elements is added between meshes being attached together. Generally, for interface element methods, an interface layer is used to attach domains.

Interface elements may be classified as either two-field or three-field methods depending on the number of used field parameters. In two-field methods, displacements on bounding domains and Lagrange multipliers for constraints between displacements are treated as field variables. In three-field methods, the displacement of an interface element is treated as an additional field variable. In three-field methods, the interface layer should be discretized. Cho and Kim [9] improved the three-field method by adding penalty functions. The continuity of the displacement field over a boundary is only guaranteed though penalty parameters. Their method simplifies the three-field method by not imposing Lagrange multipliers $\boldsymbol{\lambda}$. In two-field methods, domains are attached using low order polynomials or Lagrange multipliers [58]. Two-field methods with Lagrange multipliers can be seen as interface element methods, because the Lagrange multipliers have to be discretized, and the methods form an interface mesh.

Dissimilar meshes can be connected using interface elements that map displacements between domains Ω^i and Ω^j. In Figure 5.2 this concept is schematically expressed.

Since the use of interface elements is straightforward, they are used in commercial codes for attaching dissimilar meshes. Interface elements introduce additional coordinates into the finite element model. Also, interface element approaches are typically more computationally demanding than methods that directly interpolate boundary degrees of freedom. Interface elements act as a mathematical constraint between two meshes. In general, there is no need to have a nodal point match between the interface layer and any of the element domains. The interface element layer is also discretized into several grid points, which are not finite element

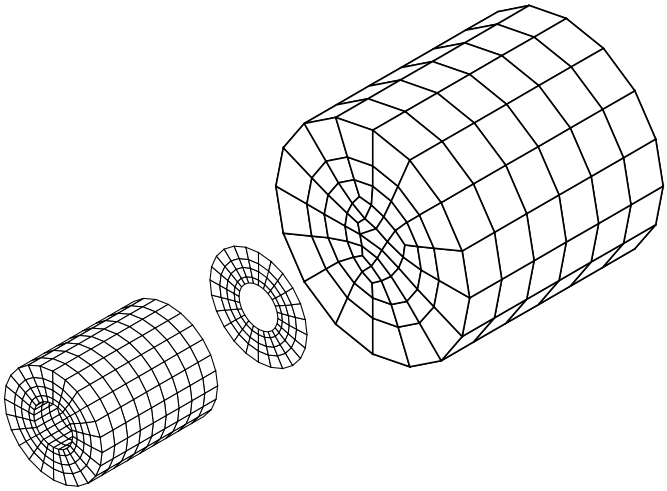

Figure 5.2. Concept of using interface elements with non-matching meshes

nodes. Even though interface elements are called elements, strictly speaking they are not finite elements in the traditional sense, since they do not have mass or volume. A complicated element interface surface can be described using B-spline functions [16]. A curve can be fit using a least squares approximation.

5.4 Field formulations

In two-field formulations, displacements of separate domains and Lagrange multipliers for constraints between domains are treated as field variables. In two-field formulations, Lagrange multipliers are introduced to force an approximate geometric compatibility between domains. In three-field formulations, the displacement of an interface element layer is treated as a third field variable. In four-field formulations [50] used variables are subdomain deformation modes, Lagrange multipliers, displacements of a frame and self-equilibrium modes of the frame. In the three-field hybrid variational formulation, the potential energy expression Π should be compatible between the sub domains. It can be expressed as in Equation 5.2.

$$\Pi = \Pi^{\Omega^i} + \Pi^{\Omega^j} + \int_s \boldsymbol{\lambda}^{i\,\mathrm{T}} \left(\boldsymbol{v}^s - \boldsymbol{u}^i \right) \mathrm{d}s + \int_s \boldsymbol{\lambda}^{j\,\mathrm{T}} \left(\boldsymbol{v}^s - \boldsymbol{u}^j \right) \mathrm{ds}, \qquad (5.2)$$

where $\boldsymbol{v}^s$ is the displacement vector on the interface surface $\boldsymbol{s}$, $\boldsymbol{\lambda}^i$ and $\boldsymbol{\lambda}^j$ are the vectors of Lagrange multipliers, and $\boldsymbol{u}^i$ and $\boldsymbol{u}^j$ are displacement vector on the

interface surface $\boldsymbol{s}$ for sub domains $\boldsymbol{\Omega}^i$ and $\boldsymbol{\Omega}^j$, respectively. To ensure continuity of displacement across the interface constraints, the integrals should be added. Field variables $\boldsymbol{u}^{ij}$, $\boldsymbol{v}^s$, and $\boldsymbol{\lambda}^{ij}$ are assumed independently. While assuming that displacement boundary conditions are satisfied for arbitrary $\boldsymbol{u}^{ij}$ in the sub domain and arbitrary $\boldsymbol{\lambda}^{ij}$ on the interface, the following equations should be added to reach equilibrium.

$$\boldsymbol{u}^{ij} = \boldsymbol{v}^s \tag{5.3}$$

$$\boldsymbol{\lambda}^{ij} = \boldsymbol{t}^{ij} \tag{5.4}$$

$$\boldsymbol{\lambda}^{i} + \boldsymbol{\lambda}^{j} = 0, \tag{5.5}$$

where $\boldsymbol{t}^{ij}$ is the traction on the interface for body i or j, and the the tractions sum is zero. Also, displacement field $\boldsymbol{u}^{ij}$ of the interface of the domains $\boldsymbol{\Omega}^i$ or $\boldsymbol{\Omega}^j$ is equal to the assumed displacement field $\boldsymbol{v}^s$. The displacement fields $\boldsymbol{u}^i$ and $\boldsymbol{u}^j$, and the Lagrange multipliers $\boldsymbol{\lambda}^i$ and $\boldsymbol{\lambda}^j$ are independently approximated for each finite element on the attachment surface in the sub domain. The displacement vector $\boldsymbol{u}^i$ and $\boldsymbol{u}^j$ on the interface can be expressed as follows using unknown nodal coordinates $\boldsymbol{g}^{ij}$.

$$\boldsymbol{u}^{ij} = \mathbf{N}^{ij}\boldsymbol{g}^{ij} \tag{5.6}$$

The matrix $\mathbf{N}^{ij}$ contains the element shape functions of $\boldsymbol{u}^{ij}$. The Lagrange multipliers are expressed using unknown coefficients as follows.

$$\boldsymbol{\lambda}^{ij} = \mathbf{R}^{ij}\boldsymbol{\alpha}^{ij}, \tag{5.7}$$

where $\mathbf{R}^{ij}$ is the matrix interpolating functions and $\boldsymbol{\alpha}^{ij}$; the vector of unknown coefficients. The assumed displacement field $\boldsymbol{v}^s$ can be expressed as follows.

$$\boldsymbol{v}^s = \mathbf{T}\boldsymbol{g}^s, \tag{5.8}$$

where the matrix $\mathbf{T}$ contains interpolation functions, and $\boldsymbol{g}^s$ is the displacements vector of the interface element. Now, total potential energy can be expressed as follows.

$$\Pi = \Pi^{\Omega^i} + \Pi^{\Omega^j} + \boldsymbol{\alpha}^{i\,\mathrm{T}}\mathbf{M}^{i\,\mathrm{T}}\boldsymbol{g}^i + \boldsymbol{\alpha}^{j\,\mathrm{T}}\mathbf{M}^{j\,\mathrm{T}}\boldsymbol{g}^j + \boldsymbol{\alpha}^{i\,\mathrm{T}}\mathbf{G}^{i\,\mathrm{T}}\boldsymbol{g}^s + \boldsymbol{\alpha}^{j\,\mathrm{T}}\mathbf{G}^{j\,\mathrm{T}}\boldsymbol{g}^s \tag{5.9}$$

Matrices $\mathbf{M}^{ij}$ and $\mathbf{G}^{ij}$ are integrals of surface s, and can be defined as follows.

$$\mathbf{M}^{ij} = -\int_s \mathbf{N}^{ij\,\mathrm{T}} \mathbf{R}^{ij} \mathrm{d}s \tag{5.10}$$

$$\mathbf{G}^{ij} = \int_s \mathbf{T}^{\mathrm{T}} \mathbf{R}^{ij} \mathrm{d}s \tag{5.11}$$

Integrals go over the interface surface $\boldsymbol{s}$. The three-field method gives the same load distribution over the interface as the continuous mesh.

5.5 Penalty frame method

In penalty frame method, the potential energy is expressed as follows. [9].

$$\Pi = \Pi^{\Omega^i} + \Pi^{\Omega^j} + \frac{1}{2}\int_s \left(\boldsymbol{v}^s - \boldsymbol{u}^i\right)^{\mathrm{T}} k \left(\boldsymbol{v}^s - \boldsymbol{u}^j\right) \mathrm{d}s \tag{5.12}$$

The displacement field $\boldsymbol{v}^s$ and the displacement field of sub domains $\boldsymbol{u}^{ij}$ can be approximated using the shape function matricies $\mathbf{T}^s$ and $\mathbf{N}^{ij}$ as follows.

$$\boldsymbol{u}^{ij} = \mathbf{N}^{ij} \boldsymbol{g}^{ij} \tag{5.13}$$

$$\boldsymbol{v}^s = \mathbf{T}^s \boldsymbol{g}^s \tag{5.14}$$

5.6 Multi-point constraints

Dissimilar element types can be attached using multi-point constraints. One example case of a beam-solid connection using a multi-point constraint can be seen in Figure 5.3. For solid element meshes, this approach does not guarantee displacement continuity for all nodes attached to the boundary.

The multi-point constraint approach can be used to combine models with different elements. In Figure 5.3, a multi-point constraint is applied using rigid links, so no relative displacement between attached domains is allowed.

In approaches that use multiple points to attach domains together, domains can be either slave or master. For multiple points in all domains, the displacement field is not continuous over the boundary and gaps or domain penetrations may occur, even though all constraints are satisfied. In some cases, this error can be tolerated and the approach can be used.

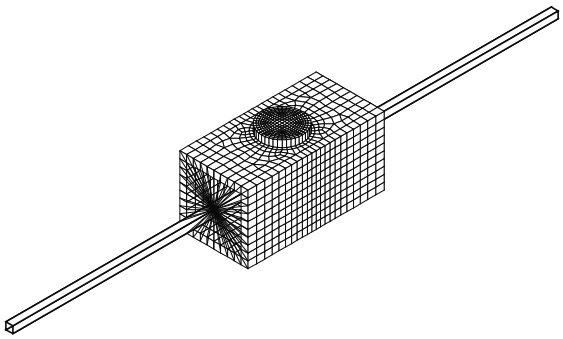

Figure 5.3. Sub-model attached to large-scale beam model with rigid webs

5.7 Meshless methods

In the literature, several meshless connection methods have been introduced [82, 29, 70], in which the concept may vary. In some methods, element shape functions are modified locally to make the displacement field continuous over the boundary. *E.g* Dohrmann *et al.* [20] presents a method for modifying shape functions of elements in the slave domain. Belytschko *et al.* presented general overview of meshless methods [6]. In meshless methods, master and slave domains are determined. Shape functions of elements in a slave domain are modified so the displacement field has a continuous bounding zone in both domains. One of the most significant benefit of using meshless methods is the reduced computational cost of refining the mesh, since there is no mesh. in linear dynamic simulation this befit can be neglected, but in particular cases like crack growth simulation, this benefit plays markable role.

5.8 Combining sub-model approach and dynamic analysis

The floating frame of reference formulation with model reduction is poorly suited for examining local stress. This is because the formulation is typically used to describe a complete body, in which structural details are omitted by model reduction since their contribution to overall dynamic performance is insignificant for a deformable body.

Irrespective of which methods are used to connect sub-models within a large-scale dynamic model; in the floating frame of reference, sub-models are attached using displacement boundary conditions on the attachment nodes of the sub-model.

These displacements are then used to solve a deformation state of the sub-model. Inside the sub-model, structural stresses are computed for fatigue life estimation from the deformation state.

The significant aspect of sub-modeling in the proposed approach is that coupling between the sub-model and the large-scale model is assumed to be unidirectional, *i.e.*, it is assumed the behavior of the reduced model in the dynamic simulation is not affected by the sub-model. That means, the large-scale model is complemented with a sub-model of the desired detail, and the sub-model does not affect the system's overall stiffness.

Information flow of the proposed method is schematically presented in Figure 5.4. In the proposed approach, the general behavior of the structure is calculated during dynamic analysis with a simplified model and the details are examined as a separate problem. This simplification makes dynamic simulation and stress calculation mutually independent. Therefore, the computation can be straightforwardly parallelized. For assessing fatigue loads on a structure, this assumption is sufficient, since any significant change in structural flexibility due to crack growth occurs late in the total life of a structure.

A fundamental motivation of the introduced approach is to keep the dynamic simulation as numerically efficient as possible. Therefore, the hosting structural model is simplified and is then reduced with the Craig-Bampton method [15]. Multibody simulation is used to produce displacement data for the sub-model, which is then analyzed to obtain fatigue data. Below in Figure 5.4, the process of using sub-modeling in fatigue analysis is shown.

Even though the proposed approach is general, boom-type structures that can be efficiently described with beam elements are studied in this work. With beam models, obtaining boundary conditions for sub-models is straightforward.

In the proposed approach, the analysis begins by creating a simplified beam model to describe the structural component. The dashed arrow in Figure 5.4 illustrates this concept. The model is reduced in this study using component mode synthesis. Next, a sub-model is created. The sub-model should be as small as possible, but it should be sufficiently large so disturbances near the boundaries do not influence stresses near the welded details. The concept of sub-modeling is shown in Figure 5.4. After every time step in the dynamic analysis, the nodal displacements for the reduced model are saved and used as external boundary conditions for the sub-models. Stress data that is suitable for fatigue assessment can be derived by solving sub-models with boundary conditions obtained from the dynamic simulation.

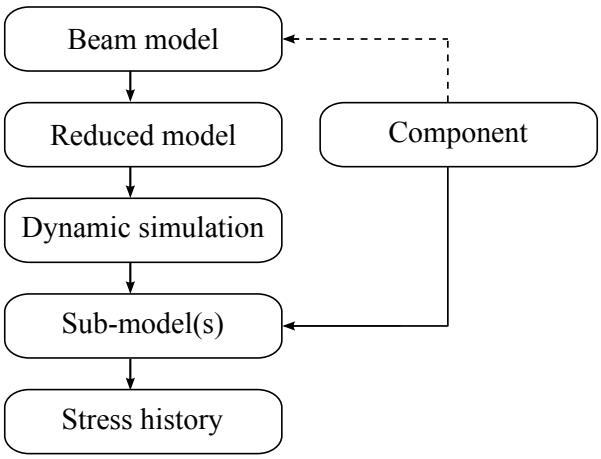

Figure 5.4. Schematic representation of the information flow in the proposed approach

From the flow chart in Figure 5.4, it should be noted that information is transferred in only one direction and all sub-models are solved independently. Even though processing of the sub-models can be easily parallelized, it can also be part of the post-processing procedure.

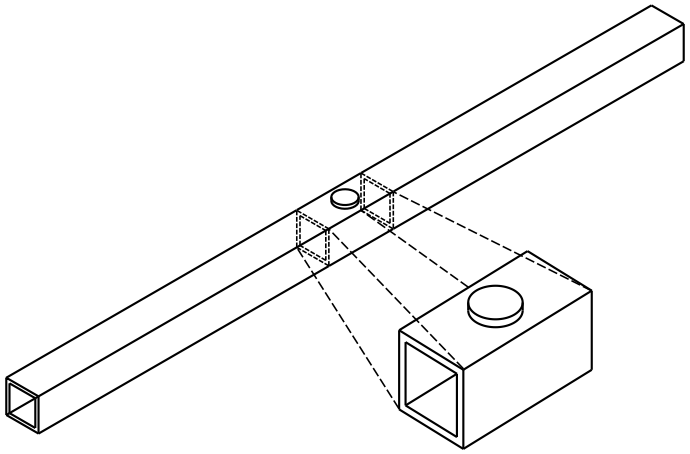

Figure 5.5. Structural component and sub-model of the volume surrounding the discontinuity

The sub-model should include not only the structural detail of interest, but also sufficient surrounding material to exclude the disturbances caused by boundary

conditions. One way to include this surrounding material is to extract elements from the large-scale model. This concept is shown in Figure 5.5. The beam model represents the center line of a structural component. The sub-model is attached to the interpolated locations of the reduced model via rigid and massless beams. Because rigid beam webs are used, the cross section is assumed constantly planar at the boundary condition points. The effect of this assumption is negligible with respect to stresses in the notch. In the dynamic simulation, translational and rotational displacements are solved as boundary conditions for the sub-model.

In general, sub-models are attached at arbitrary structural component locations, thus nodal displacement interpolation should be used. For the sake of simplicity, the sub-model coordinates are not reduced, even though using a non-reduced sub-model makes stress calculation computationally heavy. From the dynamic simulation efficiency point of view, this is not crucial, because stress can be analyzed for the sub-model independently of the dynamic simulation.

CHAPTER 6

Applying the method - numerical examples

Fatigue damage typically originates from the points of discontinuity of the structure, especially if there is residual stress in or around the discontinuity. In order for the machine system to be simulated efficiently or even in real-time, it must often be simplified, and details irrelevant in terms of structural stress neglected. The modeling of small details, such as welded clamp for a hydraulic pipe of a boom, increases the need for computational efficiency, and such details have only a localized importance. In this work the simplified dynamic simulation and relative accurate model of notch are combined together using sub-modeling techniques.

Coupling between the sub-model and the large-scale model is assumed to be one directional, *i.e.*, it is assumed that the behavior of the reduced model in dynamic simulation is not affected by the sub-model. That means, the large-scale model is complemented with a sub-model of the desired detail and it does not affect the system's overall stiffness. This crucial simplification makes dynamic simulation and stress calculation independent from each other. Therefore, the computation can be straight forwardly parallelized. Displacement boundary conditions of the sub-model, however, are acquired from the large-scale model. In the proposed approach, during dynamic analysis the general behavior of the structure is calculated with a simplified model and details are examined as a separate problem.

A fundamental motivation of the introduced approach is to keep the dynamic simulation as numerically efficient as possible. Therefore, the hosting structural model is simplified and is then reduced with the Craig-Bampton method [15].

Even though the proposed approach is general, in this work boom-type structures that can be efficiently described with beam elements are studied. With beam models, obtaining boundary conditions for sub-models is straightforward. In the proposed approach, multibody simulation is used for producing displacement data for the sub-model, which is then analyzed and fatigue data is obtained.

The beam model represents the center line of a structural component. The sub-model is attached to the interpolated locations of the reduced model via rigid and massless beams. Due to the use of rigid beam webs, the cross section is assumed to remain planar at the boundary condition points. The effect of this assumption, with respect to stresses in notch, is negligible. In dynamic simulation, translational and rotational displacements are solved as boundary conditions for the sub-model. In general, sub-models are attached at arbitrary locations of the structural component, thus nodal displacement interpolation should be used. Note that only displacement boundary conditions are transferred to the sub-model.

For sake of simplicity, the sub-model coordinates are not reduced, even though using a non-reduced sub-model makes stress calculating computationally heavy. From the dynamic simulation efficiency point of view, this is not crucial due to the fact that stress analysis for the sub model can be made independently from the dynamic simulation.

6.1 Numerical examples

In this study, a static example of a cantilever beam is used to evaluate the static error that occurs when describing a detailed finite element model as a coarse beam model. Also, error in model reduction is evaluated. For determining the decrease in computation burden, CPU times between detailed finite element model and the proposed method with non-reduced sub-model are compared. Comparison between the reduced model and the reference model in dynamic simulation with a sinusoidal tip load is shown. To show the efficiency of the method for obtaining stress history of a structural detail, a practical example of a drilling boom is studied.

6.1.1 Static example

In the following section, a comparison of static tests is made between the detailed finite element model and the beam model with reduced coordinates. The cantilever beam in Figure 6.1 is loaded on its free end with force $F_s = -10$ kN and vertical

Table 6.1. Properties of the cantilever beam and the cross section

Property	*Unit*
Height of the profile	0.1 m
Width of the profile	0.1 m
Thickness of the profile	0.01 m
Area of the profile	0.0036 m^2
Area moment of inertia	$0.492 \cdot 10^{-5}$ m^4
Shear correction factor	5/6
Length of the cantilever beam	2.0 m
Tip load	10 kN
Elastic modulus	2.1 GPa
Poisson's ratio	0.3

displacement on the free end is measured. The geometric values of the beam and cross-sectional properties used in the numerical example are shown in Table 6.1.

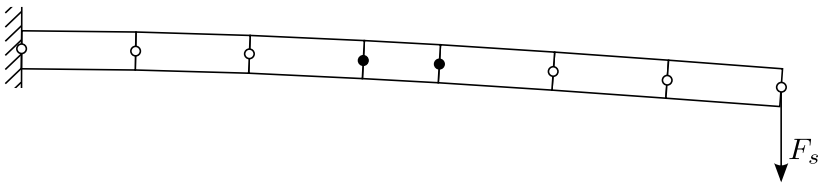

Figure 6.1. The coarse beam element model

The coarse beam element model of the cantilever beam, shown in Figure 6.1, is modeled with seven Timoshenko beams. Next, the beam model is reduced with the Craig-Bampton method and structural flexibility is described with two deformation modes. Since, in Craig-Bampton method static correction modes and unbounded modes are combined and orthogonalized, rigid body motions have to be removed. In this example, two transversal bending modes were used. The detailed finite element model is shown in Figure 6.2 (left) and is used for verification purposes. Furthermore, the finite element model contains a round attachment on the top surface in the center of the beam. In case of the coarse beam model the center is described with a sub-model, shown in Figure 6.2 (right).

The finite element mesh of the sub-model has 2000 linear, brick elements and 400 rigid, massless beams. The detailed finite element model is modeled with 9000 solid elements. At end C, the model is fixed at all nodes. The black lines seen on

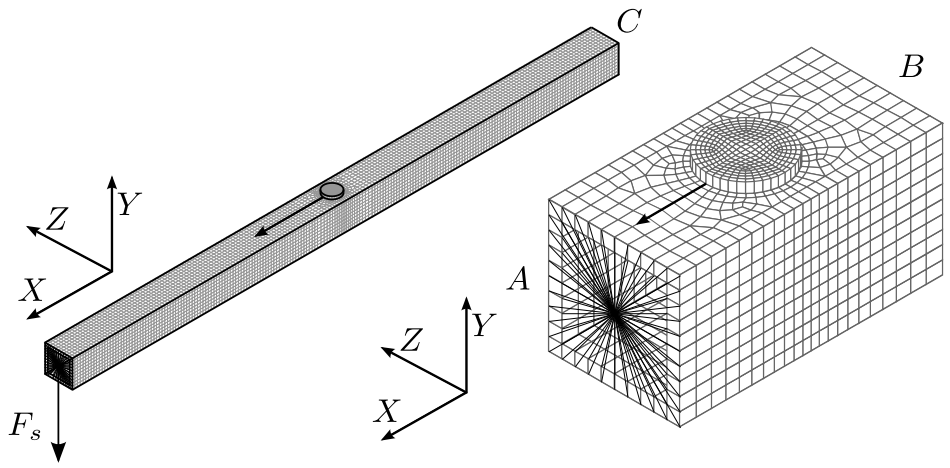

Figure 6.2. Detailed finite element model (left) and sub-model

side A, in Figure 6.2 (right), represent rigid and massless beam webs and connect the cross section of the sub-model to the dynamical model. The use of rigid beam webs keeps the boundary cross section of the sub-model planar. This clearly simplifying assumption is made because in the beam model the cross section is assumed to remains planar. In slender structures, cross-sectional deformation due to axial forces caused by bending is insignificant. Axial stress on the surface of the model is examined near the discontinuity, at the point and direction indicated by the arrow in Figure 6.2.

Since the sub-model and the reduced beam model have overlapping nodes, Figure 6.2 A and C, boundary conditions for the sub-model can be fixed based on nodal deformation from the reduced beam model. In the case of non-overlapping nodes, interpolation of nodal translational deformation and rotation deformation between nodes is required. In this case, interpolation could be made using Timoshenko beam shape functions. Since the sub-model only uses displacements obtained from the coarse model as boundary conditions, it does not interfere with the overall behavior of the model.

For comparison, the vertical displacement of the free end of the statically loaded cantilever structures are presented in Table 6.2.

Increased structural stiffness due to modal reduction can be observed.

Figure 6.3 presents the axial stress in the center cantilever beam as a function of the distance from the discontinuity, x, for the coarse beam model, the reduced model and the detailed FE model. The sub-models used with both the coarse beam

Table 6.2. Comparison of the vertical displacement of a cantilever beam at the free end

Model	*Displacement*
Detailed finite element model	-0.026135 m
Reduced model	-0.025860 m

and reduced beam models were had the same meshing as was used in the same region of the full beam model. For fatigue assessment the hot spot or structural stress is often used [46]. A linear surface extrapolation for hot spot stress [54] has been performed for each of the three stress distributions shown in Figure 6.3. The hot spot structural stress at the edge of the discontinuity, $x = 0$, is based on a linear extrapolation of surface stresses at nodes 4 mm and 10 mm from the edge of the discontinuity.

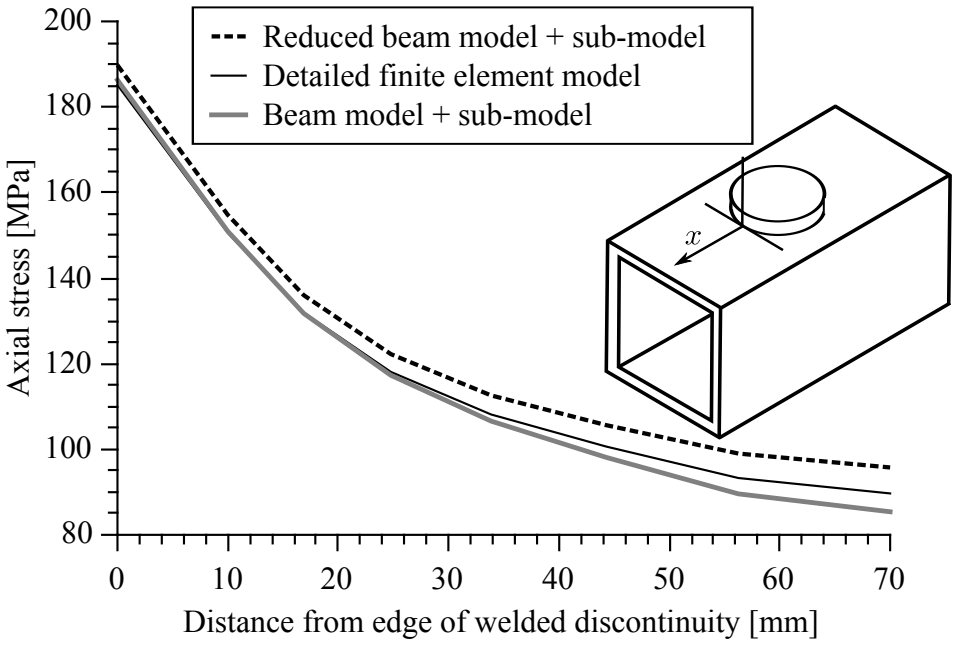

Figure 6.3. Comparison of stress results near the discontinuity

It can be noted from Figure 6.3 that, stress results close to the sub-model boundary, $x = 70$ mm, are more sensitive to local disturbances caused by boundary conditions. The influence of boundary conditions is seen in Figure 6.4 which shows the error in the computed stress results for beam and reduced models as a function of the distance from the discontinuity, x. At $x = 0$ mm the axial stress

computed from the reduced model is 2.5 % larger than the results obtained with the detailed finite element model. For the beam model the corresponding error is less than 1 %. Decreased accuracy due to modal reduction is observed for all x. This is mainly due to the inaccurate description of the displacement field near the boundary conditions using only the two lowest Craig-Bampton modes. Using more deformation modes to describe the displacement field will increase accuracy of the method while, however, burdening the computational efficiency.

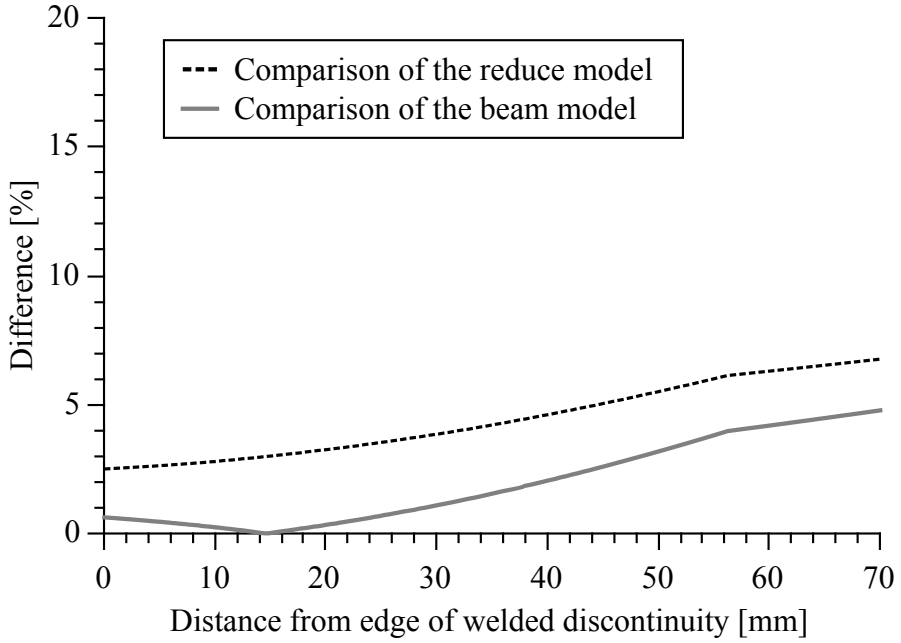

Figure 6.4. Difference in stress results near the discontinuity

6.1.2 Dynamic comparison

A comparison dynamic simulation test is made between the detailed finite element model and the reduced beam model in order to estimate both the computational time and any errors in the dynamic simulation. Stress values are computed in the post-processing phase while the sub-model in Figure 6.2 (right) is bounded on its boundary nodes. Displacement boundary conditions are obtained from dynamic simulation and are applied sequentially on the sub model. The node located on the supported end is fixed.

A harmonic load with a frequency of $\omega = 3$ rad/s is applied to the cantilever beam shown Figure 6.1. Parameters for the cantilever beam are shown in Table 6.1. The cantilever beam is loaded on its free end with force F_h.

$$F_h = 10 \text{ kN} \cdot \sin(\omega t) \tag{6.1}$$

The detailed finite element in Figure 6.2 (left) is loaded with the same force F_h as the reduced model in order to create a reference result. The hot spot stress history for the round attachment in the detailed finite element is obtained from the same model.

Time history of hot spot stresses obtained using the detailed model and the sub-modeling approach are compared in Figure 6.5. A constant time step of 10^{-4} s is used throughout the simulation.

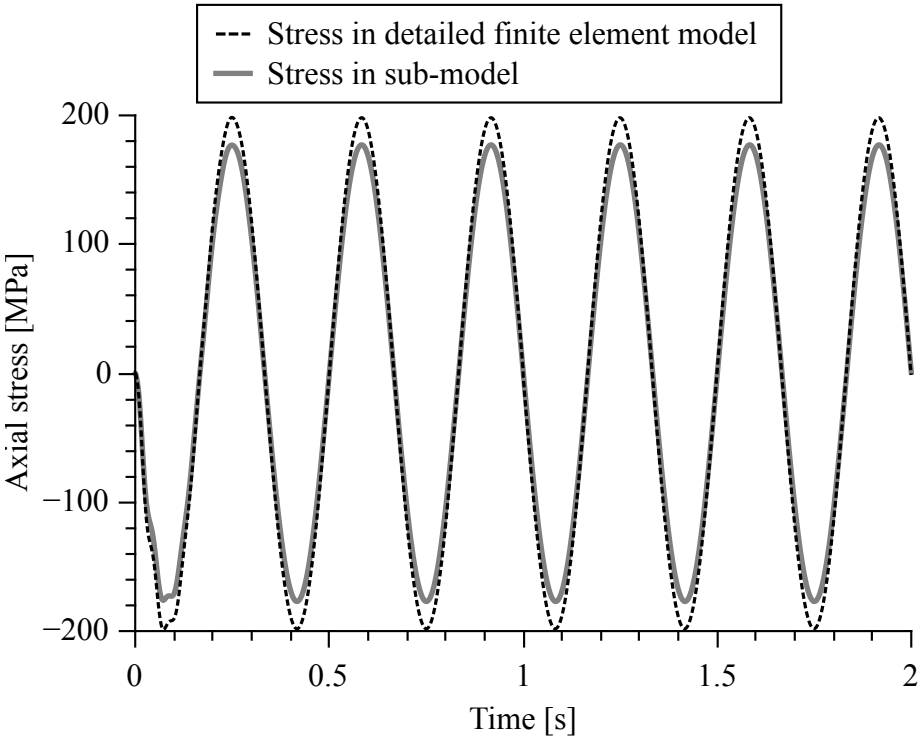

Figure 6.5. Stress comparison in harmonically loaded cantilever beam

It can be observed in Figure 6.5 that the system reaches steady state rapidly. It is also seen that the reduced beam model with sub-modeling results in a structural

Table 6.3. Comparison of the CPU times in dynamic simulation

Model	*CPU time*
Detailed finite element model	147 min 48 s
Reduced model	29 min 8 s

stress approximately 6 % greater than with the reference model. This is due to an inaccurate description of displacement field in the reduced model. In general, the error can be diminished by using more deformation modes, with the cost of an increased computational burden. Assumptions are made considering computational efficiency. From a fatigue point of view, a 6 % difference in computed stress would produce a 20 % difference in the computed fatigue life of a welded structure. In most cases this would be considered to be only a small source of error during fatigue assessment.

Even though coordinate reductions were not made in the sub-model, an 80 % decrease in computational time was observed due to the use of the proposed approach, Table 6.3. Also, the large-scale model contained only one detail. In a case of a complex detailed model, using a reduced model gives more significant benefits in terms of CPU time.

Commercial FE code (ANSYS[1] 11.0 for Linux) was used for measuring CPU times. One Intel T7200 core at 2.00 GHz was used. The operating system had Linux generic kernel version 2.6.32-34.

6.2 Drilling boom

A more detailed industrial example is illustrated using a simulation model of a hydraulic drilling boom. The model is of a Sandvik mining drill that is used to drill holes for explosives in tunnel mining operations, see Figure 6.6. The usual work cycle consists of the drill being positioned with the explosion pattern on the tunnel wall and then drilling a hole for the explosive charge. However, the machine is often misused, *e.g.*, by scaling which mean that the boom is used to pry loose rocks from the wall. Misuse severely compromises the longevity of the structure. The effects of such misuse are difficult and expensive to measure on real machines. Therefore, this is an ideal case to be used as a test scenario. The drilling boom is misused by bending it against the tunnel wall and the displacements of

[1]Website of Ansys software: http://www.ansys.com/Products/

two nodes of the beam are used as the boundary conditions for the stress analysis of a component from the beam.

6.2.1 Drilling boom model composition and work cycle

The drilling boom model consists of 12 bodies and 15 constraints. In addition to the structural components, the boom model also includes a complete hydraulic system, which is modeled using lumped fluid theory [76]. The model is currently used in the product development department of Sandvik Mining and Construction[2]. The model has been previously created by Mevea Ltd.[3] and is used with permission from both companies. The model has been verified using measurements from the real drilling boom and it is accurate enough to be used for product development purposes. The drilling boom is visualized in Figure 6.6.

Figure 6.6. Simulation model of a feed boom of a tunnel drill

The feed boom model consists of a Timoshenko beam model with 22 nodes as shown in Figure 6.7. The number of nodes was optimized to be as small as possible to allow for faster calculation but also large enough to keep the simulation

[2]Website of Sandvik Mining and Construction: http://www.miningandconstruction.sandvik.com/
[3]Website of Mevea Ltd.: http://www.mevea.fi/

Table 6.4. Feed boom FE-model cross-sectional properties

Property	*Profile 1*	*Profile 2*
Area of the profile	0.0114 m^2	$1.0 \cdot 10^{-9}$ m^2
Area moment of inertia (zz)	$4.86 \cdot 10^{-5}$ m^4	1 m^4
Area moment of inertia (yy)	$4.35 \cdot 10^{-5}$ m^4	1 m^4

stable with larger time-steps. The boom and the finite element beam model are shown in Figure 6.7. The beam has modeled using two different cross-sectional profiles (1 and 2, presented in Figure 6.7) and its properties are presented below in Table 6.4. The elastic coefficient for all of the elements was $70.0 \cdot 10^9$ Pa, Poisson's ratio 0.33 and density was scaled to 70007.35 kg/m^3 in order to achieve total mass of the system at 370 kg. Flexibility of the reduced model was described with two Craig-Bampton modes, a horizontal mode and a vertical mode with frequencies 14.30 Hz and 15.11 Hz, respectively.

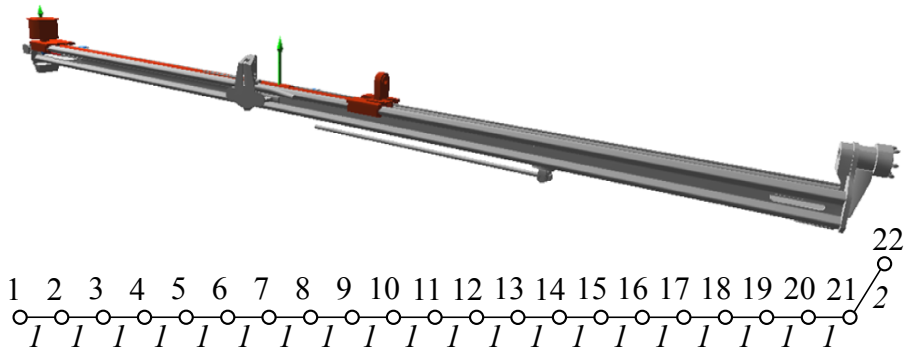

Figure 6.7. Feed boom of the tunnel drill and the beam element composition

Beam model of the feed boom, Figure 6.7, was compared with the full finite element model. Comparison was made between transversal static displacements and first and second eigenmodes. Eigenmodes for the comparison were calculated for fixed-free boundary condition *i.e.*, the beam was supported rigidly from node 1 and horizontally and vertically at node 21. Static displacement comparison was made using 1000 N force. Comparison results are presented in Table 6.5.

The simulated work cycle consisted of the end of the drill being first axially pressed against the tunnel wall. External load, due to contact between the wall and the feed boom, is applied on the tip of the feed boom (node 22). After a sufficient pressure for proper grip was established, the drill was turned to one side

Table 6.5. Comparison between the beam model and the full scale finite element model

Measure	*Full scale FE-model*	*Beam model*	*Difference*
Horizontal tip displacement	0.038895 m	0.037112 m	4.58 %
Vertical tip displacement	0.03646 m	0.033253 m	6.76 %
1. eigenmode (horizontal)	2.0 Hz	2.25 Hz	6.40 %
2. eigenmode (vertical)	2.08 Hz	2.38 Hz	14.40 %

so as to produce the prying action previously described. This operation produces a significant bending moment on the boom. The boom was then abruptly moved away from the wall releasing the axial stress and bending moment. The abrupt movement created significant dynamic vibrations and stress fluctuations. The nodal displacements from this reference run are presented in Figure 6.8. Both translational and rotational displacements were observed.

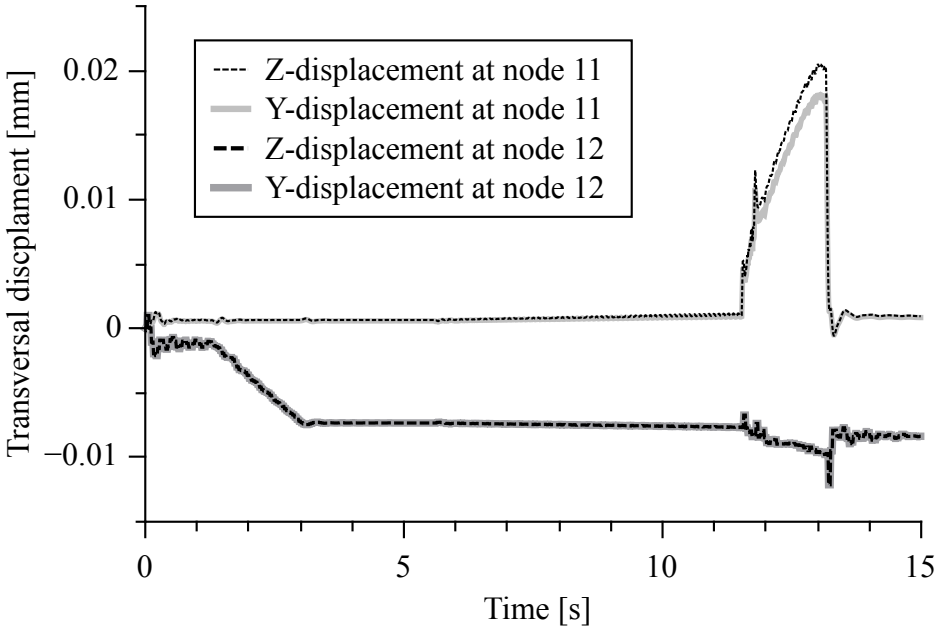

Figure 6.8. Transversal displacements of boundary nodes during simulation

6.2.2 Drilling boom model stress analysis

This displacement data is then used then as a boundary condition for the sub-model in Figure 6.9. Attachment nodes are nodes 11 and 12 depicted in Figure 6.7. The

sub-model contains the stress concentrations where fatigue damage can possibly occur. Nodal displacement history is applied as boundary conditions on the sub-model as a sequential set of static boundary conditions. In Figure 6.8, the sub-model for the feed boom is presented. It is modeled with 3000 solid elements and 400 beam elements were used for the rigid web.

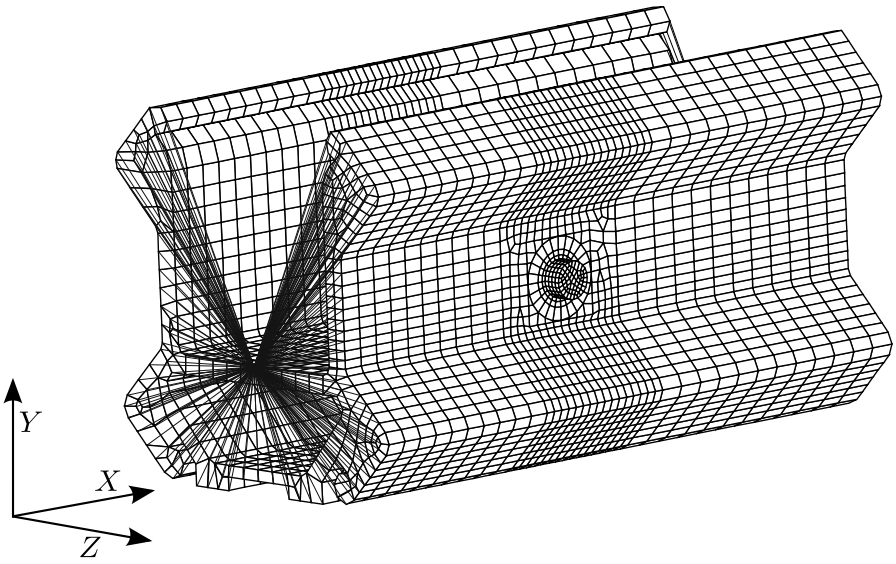

Figure 6.9. Sub-model attached to feed boom model

The welded notch in the sub-model is analyzed using displacements obtained from simulation. The linear surface extrapolation procedure for hot spot stress previously mentioned is used. Axial direction (x-direction) is selected for extrapolating hot spot stress on the edge of the notch. The selection of the direction of hot spot extrapolation is made based on the assumption that the majority of stresses are acting in the axial direction.

Hot spot stress history that was obtained using linear surface extrapolation [54] is shown in Figure 6.10. Stress component used as a raw data for extrapolation was the axial stress component on surface.

The stress history obtained for the welded detail can later be processed using the rainflow counting algorithm, fatigue assessment or for any other post-processing action. The purpose of presenting the second numerical example was to show practicality of the proposed approach. Error due to sub-modeling procedure was shown in previous example, thus the most significant source of error is the reduction of large-scale model into beam model.

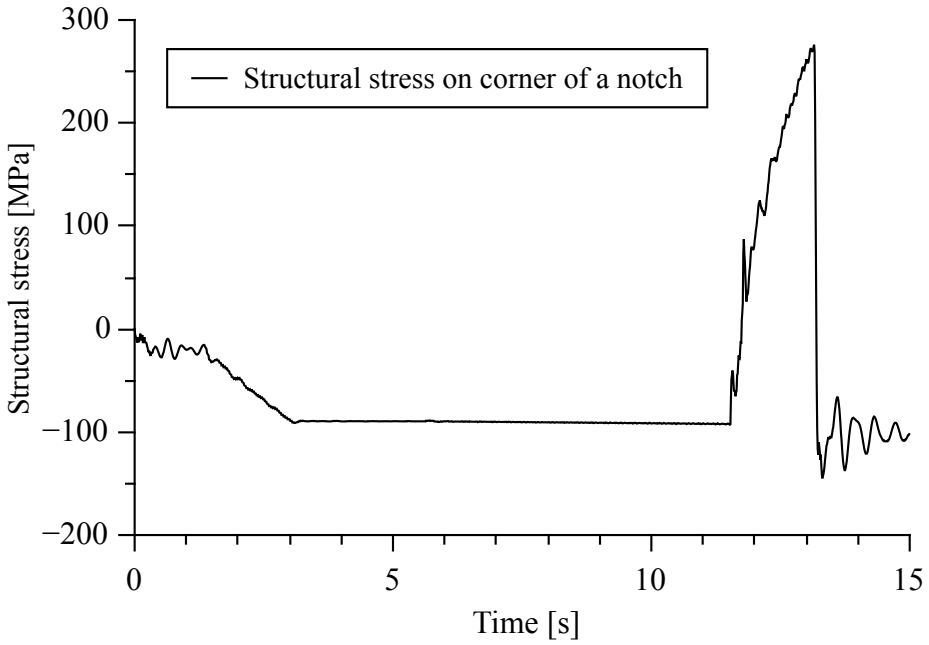

Figure 6.10. Stress history of a notch at the feed boom

The results of this numerical experiment show that the developed method can be used to determine the stresses of a structural detail using a real-time simulation model. This method enables a wide variety of uses from determining stresses from positions that cannot be measured from the real machine to determining the best practices for machine operation. Measuring bearing housing stresses, for example, in a real machine during an operation cycle is next to impossible. This method enables the determination of stresses during the entire operation cycle instead of just a suspected peak value. The method could be used to improve estimations on the machine durability as well as improving the machine durability already in the machine design phase. A practical example would be to use virtual prototyping in the machine product development phase. The model could then be used to run a series of reference operation cycles while recording displacement data from a structure. The recorded data could then be used to run analysis on several crucial parts of the structure in order to determine the life expectancy under operating conditions as well as different operators.

CHAPTER 7

Conclusions

In this work one approach of making fatigue analysis more usable among multibody simulation based product development is studied. In order to combine dynamic simulation and fatigue design this study introduces a novel approach for efficiently obtaining stress history from dynamic simulation.

This dissertation presents an approach in which the stress history for fatigue life estimation of an arbitrary structural discontinuity in a large-scale structure can be efficiently obtained in multibody simulation. In the proposed approach the structure is modeled with structured elements (*i.e.* planes or beams) in order to get rid small structural details to minimize nodal degrees of freedom. After that model is further reduced using component mode synthesis, in numerical examples, Craig-Bampton method was used, this model is called as reduced model. Reduced model is used to represent flexible body in multibody simulation. Small structural details are modeled separately and are attached to reduced model using suitable methods. In this dissertation, in numerical examples sub-models were attached to reduced model using rigid beam webs. Sub-models were analyzed quasi-statically within finite element codes using displacements, obtained from dynamic simulation, as boundary conditions. This analysis can be made during the dynamic simulation or in post-processing phase. Computations involving sub-modeling allow the fatigue assessment calculation to be separated from the dynamic simulation and structural details can be analyzed independently.

The presented method for using sub-modeling together with the floating frame of reference formulation can further be coupled with rainflow counting to obtain a computationally efficient method for estimating fatigue life of a component. A stress history obtained with multibody dynamic simulation can be used as

initial data for the fatigue analysis of the component. In such cases, one should make sure that the simulated operations describe the operating conditions of the machine with sufficient accuracy. Also, the stress history can be used as initial data in component dimensioning. This allows for producing loading data, which is otherwise difficult to obtain, with regards to machine simulation.

In many previous studies the entire structure is tried to solve and analyze at once, which is computationally overwhelming in a case of complex structures. In the proposed method problem is heavily simplified, but using sub-modeling techniques accuracy in deformation results is preserved locally. In other words, computational capacity is used on those areas that are assumed to be crucial from fatigue point of view. Note, stress history is not only obtained for some nodes, but for the entire area of concentrated stress.

One of the leading ideas in the proposed methods is to separate dynamic simulation and stress recovery from each other. It makes possible to freely select sub-models to be analyzed. Also, if it seems that some areas are not severe, they can be dropped away from analysis without modifying large-scale model or dynamic simulation model. All the main components of the proposed method were introduced and because method requires an appropriate selection of a certain component, interchangeable approaches were introduced.

The proposed method was introduced presenting set of numerical examples. In presented examples, the sub-model was coupled with a simplified beam model, which described the general behavior of the structure. Even though the approach is general, for the sake of simplicity, reduced beam models are used as an example of structures in dynamic simulation. The first example presented demonstrates that sub-modeling is suitable for a case in which the sub-model is coupled with the beam model, although in solid element models and beam element models, the boundary conditions correspond to each other only approximately. With the industrial example, a practical case was studied and the usability of a method for producing stress history was shown.

The assumption related to one directional coupling of the beam model and sub-model leads to a situation in which the sub-model is loaded by a series of static boundary conditions. In the future, coordinate reduction for the sub-model should be considered in order to reduce the computational burden. Also, multi-axial failure criteria can be discussed. Linear surface hot spot extrapolation used with axial stress does not take shear stresses into account. Torsion load on a crane can induce significant shear stresses in a notch and may have a considerable effect on fatigue life. This can be taken into account by using alternative damage hypotheses that considers shear stresses. This is a straightforward assumption,

but it may underestimate shear stress levels. Shear stress in a welded notch of a crane structure may occur if torsion is applied and distortion is present.

In future work the integration of fatigue analysis and produced stress history could be improved. The way how stress data is analyzed and compared to real fatigue test results differs from the stress results that can be straightforwardly obtained from dynamic simulation. In numerical examples, this aspect is taken into account using linear surface extrapolation to estimate hot-spot stress. The problem using that approach is the difficulty of knowing the most probable crack growth direction. In reality, crack may change the direction of growing depending on geometry and/or loading conditions. Also, in future work methods of attaching sub-model into simulation model should be studied carefully. Possibility to use coordinate reduction for sub-models and what kind of limitations it provides to attachment for sub-models.

BIBLIOGRAPHY

[1] AGRAWAL, O. P., AND SHABANA, A. A. Dynamic analysis of multibody systems using component modes. *Computers & Structures 21*, 6 (1985), 1303–1312.

[2] AMINPOUR, M. A., KRISHNAMURTHY, T., AND FADALE, T. Coupling of independently modeled three-dimensional finite element meshes with arbitrary shape interface boundaries. *AIAA Paper 98-2060* (1998), 3014–3024.

[3] AMZALLAG, C., GEREY, J., ROBERT, J., AND BAHUAUD, J. Standardization of the rainflow counting method for fatigue analysis. *International Journal of Fatigue 16*, 4 (1994), 287–293.

[4] ARCZEWSKI, K., AND FRĄCZEK, J. Friction models and stress recovery methods in vehicle dynamics modelling. *Multibody System Dynamics 14*, 3-4 (2005), 205–224.

[5] BATHE, K. J. *Finite element procedures*, 1st ed. Prentice Hall, New Jersey, 1996.

[6] BELYTSCHKO, T., KRONGAUZ, Y., ORGAN, D., FLEMING, M., AND KRYSL, P. Meshless methods: An overview and recent developments. *Computer Methods in Applied Mechanics and Engineering 139*, 1–4 (1996), 3–47.

[7] BRACCESI, C., AND CIANETTI, F. A procedure for the virtual evaluation of the stress state of mechanical systems and components for the automotive industry: development and experimental validation. *Proceedings of the Institution of Mechanical Engineers, Part D: Journal of Automobile Engineering 219*, 5 (2005), 633–643.

[8] CHIERICHETTI, M., MCCOLL, C., PALMER, D., RUZZENE, M., AND BAUCHAU, O. Combined analytical and experimental approaches to rotor components stress predictions. In *The 1st Joint International Conference on Multibody System Dynamics* (2010).

[9] CHO, M., AND KIM, W. A coupled finite element analysis of independently modeled substructures by penalty frame method. *Journal of Mechanical Science and Technology 16*, 10 (2002), 1201–1210.

[10] CHO, Y.-S., JUN, S., IM, S., AND KIM, H.-G. An improved interface element with variable nodes for non-matching finite element meshes. *Computer Methods in Applied Mechanics and Engineering 194*, 27-29 (2004), 3022–3046.

[11] CLAUS, H. A deformation approach to stress distribution in flexible multibody systems. *Multibody System Dynamics 6*, 2 (2001), 143–161.

[12] COOK, R., MALKUS, D., PLESHA, M., AND WITT, R. *Concepts and applications of finite element analysis*, 4th ed. John Wiley & Sons, New York, 2002.

[13] COTTREL, A. H. *Theory of Crystal Dislocations*, 1st ed. Blackie and Son, London, 1964.

[14] CRAIG, R. R., AND KURDILA, A. J. *Fundamentals of structural dynamics*, 2nd ed. John Wiley & Sons, New Jersey, 2006.

[15] CRAIG JR., R. R., AND BAMPTON, M. C. C. Coupling of substructures for dynamic analyses. *AIAA Journal 6*, 7 (1968), 1313–1319.

[16] DIERCKX, P. *Curve and surface fitting with splines*. Oxford University Press, New York, 1993.

[17] DIETZ, S. *Vibration and fatigue analysis of vehicle systems using component modes*. Doctoral thesis, Technische Universität Berlin, 1999.

[18] DIETZ, S., NETTER, H., AND SACHAU, D. Fatigue life predictions by coupling finite element and multibody systems calculations. In *Proceedings of Design Engineering Technical Conferences* (1997).

[19] DIETZ, S., NETTER, H., AND SACHAU, D. Fatigue life prediction of a railway bogie under dynamic loads through simulation. *Vehicle System Dynamics 29*, 6 (1998), 385–402.

[20] DOHRMANN, C. R., KEY, S. W., AND HEINSTEIN, M. W. Methods for connecting dissimilar three-dimensional finite element meshes. *International Journal for Numerical Methods in Engineering 47*, 5 (2000), 1057–1080.

[21] DONG, P. A structural stress definition and numerical implementation for fatigue analysis of welded joints. *International Journal of Fatigue 23*, 10 (2001), 865–876.

[22] DOWLING, N. E. *Mechanical Behavior of Materials: Engineering Methods for Deformation, Fracture, and Fatigue*, 3rd ed. Prentice Hall, New Jersey, 2007.

[23] EBERHARD, P., AND SCHIEHLEN, W. Computational dynamics of multibody systems: History, formalisms, and applications. *Journal of Computational and Nonlinear Dynamics 1*, 3 (2006), 3–12.

[24] ETUBE, L. *Fatigue and Fracture Mechanics of Offshore Structures*, 1st ed. Professional Engineering Publishing, London, 2001.

[25] FROST, N. E., MARSH, K. J., AND POOK, L. P. *Metal fatigue*, 1st ed. Clarendon Press, Oxford, 1974.

[26] GMÜR, T., AND SCHORDERET, A. A set of three-dimensional solid to shell transition elements for structural dynamics. *Computers & Structures 46*, 4 (1993), 583–591.

[27] HAAGENSEN, P. J., AND MADDOX, S. J. *IIW Recommendations on Post Weld Fatigue Life Improvement of Steel and Aluminium Structures*. International Institute of Welding, Paris, 2011.

[28] HAUG, E. J. *Computer aided kinematics and dynamics of mechanical systems, Vol. 1. basic methods*, 2nd ed. Allyn and Bacon, Massachusetts, 1989.

[29] HUERTA, A., AND FERNÁNDEZ-MÉNDEZ, S. Enrichment and coupling of the finite element and meshless methods. *International Journal for Numerical Methods in Engineering 48*, 11 (2000), 1615–1636.

[30] IIDA, K. Application of the hot spot strain concept to fatigue life prediction. *Welding in the World 22*, 9-10 (1984), 222–247.

[31] JUN, K., PARK, T., LEE, S., JUNG, S., AND YOON, J. Prediction of fatigue life and estimation of its reliability on the parts of an air suspension system. *International Journal of Automotive Technology 9*, 6 (2008), 741–747.

[32] KNIGHT, N. F., RANSOM, J. B., GRIFFIN, O. H., AND THOMPSON, D. M. Global/local methods research using a common structural analysis framework. *Finite Elements in Analysis and Design 9*, 2 (1991), 91–112.

[33] KORKEALAAKSO, P., MIKKOLA, A., RANTALAINEN, T., AND ROUVINEN, A. Description of joint constraints in the floating frame of reference formulation. *Proceedings of the Institution of Mechanical Engineers, Part K: Journal of Multi-body Dynamics 223*, 2 (2009), 133–145.

[34] KORKEALAAKSO, P., MIKKOLA, A., AND ROUVINEN, A. Multi-body simulation approach for fault diagnosis of a reel. *Proceedings of the Institution of Mechanical Engineers, Part K: Journal of Multi-body Dynamics 220*, 1 (2006), 9–19.

[35] KOUTSOVASILIS, P., AND BEITELSCHMIDT, M. Comparison of model reduction techniques for large mechanical systems. *Multibody System Dynamics 20*, 2 (2008), 111–128.

[36] LEE, S.-H., PARK, T.-W., PARK, J.-K., YOON, J.-W., JUN, K.-J., AND JUNG, S.-P. Fatigue life analysis of wheels on guideway vehicle using multibody dynamics. *International Journal of Precision Engineering and Manufacturing 10*, 5 (2009), 79–84.

[37] MADDOX, S. J. The effect of mean stress on fatigue crack propagation a literature review. *International Journal of Fracture 11*, 3 (1975), 389–408.

[38] MADDOX, S. J. *Fatigue strength of welded structures*, 2nd ed. Abington Publishing, Cambridge, 1991.

[39] MARQUIS, G. *Variable Amplitude Loading*. Woodhead Publishing Ltd, Cambridge, 2011, ch. 8, pp. 208–238.

[40] MEIROVITCH, L., AND KWAK, M. K. Rayleigh-Ritz based substructure synthesis for flexible multibody systems. *American Institute of Aeronautics and Astronautics Journal 29*, 5 (1991), 1709–1719.

[41] MELZER, F. Symbolic computations in flexible multibody systems. *Nonlinear Dynamics 9*, 1-2 (1996), 147–163.

[42] MIKKOLA, A. M. *Studies on fatigue damage in a hydraulically driven boom system using virtual prototype simulations*. Doctoral thesis, Lappeenranta University of Technology, 1997.

[43] MINER, M. A. Cumulative damage in fatigue. *Journal of Applied Mechanics 12*, 3 (1945), 159–164.

[44] MURAKAMI, Y. *Metal Fatigue: Effects of Small Defects and Nonmetallic inclusions*, 1st ed. Elsevier Science, Oxford, 2002.

[45] NIEMI, E. *Stress determination for fatigue analyses of welded components*, 1st ed. Abington Publishing, Cambridge, 1995.

[46] NIEMI, E., FRICKE, W., AND MADDOX, S. J. *Fatigue analysis of welded components: Designer's guide to the structural hot-spot stress approach*, 1st ed. Woodhead Publishing, Cambridge, 2006.

[47] NIKRAVESH, P. E., AND CHUNG, I. S. Application of Euler parameters to the dynamic analysis of three-dimensional constrained mechanical systems. *Journal of Mechanical Design 104*, 4 (1982), 785–791.

[48] PALMGREN, A. Die Lebensdauer von Kugellagern. *Zeichscrift des Verein Deutscher Ingenieure 68*, 14 (1924), 339–341.

[49] PANTANO, A., AND AVERILL, R. C. A penalty-based finite element interface technology. *Computers & Structures 80*, 22 (2002), 1725–1748.

[50] PARK, K. C., FELIPPA, C. A., AND G., R. A simple algorithm for localized construction of non-matching structural interfaces. *International Journal For Numerical Methods In Engineering 53*, 9 (2002), 2117–2142.

[51] PETERSON, R. E. *Stress concentration factors*, 1st ed. John Wiley & Sons, New York, 1974.

[52] PILKEY, W. D. *Peterson's Stress Concentration Factors*, 2nd ed. John Wiley & Sons, New York, 1997.

[53] POOK, L. *Metal Fatigue What it is, why it matters*, 1st ed. Springer, Dordrecht, 2007.

[54] POUTIAINEN, I., TANSKANEN, P., AND MARQUIS, G. Finite element methods for structural hot spot stress determination - a comparison of procedures. *International Journal of Fatigue 26*, 11 (2004), 1147–1157.

[55] QU, Z.-Q. *Model order reduction techniques with applications in finite element analysis*, 1st ed. Springer, London, 2004.

[56] RANSOM, J. B., MCCLEARY, S. L., AND AMINPOUR, M. A. A new interface element for connecting independently modeled substructures. In *AIAA/ASME/ASCE/AHS/ASC 34th Structures, Structural Dynamics, and Materials Conference* (1993).

[57] RANTALAINEN, T. T., MIKKOLA, A. M., MOISIO, S. M., AND MARQUIS, G. B. A method for obtaining the fatigue stress history from a flexible multibody simulation using the sub-modeling approach. *Mechanics Based Design of Structures and Machines* (Accepted).

[58] RIXEN, D., FARHAT, C., AND GÉRADIN, M. A two-step, two-field hybrid method for the static and dynamic analysis of substructure problems with conforming and non-conforming interfaces. *Computer Methods in Applied Mechanics and Engineering 154*, 3-4 (1998), 229–264.

[59] RYU, J., KIM, S.-S., AND KIM, S.-S. An efficient computational method for dynamic stress analysis of flexible multibody systems. *Computers & Structures 42*, 6 (1992), 969–977.

[60] SAKAI, T., AND SHIOZAWA, K., Eds. *Databook on Fatigue Strength of Metallic Materials*. Elsevier Science, Amsterdam, 1996.

[61] SCHIEHLEN, W. Multibody system dynamics: Roots and perspectives. *Multibody System Dynamics 1*, 2 (1997), 149–188.

[62] SCHWERTASSEK, R., DOMBROWSKI, S., AND WALLRAPP, O. Modal representation of stress in flexible multibody simulation. *Nonlinear Dynamics 20*, 4 (1999), 381–399.

[63] SHABANA, A. A. Flexible multibody dynamics: Review of past and recent developments. *Multibody System Dynamics 1*, 2 (1997), 189–222.

[64] SHABANA, A. A. *Dynamics of Multibody Systems*, 3rd ed. Cambridge University Press, Cambridge, 2005.

[65] SHYU, W.-H., MA, Z.-D., AND HULBERT, G. M. A new component mode synthesis method: Quasi-static mode compensation. *Finite Elements in Analysis and Design 24*, 4 (1997), 271–281.

[66] SMITH, R. A., AND MILLER, K. J. Prediction of fatigue regimes in notched components. *International Journal of Mechanical Sciences 20*, 4 (1978), 201–206.

[67] SOCIE, D. F., AND MARQUIS, G. B. *Multiaxial fatigue*, 1st ed. Society of Automotive Engineers, Warrendale, 2000.

[68] STEPHENS, R. I., FETEMI, A., STEPHENS, R. R., AND FUCHS, H. O. *Metal fatigue in engineering*, 2nd ed. John Wiley & Sons, New York, 2001.

[69] TAYLOR, D., AND WANG, G. A critical distance approach which unifies the prediction of fatigue limits for large and small cracks and notches. In *Proceedings of Fatigue'99* (1999).

[70] TIAN, R., AND YAGAWA, G. Non-matching mesh gluing by meshless interpolation - An alternative to Lagrange multipliers. *International Journal for Numerical Methods in Engineering 71*, 4 (2007), 473–503.

[71] TOBIAS, C., AND EBERHARD, P. Stress recovery with Krylov-subspaces in reduced elastic multibody systems. *Multibody System Dynamics 25*, 4 (2011), 377–393.

[72] WALLRAPP, O. Flexible bodies in multibody system code. *Vehicle System Dynamics 30*, 3-4 (1998), 237–256.

[73] WALLRAPP, O., AND WIEDEMANN, S. Comparison of results in flexible multibody dynamics using various approaches. *Nonlinear Dynamics 34*, 1 (2003), 189–206.

[74] WASFY, T. M., AND NOOR, A. K. Computational strategies for flexible multibody systems. *Applied Mechanics Reviews 56*, 6 (2003), 553–613.

[75] WATSON, P., AND DABELL, B. J. Cycle counting and fatigue damage. *Journal of the Society of Environmental Engineers 15*, 3 (1976), 3–8.

[76] WATTON, J. *Fluid power systems: Modeling, simulation, analog and microcomputer control*, 1st ed. Prentice Hall, New York, 1989.

[77] WINFREY, R. C. Elastic link mechanism dynamics. *ASME Journal of Engineering for Industry 93*, 1 (1971), 268–272.

[78] YEH, H.-F., AND DOPKER, B. Deformation mode selection and mode orthonormalization for flexible body system dynamics. *Computers & Structures 34*, 4 (1990), 615–627.

[79] YIM, H. J., HAUG, E. J., AND DOPKER, B. Concurrent engineering of mechanical systems. Tech. Rep. R-79, The University of Iowa, 1989.

[80] YIM, H. J., AND LEE, S. B. An integrated CAE system for dynamic stress and fatigue life prediction of mechanical systems. *Journal of Mechanical Science and Technology 10*, 2 (1996), 158–168.

[81] YOUNG, W., AND BUDYNAS, R. *Roark's Formula for Stress and Strain*, 7th ed. McGraw-Hill, New York, 2002.

[82] ZHAO, C., HOBBS, B. E., MÜHLHAUS, H. B., AND ORD, A. A consistent point-searching algorithm for solution interpolation in unstructured meshes consisting of 4-node bilinear quadrilateral elements. *International Journal for Numerical Methods in Engineering 45*, 10 (1999), 1509–1526.

ACTA UNIVERSITATIS LAPPEENRANTAENSIS

452. PHAM, ANH TUAN. Sewage sludge electro-dewatering. 2011. Diss.

453. HENNALA, LEA. Kuulla vai kuunnella – käyttäjää osallistavan palveluinnovoinnin lähestymistavan haasteet julkisella sektorilla. 2011. Diss.

454. HEINIMÖ, JUSSI. Developing markets of energy biomass – local and global perspectives. 2011. Diss.

455. HUJALA, MAIJA. Structural dynamics in global pulp and paper industry. 2011. Diss.

456. KARVONEN, MATTI. Convergence in industry evolution. 2011. Diss.

457. KINNUNEN, TEEMU. Bag-of-features approach to unsupervised visual object categorisation. 2011. Diss.

458. RUUSKANEN, VESA. Design aspects of megawatt-range direct-driven permanent magnet wind generators. 2011. Diss.

459. WINTER, SUSANNA. Network effects: scale development and implications for new product performance. 2011. Diss.

460. JÄÄSKELÄINEN, ANSSI. Integrating user experience into early phases of software development. 2011. Diss.

461. KÄÄRIÄINEN, TOMMI. Polymer surface modification by atomic layer deposition. 2011. Diss.

462. KOCHURA, ALEKSEY. Growth, magnetic and transport properties of InSb and II-IV-As2 semiconductors doped with manganese. 2011. Diss.

463. PUTKIRANTA, ANTERO. Possibilities and challenges of longitudinal studies in operations management. 2011. Diss.

464. HAPPONEN, ARI. Muuttuvaan kysyntään sopeutuva varastonohjausmalli. 2011. Diss.

465. VASAVA, PARITOSH. Application of computational fluid dynamics in modelling blood flow in human thoracic aorta. 2011. Diss.

466. PURO, LIISA. Identification of extractives and polysaccharides as foulants in membrane filtration of pulp and paper mill effluents. 2011. Diss.

467. LAPPALAINEN, PIA. Socially Competent Leadership – predictors, impacts and skilling in engineering. 2012. Diss.

468. PLAMTHOTTATHIL, ANSHY OONNITTAN. Application of electrokinetic Fenton process for the remediation of soil contaminated with HCB. 2012. Diss.

469. EBRAHIMI, FATEMEH. Synthesis of percarboxylic acids in microreactor. 2012. Diss.

470. JANTUNEN, SAMI. Making sense of software product requirements. 2012. Diss.

471. VILKO, JYRI. Approaches to supply chain risk management: identification, analysis and control. 2012. Diss.

472. TANSKANEN, VESA. CDF modelling of direct contact condensation in suppression pools by applying condensation models of separated flow. 2012. Diss.

473. HUHTANEN MIKKO. Software for design of experiments and response modelling of cake filtration applications. 2012. Diss.

474. PARJANEN, SATU. Creating possibilities for collective creativity Brokerage functions in practice-based innovation. 2012. Diss.

475. KUKKONEN, SAKU. Generalized differential evolution for global multi-objective optimization with constraints. 2012. Diss.

476. LAAKSONEN, JONNA. Tactile-proprioceptive robotic grasping. 2012. Diss.

477. KALLIO, ANNE. Enhancing absorptive capacity in a non-research and development context An action research approach to converting individual observations into organizational awareness. 2012. Diss.

478. LÄTTILÄ, LAURI. Improving transportation and warehousing efficiency with simulation based decision support systems. 2012. Diss.

479. OYOMNO, WERE. Usable privacy preservation in mobile electronic personality. 2012. Diss.

480. LINNALA, MIKKO. Simulation and optimization tools in paper machine concept design. 2012. Diss.

481. KORPIJÄRVI, JUHA. Aging based maintenance and reinvestment scheduling of electric distribution network. 2012. Diss.

482. KORHONEN, JUHAMATTI. Active inverter output filtering methods. 2012. Diss.

483. KŁODOWSKI, ADAM. Flexible multibody approach in bone strain estimation during physical activity: quantifying osteogenic potential. 2012. Diss.

484. VUORENMAA, MARKKU. Osaamisen johtaminen pk-yrityksen kansainvälisen kasvun elinkaarella. 2012. Diss.

485. RAUTIAINEN, MARITA. Dynamic ownership in family business systems – a portfolio business approach. 2012. Diss.

486. LILIUS, REIJO. THE FINNISH IT INDUSTRIES IN TRANSITION Defining and measuring the Finnish software product and IT services industries by applying theoretical frameworks . 2012. Diss.

487. TUOMINEN, PASI. The purpose of consumer co-operation: implications for the management and governance of co-operatives. 2012. Diss.

488. SAARI, ESA. Suurnopeus-turbokoneroottoreiden termodynaaminen ja mekaaninen mallinnus sekä rakenneanalyysi. 2012. Diss.

489. PAANANEN, MIKKO. On innovative search: the use of internal and external sources of innovation among Finnish innovators. 2012. Diss.

490. BELOVA, POLINA. Quasiclassical approach to the vortex state in iron-based superconductors. 2012. Diss.

491. HIETANEN, IIRO. Design and characterization of large area position sensitive radiation detectors. 2012. Diss.

492. PÄSSILÄ, ANNE. Reflexive model of research-based theatre – processing innovation of the cross-road of theatre, reflection and practice-based innovation activities. 2012. Diss.

493. RIIPINEN, TOMI. Modeling and control of the power conversion unit in a solid oxide fuel cell environment. 2012. Diss.